# Numerical Investigation of Erosion Mitigation Method for Multiphase flow Pipelines



Author

Nauman Khan

(Registration No: 00000328935)

Thesis Supervisor: Dr. Muhammad Rehan Khan

DEPARTMENT OF MECHANICAL ENGINEERING

COLLEGE OF ELECTRICAL & MECHANICAL ENGINEERING

NATIONAL UNIVERSITY OF SCIENCES AND TECHNOLOGY

ISLAMABAD, PAKISTAN

(2024)

# THESIS ACCEPTANCE CERTIFICATE

Certified that final copy of MS/MPhil thesis written by Ms. **NS Nauman Khan**, Registration No. **00000328935** of **NUST College of E&ME** has been vetted by undersigned, found complete in all respects as per NUST Statutes/Regulations, is free of plagiarism, errors, and mistakes and is accepted as partial fulfillment for award of MS/MPhil degree. It is further certified that necessary amendments as pointed out by GEC members of the scholar have also been incorporated in the said thesis.

Signature: _____
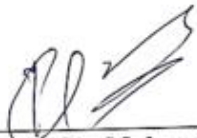
Name of Supervisor: **Dr. Muhammad Rehan Khan**

Date: _____ 12-2-2024 _____

Signature (HOD): _____
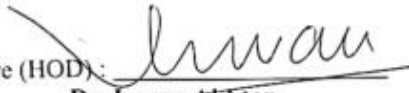
Name: **Dr. Imran Akhtar**

Date: _____ 12-2-2024 _____

Signature (Dean): _____

Name: **Dr. Nasir Rashid**

Dated: _____ 1 2 FEB 2024 _____

**Dedicated to my exceptional parents and adored siblings whose tremendous support and cooperation led me to this wonderful accomplishment**

# ACKNOWLEDGEMENTS

In the name of Allah Subhana-Watala, the Almighty, the most Gracious, the most Merciful. All praises to Allah Subhana-Watala for His help and blessings by giving me the opportunity, strength, and energy to carry out and complete this work. I acknowledge that whosoever helped me throughout the course of my thesis, whether my parents or any other individual was Your will. So indeed, none be worthy of praise but You.

I want to express my deep gratitude to my beloved elder brother, Zahid Noor, who has inspired and motivated me throughout my life. He has overcome many hardships and challenges, especially after our father's demise, but he never gave up hope. He is the reason for all my accomplishments, and I hope to honour him with this work.

I am especially thankful to my supervisor, Dr. Muhammad Rehan Khan, for his invaluable guidance and support throughout my thesis. He has been a great mentor and friend who constantly facilitated me in following my research interests and goals and was always accessible whenever I needed help or guidance. I appreciate his patience and guidance throughout the whole process.

I am also grateful to Dr. Tariq Talha and Dr. Muhammad Ali Khan for being part of my thesis guidance and evaluation committee and for providing me with their support and direction whenever I sought it.

Finally, I would like to express my gratitude to all the individuals who have rendered valuable assistance to my study.

# ABSTRACT

Erosion which can lead to leakages, interruptions and expensive repairs is a major concern in piping systems. Design modification is a promising technique for mitigating erosion and extending the lifespan of piping systems. In this study, computational fluid dynamics (CFD) was used to explore the erosion behaviour of different elbow designs in the multiphase air-sand, and water-sand flows to identify the optimal elbow design for mitigation erosion. The elbow designs considered were the standard 90-degree elbow, the 18-degree gored elbow, the 22-5-degree gored elbow, and the 30-degree gored elbow. The results showed that the 22.5-degree gored elbow consistently decreased the erosion rate by 0.68 to 0.95 times (5-32%) across various flow conditions, indicating its potential for erosion mitigation in multiphase air-sand flows. The 18-degree and 30-degree gored elbows show less consistent results, with both erosion reduction and increase observed. In water-sand flows across all the operating conditions, the erosion rate of gored elbows was enhanced compared to the standard 90-degree elbow. The 30-degree gored elbow showed consistently worsened erosion, while the 18-degree gored elbow showed the least erosion increase relative to the baseline. The standard 90-degree elbow was the least effective at reducing erosion in air-sand flows, but it had the highest erosion resistance in multiphase water-sand flows. Regression analysis revealed that flow rate, air velocity, and elbow design significantly affected erosion rate in air-sand flow. The 22.5-degree gored elbow exhibited the highest erosion resistance, while the standard 90-degree elbow had the lowest resistance for the Oka erosion model. Conversely, in water-sand flow, elbow design had the most significant effect on erosion, followed by flow rate and water velocity, respectively. The standard 90-degree elbow has the highest erosion

iii

resistance, while the 30-degree gored elbow has the lowest erosion resistance. Sand size had minimal impact on the erosion rate in both flows.

# TABLE OF CONTENTS

# LIST OF TABLES

# LIST OF FIGURES

# CHAPTER 1: INTRODUCTION

## 1.1 Background of Study

Elbow pipes, or simply elbows, are curved fittings that connect two pipes at an angle to change the direction of the fluid flow. They are commonly used in piping systems for a variety of industrial applications, such as oil and gas, petrochemical and process manufacturing industries [1]. Elbow pipes allow fluids to change direction around obstacles and in narrow spaces while increasing turbulence, pressure drop, and energy losses. The pressure drop and energy losses in the elbows are influenced by the fluid velocity, pipe roughness, pipe diameter, bend radius, and bend angle [2]. These parameters determine how the pressure and energy change in the elbow system with different intensities. Elbow pipes are versatile and can accommodate a wide range of fluids and boundary conditions due to their availability in various materials, sizes and shapes [3].

However, elbow pipes are prone to erosion due to high fluid velocities near the inner wall caused by the flow direction. Erosion occurs when a fluid carrying solid particles repeatedly impacts the surface of the material, causing wear [4]. Substantial wear and tear damage can lead to component failure, pipeline leakage and other dangerous consequences. Research has demonstrated that components such as elbows, tees, valves, chokes, u-bend and other geometries that cause rapid changes in flow direction are more susceptible to wear damage [5].

Elbows in pipeline systems are highly susceptible to erosion, as they experience an erosion rate up to 50 times higher than straight pipes. The fluid changes direction at the elbow, which enhances its speed, and this results in the particles striking the elbow wall with higher intensity, causing erosion. Erosion is influenced by various factors, such as fluid velocity, fluid properties, particle size and concentration, angle of elbow, particle and targeted material and flow pathway geometry. An explanation of the factors affecting the erosion is given [6].

- **Fluid velocity**

The major cause of piping system failure, especially in standard 90° elbows, is solid particle erosion. This occurs when the abrasive action of these particles, such as sand, dirt or other

contaminants, abrades the pipe wall. The wear rate of the pipe wall is proportional to the fluid speed and the impact force of the particles. Higher fluid velocity boosts the kinetic energy and impact force of the particles, which in turn enhances the erosion intensity.

- **Fluid properties**

The properties of the fluid, such as concentration, hardness, viscosity, corrosiveness, chemical composition, pressure and temperature, can have a significant impact on erosion in the piping system. These properties that influence the erosion rate are crucial for piping system design and maintenance.

- **Particle size and concentration**

The size and concentration of particles in a fluid also affect the erosion intensity in several ways. Larger and more concentrated particles can cause more abrasive wear, higher impact force and faster erosion rate. This can cause more material removal and slurry behaviour, which can enhance erosion severity. Therefore, particle size and concentration are important parameters to consider for erosion prevention and control.

- **The angle of the elbow**

The angle of an elbow in a piping system can affect erosion by causing variations in the fluid flow patterns and force distribution on the elbow's inner surface. Sharper angles, such as 90° bends, can create more pressure drop, more turbulence, fluid direction changes, boundary layer separation, and vortex formation, leading to higher erosion rates.

- **Material properties**

Erosion is influenced by the material properties of both the erodent and impacted surface. The erodent properties, such as size, shape, concentration, hardness and velocity, affect its erosive potential and impact force on the surface. The impacted surface properties such as hardness, toughness, corrosion resistance, wear resistance, chemical computability and surface finish affect its resistance to wear and deformation caused by the erodent.

- **Design consideration**

Design consideration and modification are crucial for influencing the erosion in piping, elbows and other fluid-handling applications. The following design factors are important for erosion in fluid processing systems

- Removing dead zones and sudden shifts in the flow direction

- Maintaining appropriate ranges of fluid velocities and pressure levels

- Lowering the chances of turbulence and flow separation

- Applying particle filtration and separation systems

## 1.2 Problem Statement

Erosion is a major concern in oil and gas piping system elbows, as it can lead to leakage, failure, malfunction, or burst of the pipelines. The main cause of erosion is the collision of solid particles, such as sand, on the elbow surface, which are entrained by the fluid flow. Erosion in the elbows is influenced by several factors, such as the speed, size and shape of the particle, the angle, material and roughness of the elbow surface, and the shape of the flow channel. Previous investigation has revealed that particle velocity is the most influential factor in erosion and that lowering particle velocity can greatly reduce erosion.

Design modification is an effective technique for mitigating erosive wear in the elbow. Previous studies have shown that vortex-chamber, plugged tee, twisted tape insertion, and innovative pipe wall can significantly reduce elbow erosion. The performance of a gored/segment elbow in reducing erosion will be examined in this study. A gored/segment elbow is an elbow that consists of a number of segments that are connected to form a smooth curve. The segments of a gored elbow can be welded or mechanically joined. Gored elbows are available in various sizes and angles.

CFD is a proven, powerful, and efficient tool to simulate fluid flow and erosion processes in piping systems. CFD-based erosion modelling has been widely used and validated in various industrial applications. It provides reliable predictions of erosion behaviour under different

boundary conditions. This research aims to use CFD-based erosion modelling to examine the influence of gored elbows on erosion rate and to propose optimal solutions for mitigating erosion in piping systems.

## 1.3 Objectives

The research objectives are:

- To review the literature on erosion mitigation methods for standard elbows
- To investigate the impact of gored elbows on erosion
- To explore optimal design and orientation angles of the gored elbow for erosion mitigation
- To compare the erosive wear of gored and standard elbows for diverse particle sizes, concentrations, and flow velocities
- To develop effective strategies for preventing erosion of elbows

## 1.4 Scope of the study

The scope of this research is to inspect the effect of gored elbows on erosion rate and to devise effective strategies for erosion prevention in oil and gas piping systems. The study will address the following key aspects:

- Conducting a comprehensive literature review on erosion mitigation methods for standard elbows.
- Analyzing the influence of gored elbows on erosion rates.
- Exploring optimal design and orientation angles of gored elbows to mitigate erosion.
- Comparing erosion rates between gored and standard elbows under various particle sizes, concentrations, and flow velocities.
- Formulating effective strategies for preventing erosion in elbows.

This study will focus on elbows and exclude other components, such as tees, valves, or chokes, that may also be prone to erosion. This study will also not consider other factors that may

influence erosion, such as fluid properties, corrosiveness, or temperature. This study will be based on a literature review and computational fluid dynamic (CFD) simulation using ANSYS Fluent software.

## 1.5 Outline of the Thesis

This thesis examines the erosion mechanism of elbow pipelines, which are widely used in diverse industrial sectors. The goal is to improve the performance, reliability, and safety of pipeline systems. The thesis is composed of five chapters, each presenting a different aspect of the research on the erosion rate of elbow pipelines. Chapter 1 introduces the study of erosion rate in pipelines with bends and provides the background, problem, objectives, and scope of the research. Chapter 2 reviews the existing literature on erosion rate and highlights the key factors that influence it. This chapter also explores the latest developments in erosion mitigation techniques in elbows. Chapter 3 presents the validation and methodology used to simulate the erosion rate in various designs of gored or segment elbow pipelines under different conditions. Chapter 4 presents and analyses the numerical results, mechanism and the influence of various parameters on wear rate in detail. Chapter 5 reports the key findings, conclusions, and recommendations for future work.

# CHAPTER 2: LITERATURE REVIEW

## 2.1 Introduction

One of the major problems for the hydrocarbon industry is erosion, which affects the efficiency and reliability of pipeline systems. Erosion is triggered by the influence of solid particles carried by a fluid flow, which wear away the material surface [7]. As a consequence, elbows, which are pipe fittings that alter the flow orientation, are more susceptible to erosion than straight pipes [2]. However, the standard 90° bend is the most commonly used flow-changing device in the oil and gas industry. Therefore, many researchers have investigated the erosive wear behaviour and mechanism of 90° elbows using experimental and numerical methods. For example, Khan (2020) used a multi-layer paint modelling technique and computational fluid dynamics (CFD) for erosion analysis distribution inside an elbow under liquid-solid flow conditions. They found that elevating the slurry speed significantly changed the way particles impacted the wall, resulting in an increase in material loss in the underside of the elbow [8].

The erosive wear mechanism of 90° bends has been extensively explored by various experimental and numerical studies. For instance, Solnordal (2015) aimed to determine the wear rate of a standard 90° elbow under pneumatic conveying of sand particles using experimental and numerical approaches. They used a surface profiler to measure the erosion depth of the elbow and then simulated the flow patterns and particle tracks using CFD and discrete phase model (DPM). Moreover, the authors evaluated different particle-wall collision models and found that the rough wall model best fitted with the experimental data[9].

In another study, Mazumder (2005) conducted an experimental and computational analysis of elbow erosion in mixed-phase flow. They measured the erosion rates of elbows in an erosion test loop and simulated the fluid and particle flow using CFD. The authors concluded that the mechanistic model developed in their study could be used to estimate erosion in elbows in multiphase fluid flow, and could be used to optimize the elbow design and operation[10].

Kesana and colleagues (2013) examined the erosive wear tendencies induced by the mixed-phase interaction of air and sand particles traversing a standard elbow. Employing ultrasonic

technology alongside numerical simulations, they quantified and replicated the dispersion and extent of erosive impact spanning the surface of the elbow. The authors verified the accuracy of their numerical model by comparing it with experimental data from various sources and evaluated the performance of different collision models. They also investigated the influence of particle size and hardness on erosion behaviour. The research revealed the exact location and intensity of maximum erosion for different flow conditions and orientations. This scholarly contribution enhances the understanding and prevention of the erosion phenomenon in industrial pipe elbows [11].

Erosion is a significant issue for elbows in pipeline systems, as they undergo much more material damage than straight pipes. Although erosion cannot be totally prevented, various methods have been developed by researchers to lessen the severe impacts of wear and tear on elbow parts. Hence, understanding and mitigating erosion in 90° bends is crucial for ensuring the safety and performance of pipeline systems.

## 2.2 Mechanism of Erosion

Erosion is a complex process that occurs due to the interaction between fluid flow and solid particles. The primary mechanism of erosion is the impact of these particles on a material surface, leading to material removal over time. This impact generates mechanical forces that can cause material detachment, surface abrasion, and eventual degradation. The erosion wear mechanism depends on various factors such as the properties of the particles, the angle of incident, the fluid, the surface as well as the flow conditions [12].

Literature reveals that the erosive wear mechanism is different for ductile and brittle materials. The mechanism of material removal from ductile material surfaces is cutting, deformation, fatigue and corrosion.

Cutting: This occurs when a hard, sharp particle strikes a soft, smooth surface, resulting in a deep groove or chip. This is the most severe type of erosive wear and leads to high erosion rates and significant material loss.

Deformation: This occurs when a soft and round particle collides with a hard and rough surface, resulting in a shallow pit or dent. This is the least severe type of erosive wear, and it leads to low erosion rates and low material loss.

Fatigue: This occurs when a hard and sharp particle impacts a hard and rough surface repeatedly, causing cracks or spalls. This is a moderate type of erosive wear and leads to moderate erosion rates and moderate material loss.

Corrosion: This occurs when a particle impacts a surface in a corrosive environment, causing oxides or other compounds to form on the surface. This can either enhance or reduce the erosion wear, depending on whether the surface is protecting or weakening, which leads to variable erosion rates and material loss [13].

Another study investigated the amount of material loss due to the energy transfer from the particle to the surface, which varied with the particle, fluid, flow, and surface features. The angle of impact also influenced the erosion rate and pattern. Moreover, this study indicated that low-impact angles produced deep grooves (cutting), while high-impact angles produced shallow pits (deformation), and intermediate angles produced both (cutting and deformation) [14]. The mechanism of ductile material erosion is explained in Figure 1.



(a)                              (b)                              (c)
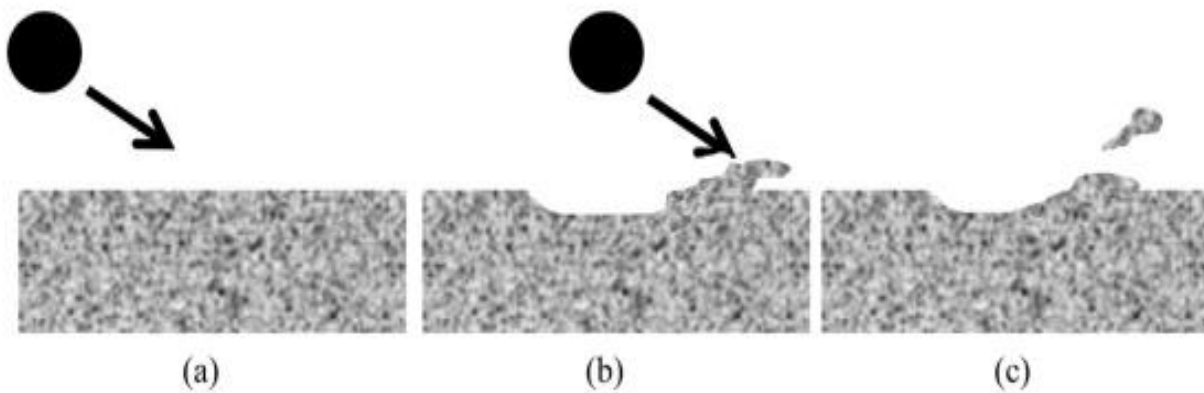
**Figure 1:** Erosion progression in ductile material (a): Prior to the particle contact, (b): Crater development and material piling at one side of the crater, (c): Material removal from the surface [14].

Alternatively, the predominant erosion mechanism in brittle materials involves the initiation of cracks due to high-velocity impact particles, resulting in the transfer of their kinetic energy. The impact instigates the development of radial, lateral, and medium cracks, which have the potential

to extend and intersect. The eventual removal of material takes place when cracks either reach unbounded edges or merge to form fragments. The cracking mechanism is dependent upon diverse factors, including particle attributes such as size, shape, hardness, and velocity, as well as surface characteristics encompassing hardness, toughness, and surface roughness. Additionally, the angle of incidence of the particle plays a pivotal role in influencing stress distribution, as well as the instigation and progression of crack formation [15].

## 2.3 Variables Affecting the Erosion Rate

Erosion dynamics is a complex field that involves many factors that affect how material degrades over time. This section explores how these factors work together to determine the erosion rate in various systems. The factors include the characteristics of the fluid and the particles, the properties of the surface, the condition of the flow, the environmental influences, and the interaction between the particle and the target [16]. By understanding how these factors interact, we can obtain a better insight into the mechanism of erosion. We can also learn how to design materials and strategies that can reduce erosion and improve performance.

### 2.3.1 The Effect of Particle Characteristics on the Rate of Erosion.

According to a study, particle size is a vital factor that influences the erosion characteristics of materials such as stainless steel, copper, and aluminium. Researchers utilized a slurry jet erosion test to investigate the impact of particle size on the erosion rate and mechanism of these materials at varying impact angles. The findings revealed that as the particle size increased from 50 to 300 micrometres, the erosion rate increased, and the erosion mechanism transitioned from cutting to deformation. Additionally, this study also demonstrated that as the impact angle varied from 15 to 90 degrees, the erosion rate enhanced. This finding provides valuable insight into the relationship between impact angle and erosion rate [17].

In contrast, another study claims that the resistance of materials to solid particle erosion (SPE) is influenced by a variety of factors. The authors of this review paper summarize the current understanding of these factors, including flow conditions, particle characteristics, and material properties. They discuss how these factors affect the SPE rate and mechanism and conclude that the SPE and mechanism are intricately dependent on these factors. Furthermore, they suggest that

9

the optimal design of materials and coating for combating erosion requires a careful balance of hardness and toughness, as well as the careful use of surface treatment and modification [18].

Similarly, another study was carried out to analyze the impact of particle characteristics such as size, shape and flow rate on the erosion of stainless steel. The researcher conducted experiments within a test section featuring a distance between elbows equivalent to 12D, employing varying particle sizes and flow rates. Transducers were utilized to accurately and reliably measure the wall thickness loss in the elbows and assess erosion. The findings from the experiments revealed a trend of decreasing erosion rates in the initial elbow with diminishing particle sizes. Conversely, the second elbow exhibits higher erosion rates with 300 µm particle size, although the erosion in the second elbow was comparatively lower than the first elbow at the 12D distance. Notably, concerning the maximum erosion ratio between the two elbows, results demonstrated a reduction in the erosion rates ratio (second to first) with an increase in particle size. Moreover, a higher ratio between the two elbows was noted with 25 µm particle size compared to 300 µm and 75 µm [19].

### 2.3.2     *The Influence of Fluid Velocity on the Rate of Erosion.*

The erosion process in the material is significantly influenced by the velocity of the fluid flow, emphasizing the necessity for a thorough investigation. In this context, a study was designed to investigate the effects of sand loading and flow velocity on the weight loss attributed to erosion-corrosion in a mild steel specimen. Employing a submerged impingement jet setup, the authors delved into the complex interaction between erosion and corrosion phenomenon. The investigation was conducted within seawater, encompassing a wide spectrum of flow velocities from 10 m/s to 20 m/s and sand loading spanning from 300 mg/L to 600 mg/. Through matriculas experimentations, the study dissected the contributions of pure erosion, corrosion and their combined impact on weight loss. The obtained insights unveiled an intriguing linear relationship between the weight loss and both flow velocity and sand loading for cases of pure erosion and erosion-corrosion interaction. Remarkably, erosion emerged as the predominant factor across most scenarios, except in situations characterized by low velocity and sand loading conditions [20].

Another research investigation found that the rate of erosion in a 90-degree horizontal elbow increases with carrier fluid velocity. The study also revealed that the erosion rate at different

locations of the elbow bend is different, varying from 2.6 to 8.9 mm/year at the fluid speed of 2.5m/s, 4.0 to 11.2 mm/year at a fluid velocity of 3.5 m/s and 5.8 to 14.6 mm/year at a fluid velocity of 4 m/s [21].

### 2.3.3    *The Effect of Incidence Angle and Target Surface Orientation on Rate of Erosion.*

The influence of impact angle and the orientation of the targeted surface play a pivotal role in shaping the erosion dynamics. The angles at which particles strike a surface significantly affect the resulting erosion pattern and material removal. Likewise, the orientation of the surface in relation to the incoming particle can either amplify or mitigate erosion effects. Understanding the interaction between impact angle and surface orientation is crucial for designing erosion-resistant materials and optimizing system performance in various industries.

Based on the literature review, a study was conducted to examine how elbow angles affect the erosion-corrosion behaviour of 1018 steel within the context of gas-liquid-solid multiphase flow. This study was carried out in a closed flow loop at standard atmospheric pressure using plug flow conditions. This study harnessed a dispersed phase comprising silt (silica sand) at a concentration of 2.5 wt%, utilizing silt grains measuring 70 µm for experimental considerations. Notably, the ensuing analysis spotlighted a pivotal finding: changing the elbow configuration from 60 to 90 degrees within a plug flow condition increased the material degradation, up to 1.8 times, due to the slit impact [22].

In a related study, the erosive wear in 15° to 90° elbow was investigated numerically in a two-phase, air-solid flow. This study examined both the horizontal-horizontal (H-H) arrangement and the vertical-horizontal (V-H) arrangement of the pipe. The assessment of the results shows that the maximum erosion rate in the V-H arrangement is greater than in the H-H configuration. The result also revealed that the point of maximum erosion on the elbow's wall in the H-H flow configuration is at around 50° while in the V-H flow configuration it is at about 55°. An elliptical pattern of material loss with elbow angles from 15° to 45° can be seen. However, a V-shape scar emerges with an increase in elbow angle and is more visible at 60° to 90°. These V-shape scars are comparatively more visible in the H-H configuration [23].

### 2.3.4    *The Effect of Design Elements on the Rate of Erosion.*

Another influential parameter in the field of pipeline engineering is the design of elbows and pipelines, which play a crucial role in determining their erosion rates. The curvature of these components and the material used in their construction are key factors in their susceptibility to erosion. Elbows that are designed with smooth curves and streamlined shapes can reduce turbulence caused by high-speed fluid flow, acting as a barrier against erosion. However, if these design elements are not carefully considered, erosion can occur, causing material degradation and weakening the structural integrity of the pipelines.

One such study was performed by examining a vertex chamber in comparison to a standard 90° elbow. The basic geometric parameters, such as pipe diameter, domain size, and curvature radius, were kept constant. A semi-sphere was constructed at the opposite side of the inlet. This research work concluded that the erosion rate in the vertex chamber was considerably dropped, and in the worst-case scenario, it was half of that in the 90° elbow. In addition to that, the vortex chamber could have a longer life span due to the more even distribution of erodent particles impact on its surface [24]. The representation of the standard 90-degree elbow's geometry and the vortex chamber can be found in Figure 2.
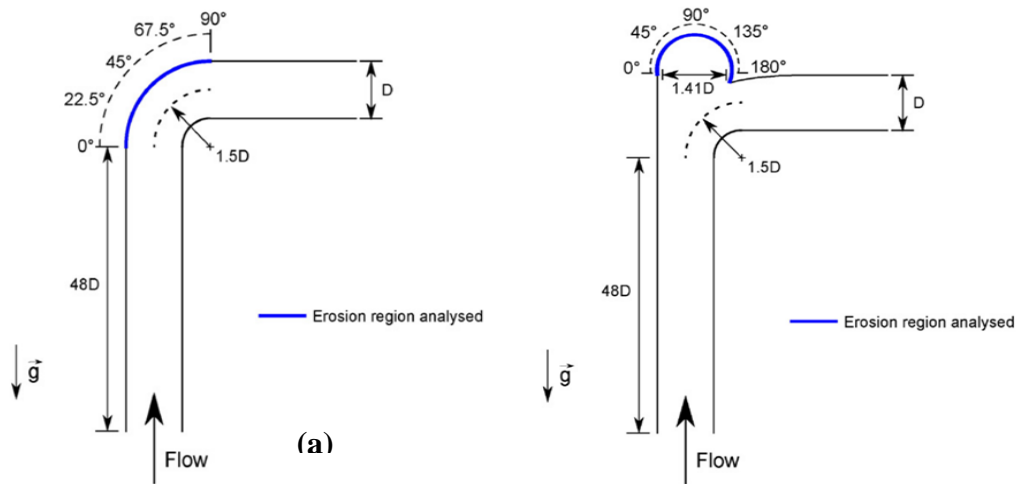


**Figure 2:** (a) Standard 90-Degree Elbow: (b) Vortex Chamber Elbow [24].

## 2.4 Erosion Mitigation Techniques

The problem of erosion poses significant challenges for many industrial applications, requiring the development of effective countermeasures to prevent or mitigate its detrimental

effects. This section provides a comprehensive analysis of the diverse range of innovative strategies that have been devised to address this issue, covering both passive and active methods of erosion control. Passive methods rely on the selection of suitable materials and the enhancement of surface properties to resist erosion, while active methods involve manipulating the flow conditions or deploying protective mechanisms to reduce erosion. The section demonstrates the practical value of these strategies by illustrating their diversity and adaptability in various industrial contexts.

A study dedicated to erosion mitigation was conducted, wherein the authors investigated the effects of trapezoidal rib on the extrados of a 90° elbow to minimize erosion. Using the CFD-DPM approach, the authors assessed the performance of the rib. They validated their CFD erosion prediction with experimental data for a standard elbow. They observed an elliptical erosion zone with a vee-shaped scar on the extrados caused by particle impacts, but it also suffers erosion itself. The rib, at $\theta=25°$, achieved the highest reduction of elbow erosion peak by 31.4%. The position and velocity of the rib influence its erosion rate and protection effect. Elbow erosion also increased with higher particle mass loading. The optimal choice was to install the rib at $\theta=25°$, considering the erosion rate and protection effect [25]. The configuration of both the rib and the pipe geometry is visually represented in Figure 3.
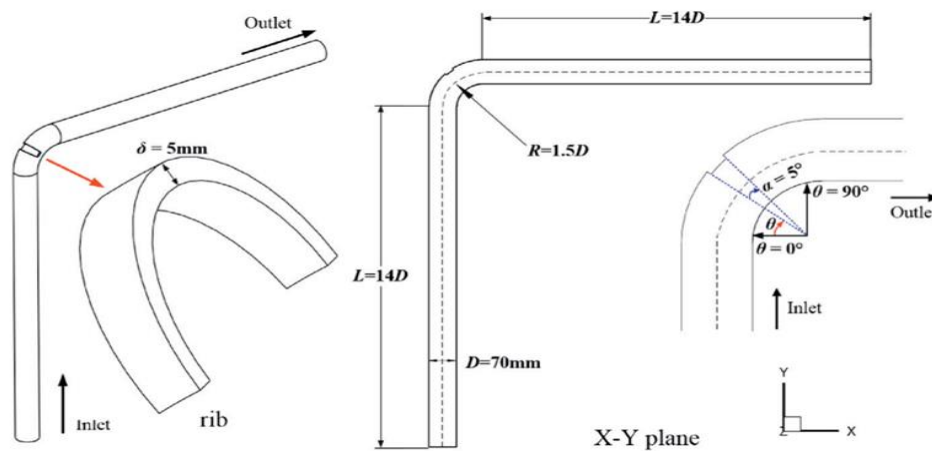


**Figure 3:** Rib and Pipe Stricture [25].

### 2.4.1 Passive Erosion Mitigation

Passive strategies for erosion mitigation involve employing altercations in geometry or materials to curtail erosion rates and ensure a more even distribution of erosion patterns. For example, some studies have investigated the use of swirl pipes, vortex chambers, plugged tees or curved pipes upstream of the elbow to induce a swirling flow, thus modifying particle trajectories and impact angles. By implementing such measures, the ultimate erosion rate can be reduced, and the longevity of the elbow extended. Another approach involves the application of advanced materials or coating to strengthen the resistance of pipe and elbow surfaces against erosion [26]. Notably, studies have showcased the efficacy of coating such as TiN, CrN, or WC-Co on steel pipes. These coatings distinctly enhance attributes such as hardness, toughness, and corrosion resistance, thereby elevating the overall performance of pipes and elbows. Passive erosion mitigation operates without the need for external energy sources or control systems.

A study was conducted to examine how swirling flow can effectively mitigate elbow erosion in solid particle pipelines. The study presents a simulation of the effects of various factors on the erosion pattern and rate of elbows. The results show that the introduction of a twisted tape generates a swirling flow that more evenly disperses solid particles within the pipeline, reducing the erosion of the elbow. Additionally, the effectiveness of this erosion reduction is greater when the twist ratio is lower and the twisted tape is positioned close to the elbow. As the gas velocity increases in the presence of swirling flow, particle impact energy rises, and the collision mode transitions from sliding to direct. While the erosion rate of an elbow fitted with a twisted tape also increases with the gas velocity, the presence of swirling flow reduces the velocity exponent of the erosion rate to some degree. The paper suggests a new approach to mitigating elbow erosion through swirling flow and provides insight into the mechanism and factors [27]. The schematics of the twisted tape and the elbow are shown in Figure 4.
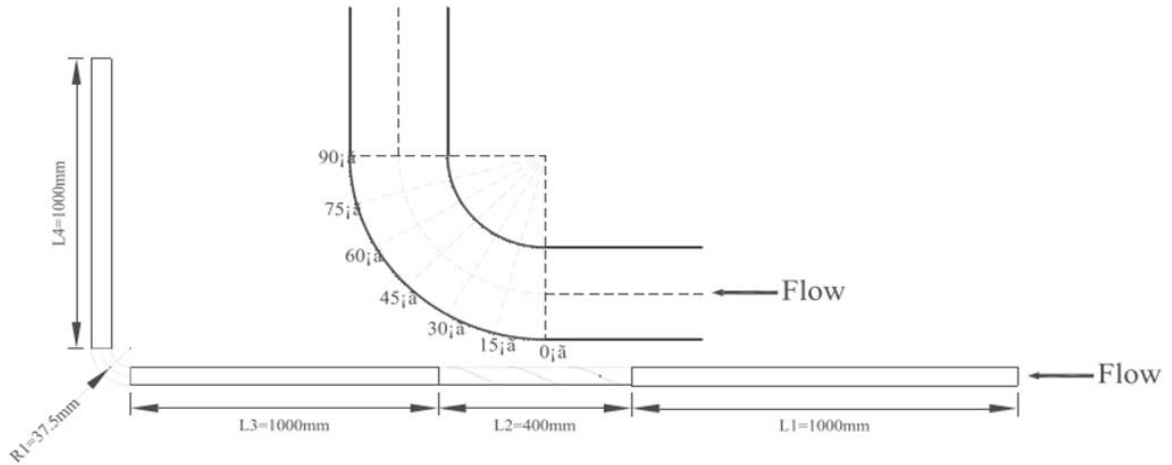
**Figure 4:** Twisted Tape and Elbow Geometry [27]

An additional investigation was conducted to measure the erosion resistance of different configurations within a dilute gas-solid multiphase flow context. These configurations comprised the plugged tee, vortex chamber, and a conventional 90° elbow. The study concludes that, with respect to erosion reduction, the plugged tee geometry surpasses both the vortex chamber and conventional elbow. However, it is recognized that the inherent flow dynamics of the plugged tee design exhibit limitations when addressing erosive processes under conditions of higher mass loading. As a solution in scenarios characterized by substantial mass loading, the vortex chamber elbow emerges as the optimal choice [28]. The configuration of the plugged tee, vortex chamber and the conventional 90° elbow is illustrated in Figure 5.
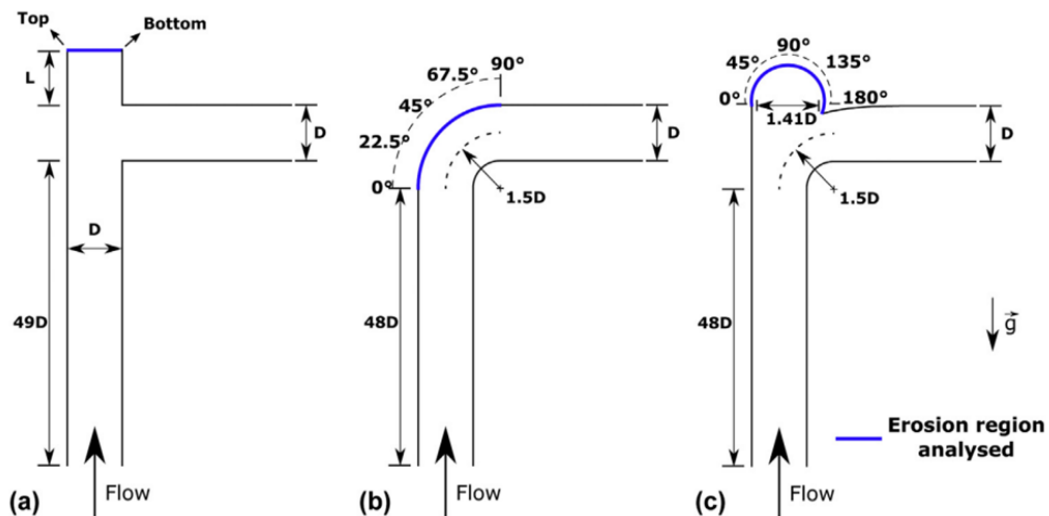


**Figure 5:** (a) Plugged Tee: (b) Conventional 90° Elbow: (c) Vortex Chamber [28].

15

A novel study introduces an innovative pipe wall design aimed at reducing the erosion of 90° elbow. The design involves twisting the pipe wall along the flow streamline direction, creating a swirling flow upstream of the elbow. The design of the twisted pipe wall and other parameters are displayed in Figure 6. This redistributes transported particles, preventing their concentration at a single point on the elbow. The authors used a CFD model based on the Euler-Lagrange approach to validate their design. The result shows an erosion reduction of 33% on the 90-degree elbow using this novel pipe wall configuration [29].
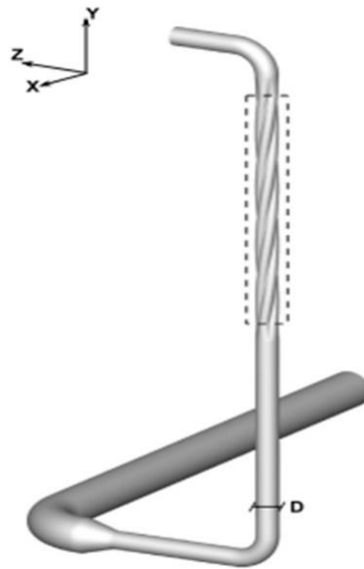


**Figure 6:** Twisted Pipe Wall [29]

The existing literature shows that a similar study was conducted to explore innovative strategies addressing the issue of elbow erosion. A novel solution for mitigating elbow erosion in pneumatic conveying systems was proposed by using hemispherical protrusions. The study investigated the influence of arrangement angles, protrusion radius, and number of protrusion rows on the erosion rate density using the CFD-DPM approach. The study reveals that a small arrangement angle and large protrusion radius for a single row of protrusions resulted in a significant reduction in the maximum erosion rate by 36.59%. Introducing multiple protrusion rows further increased erosion reduction to 39.09%, but at the cost of increased flow resistance [30]. The schematic of the pipe and protrusions in the elbow is illustrated in Figure 7.
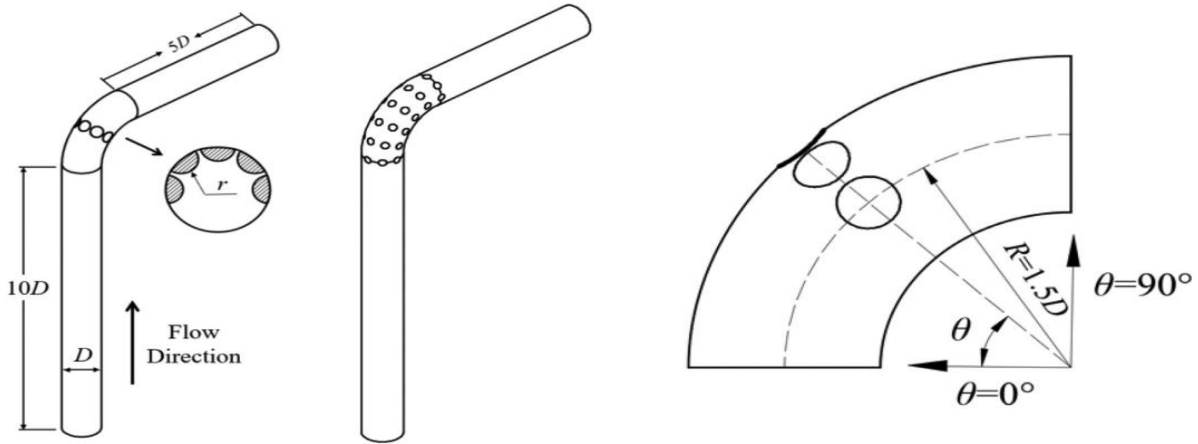
**Figure 7:** Pipe and Protrusions in Elbow [30]

*2.4.2        Active Erosion Mitigation*

Active erosion mitigation involves the utilization of external apparatus or systems to regulate or oversee the erosion phenomenon. As an illustration, certain investigations have suggested harnessing electrodynamic fields, ultrasonic waves, or acoustic emission sensors to manipulate or identify erosion dynamics. These approaches possess the potential to alter particle attributes such as charge, velocity, or trajectory or to gauge material attrition, surface texture, or fracture advancement. Moreover, the integration of an online erosion monitoring system stands as another example. These systems furnish real-time erosion data encompassing erosion rate, localization, and intensity. Active erosion mitigation requires the utilization of external energy sources or control systems for its operations.

## 2.5 Computational Approach and Modeling

Computational methods and models have greatly advanced the study of erosion and its complex interactions with various factors. By simulating the effect of erosion using computational techniques, researchers can gain a deeper understanding of the mechanisms, rates, and mitigating strategies of erosion. This section explores the importance of computational approaches for comprehending and forecasting erosion phenomena.

Researchers are widely applying computational fluid dynamics (CFD) in research studies due to its high flexibility, computational efficiency, and time-saving potential [31]. Computational

fluid dynamics (CFD) is an essential tool to study and analyze fluid flow in pipes and elbows, which are common components in many industrial processes such as oil and gas transportation, hydraulic fracturing, and chemical engineering [32]. The literature review revealed that CFD techniques are extensively utilized to perform numerical simulations related to erosion studies [33]. Numerical modelling has always been used as a powerful tool for predicting erosive wear rate and mechanism, as well as optimizing the design and performance of pipe systems. By numerically solving complex equations that describe the erosion mechanism, computational modelling provides a systematic way to examine erosion. These models consider the variables that influence the erosion rates, such as particle properties, fluid speed, incidence angles, and design features. Computational simulations enable researchers to investigate erosion patterns under various conditions that may be difficult to reproduce in real-world experiments [34].

Different computational models have been proposed to study erosion comprehensively. Empirical models use experimental data to determine the relationship between erosion rates and relevant factors. These models are useful for their simplicity and applicability but may not be accurate enough to predict erosion under different conditions. On the other hand, mechanistic models aim to understand erosion at a fundamental level. They apply physical principles, such as fluid dynamics and particle interactions, to simulate the erosion process in a more detailed way. These models reveal the underlying physics of erosion but may need complex numerical simulations and specific input parameters [35].

Creating accurate computational erosion models is challenging due to the multidimensional nature of erosion phenomena. Robust numerical methods and high-performance computing resources could accurately establish the interactions between particles, fluids, and target surfaces. Moreover, getting precise input parameters for these models can be difficult, as it needs careful experimental characterization. Recent progress in computational fluid dynamics (CFD) and numerical methods has improved the accuracy and efficiency of erosion simulations. A better understanding of turbulence, particle dynamics, and surface interactions enables a more realistic representation of erosion processes [36].

In summary, computational methods and models have greatly improved our knowledge of erosion processes. The use of computational fluid dynamics (CFD) techniques allows for

flexibility and efficiency in studying the integrations of erosion with various factors. These simulations reveal the mechanism, rates, and mitigation strategies of erosion. While empirical models are simple, mechanistic models go deeper into the physics of erosion despite requiring complex simulations and precise input parameters. Despite the changes, recent advances in computational methods enhance the accuracy of representing turbulence, particle dynamics, and surface interactions. These improvements enable researchers to develop better erosion control strategies and make informed decisions based more comprehensive understanding of erosion phenomenon.

## 2.6 Summary

The literature on this topic indicates that erosion is the process of solid particles in a fluid stream hitting and damaging the inner pipe wall, causing wear and deterioration. It is a serious problem for the hydrocarbon industry, as it can lead to pipeline failure and environmental hazards. One of the most critical components of pipeline systems that are prone to erosion is the conventional 90-degree bend, which is used to change the direction of the flow. Moreover, the literature reveals that the erosion rate depends on various factors related to the particles, the fluid and the surface. Elbow pipes are particularly suspectable to erosion due to their complex flow pattern and high particle impact angle.

The literature on erosion mitigation strategies emphasizes the effectiveness of design modification in reducing elbow erosion. However, there is limited information available on elbow erosion, and mitigation strategies are still being developed. Although there is extensive research on erosion mitigation strategies for piping systems, the knowledge about gored elbow erosion is still limited. As indicated by the literature, design modifications have been shown to be effective in mitigating erosion in conventional elbows. However, their application to gored elbows is a new and relatively unexplored area.

Gored or segmented elbows have the unique characteristic of being made up of segments that can be customized in terms of size and shape, providing opportunities for innovative erosion mitigation methods. However, the current body of literature on erosion in gored elbows is limited,

resulting in a lack of understanding of erosion patterns, underlying mechanisms, and optimal mitigation techniques for these specific components.

The various dimensions and configurations of gored elbows, including parameters such as bend angle, segment angle, segment length and segment diameter, have a significant impact on erosion behaviour. Additionally, the different combinations of quantities and arrangements, such as three-segment, four-segment, and five-segment gored elbows, introduced complex factors that require further investigation.

The primary aim of this study is to bridge the existing research gap by reviewing the current knowledge on erosion mechanisms and factors, with a particular focus on 90° elbows. Additionally, this study seeks to investigate the effectiveness of various design modifications, such as altering the curvature or introducing surface features, in reducing the erosion rate in gored elbows by changing flow patterns and particle angles. The effectiveness of these modifications will be confirmed through the use of CFD models.

Furthermore, this study aims to compare the performance of gored elbows with 90° elbows using CFD simulations. This comparison can help determine whether gored elbows are optimal for certain applications and operation conditions, as well as identify which gored configuration exhibits the least erosion among different options.

Overall, this research can contribute to the understanding and mitigation of gored elbow erosion in pipeline systems.

# CHAPTER 3: METHODOLOGY

## 3.1 Introduction

This chapter aims to optimize the erosion rates of important pipeline components in the gored elbows in comparison to the conventional 90-degree elbow. Numerical methods and computational models are used to study the erosion behaviour and design aspects of these diverse configurations. The gored elbows are designed with different gored angles: 18 degrees, 22.5 degrees and 30 degrees. The objective is to determine the gored elbow with the lowest erosion rate and the best design for minimizing erosion.

This chapter is organized into several sections, each with a specific role in the analysis. The first section (3.2) describes the geometrical features of both the gored and 90-degree elbows, as they are crucial for understanding the erosion patterns. The second section (3.3) explains the grid generation process, which is important for creating a computational domain that reflects the physical system. The third section (3.4) discusses the operating conditions which are necessary for realistic erosion simulations.

The numerical modelling section (3.5) is the main part of the analysis, where various techniques are used to model the fluid flow and erosion. The Euler-Lagrange approach is used, which treats the fluid as a continuous phase and the eroding particles as a discrete phase. The continuous phase model is used for the fluid flow, while the discrete phase model is used for the particle tracking. The K-Epsilon turbulence model is utilized for the turbulence effects, and standard wall treatment is used for the boundary layer phenomenon. Erosion modelling methods are also presented to estimate erosion rates based on fluid flow and particle trajectories.

The final section (3.6) provides a comparison between the computational results and the empirical data obtained from previous research to validate the accuracy and reliability of the numerical models. This validation process is a vital step in ensuring that the approach confirms the experimental findings on the flow dynamics and erosion rates in the 90-degree elbow. The objective is to demonstrate the applicability and resilience of the numerical methods for simulating complex fluid flow phenomena and erosion rates in elbow pipelines.

Figure 8 presents the research methodology of this study, which shows a detailed and complex overview of the method and process used.
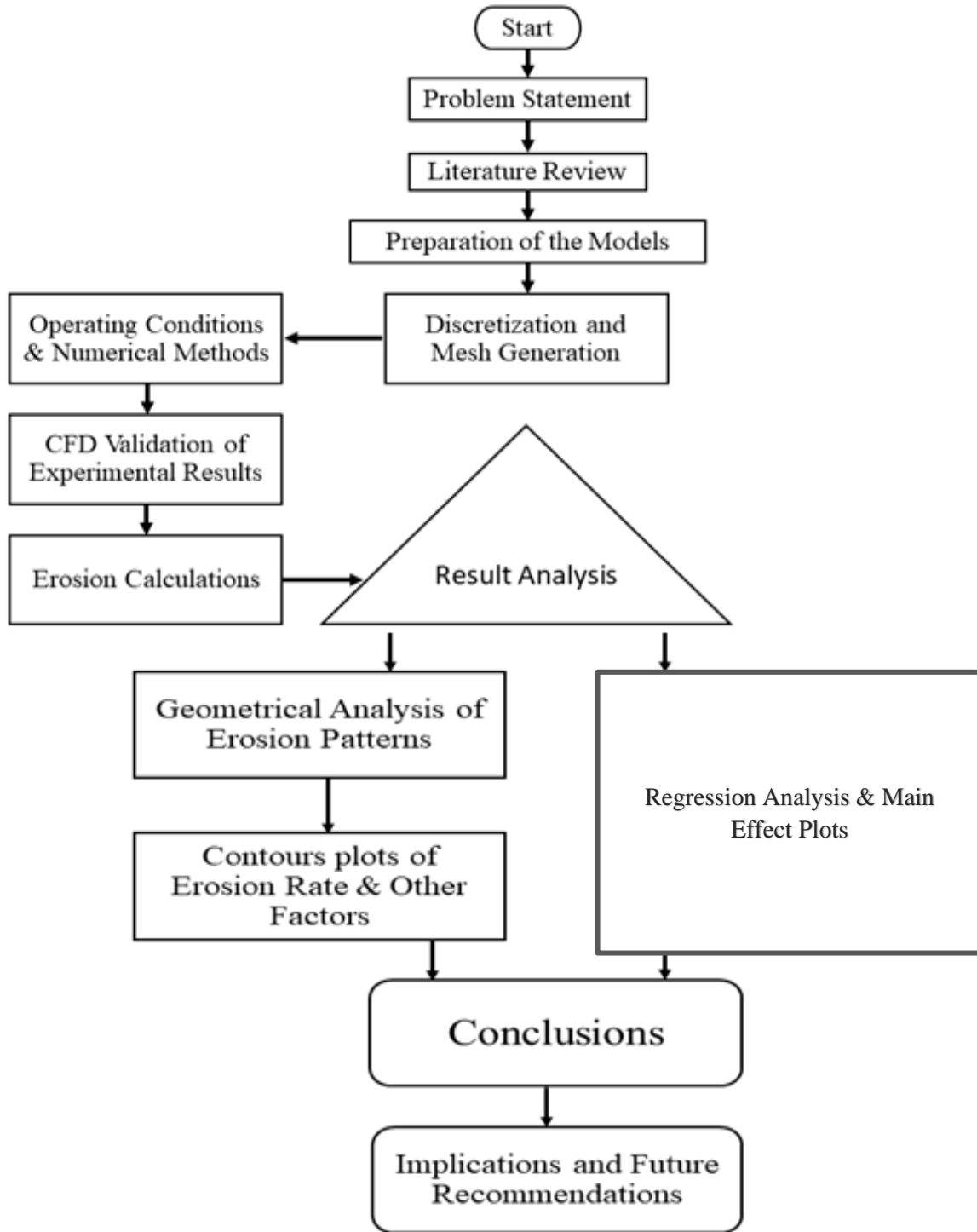


**Figure 8:** Diagram illustrating the research methodology

## 3.2 Geometry Description

The 3D model, as shown in Figure 8 and Figure 9, was created using the SOLIDWORKS software suite. The geometric parameters for the simulations were selected based on the findings detailed in the reference [37]. The fluid flow enters through an initial straight section of 1000 mm in length, which includes a 90° elbow with a radius-to-diameter (r/D) ratio of 1.5. After the elbow, there is a subsequent straight segment of 600 mm in length to accommodate the outflow of the fluid. The inner diameter (D) of the pipe is fixed at 76.2 mm, as specified in Figure 9(a). Figures 9(b), and10(a), and (b) illustrate three alternative geometries that have been modified from the main model. These geometries have different elbow curvatures, which are known as "gored" or "segmented" elbows in fluid dynamics.

The first alternative geometry has an elbow with five segments, each with an 18° angle. This geometry demonstrates the complexity of multi-segmented designs. The second alternative configuration has an elbow with four segments, each with a 22.5° angle. This outline shows the flexibility of segmented designs. The third alternative structure has an elbow with three segments, each with a 30° angle. This layout reveals the diversity of the segmented designs. These geometries were used for comparative analysis of the simulation results.
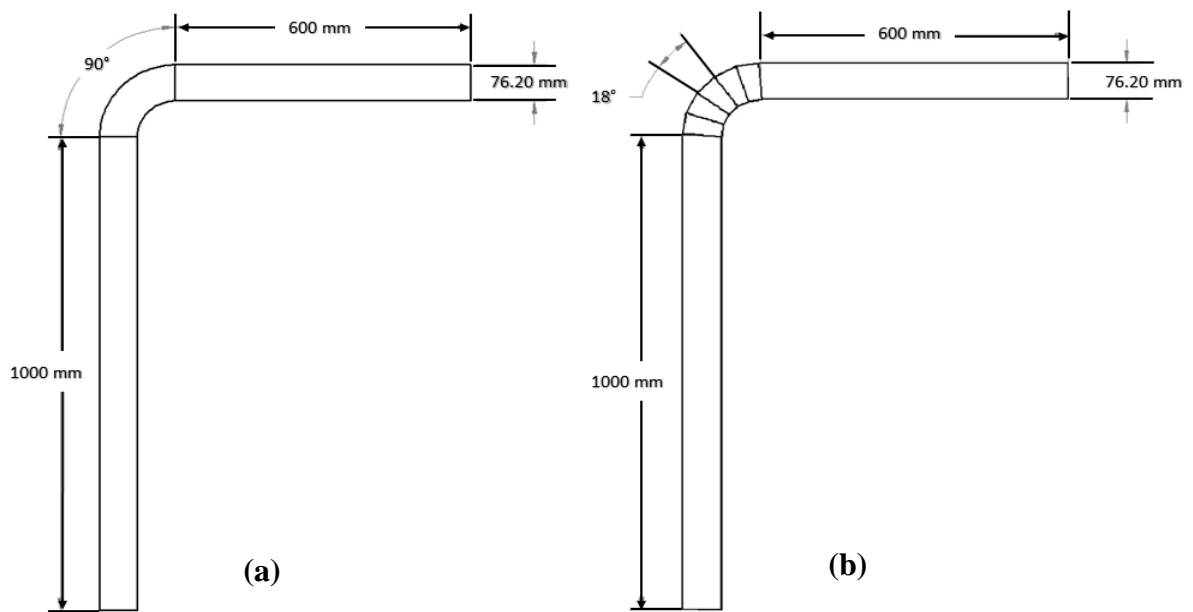


**Figure 9:** (a) Geometry Dimensions of the Standard 90° Elbow (b) Geometry Dimensions of the Gored Elbow with Five 18° Segments.
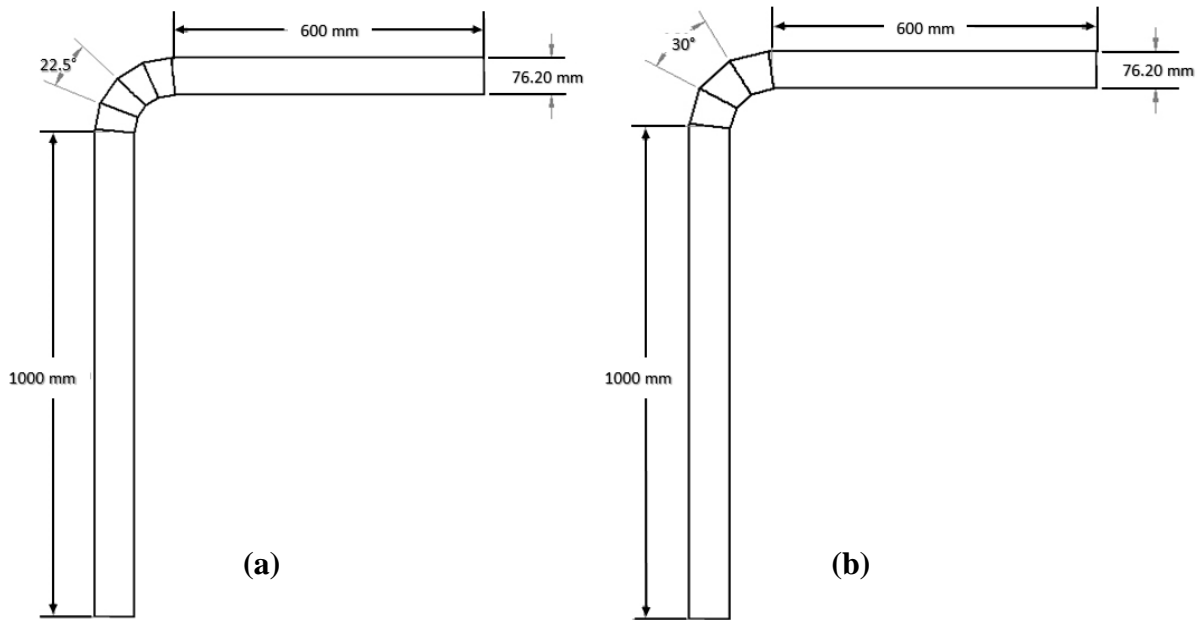
**Figure 10:** (a) Geometry dimensions of the gored elbow with four 22.5° segments (b) Geometry dimensions of the gored elbow with three 30° segments.

## 3.3 Grid Generation

Grid generation is a critical step in computational modelling and simulations. It allows the representation of the physical system's geometry within a computational domain by creating a mesh of points or cells that cover the domain and serves as the basis for numerical simulations. These simulations enable the estimation of various physical quantities, such as fluid flow, temperature, or erosion behaviour, at discrete locations within the domain. The quality and resolution of the grid have a direct influence on the accuracy and efficiency of the simulations, as they determine the reliability of the results. Therefore, careful selection and application of methods and techniques are required to produce grids suitable for specific research objectives. One of the methods and techniques that was employed for the research purpose was a mesh refining study, which is presented and discussed below.

A mesh refining study is a process of testing different meshes with varying levels of refinement and comparing the results with a reference solution or experimental data. The error rate of each mesh is calculated by comparing the results of each mesh with the result of the reference solution. The error rate is defined as the relative difference between the two solutions in terms of the maximum erosion rate.

24

Seven different meshes were applied with varying levels of refinement to the standard 90-degree elbow geometry to evaluate the accuracy and validity of our numerical simulations. The maximum erosion rate obtained from each mesh was compared with the finer meshes as well as with the previous experimental results reported in the literature. The number of nodes in each mesh reneged from 450,000 to 1,960,102, and the maximum wear rate at a specified location was calculated for each mesh. The fluid flow field was divided, and a structured hexahedral mesh was generated for each case. The mesh size and the corresponding maximum wear rate for each case are illustrated in Table 1.

**Table 1:** Maximum Erosion Rate for Various Meshes with Different Node Numbers

| Mesh | Number of Nodes | Maximum Erosion |
| --- | --- | --- |
| S0 | 5.72E+05 | 1.20E-05 |
| S1 | 1.20E+06 | 2.90E-05 |
| S2 | 1.33E+06 | 4.30E-05 |
| S3 | 1.50E+06 | 4.60E-05 |
| S4 | 1.72E+06 | 4.90E-05 |
| S5 | 1.96E+06 | 5.00E-05 |
| S6 | 5.72E+05 | 5.03E-05 |

S6 was considered as the benchmark or reference solution for the other meshes. It found that S5 had the lowest error rate of 0.6%, which means that it had a high accuracy in simulating the erosion rate. S4 had a slightly higher error rate of 2.6%, which means that it still had an acceptable accuracy. S3 had a higher error rate of 8.5%, which means that it had less precision and reliability. S2 had a higher error rate of 14.5%, and S1 had a higher error rate of 42.3%, which means that they had poor accuracy and consistency. S0 had an extremely high error rate of 76%, which means that it had very low accuracy and validity.

It was also found that S6 had a high computational cost compared to S5, which took less time to run due to its coarser resolution. Therefore, S5 was selected as the optimal mesh for our

ongoing numerical analyses, as it struck an excellent balance between accuracy and efficiency. Moreover, the previous experimental data from the literature matched well with the numerical results of S5, which further validated our choice of mesh and simulation approach.

The relationship between the maximum erosion rate and the number of nodes was visualized on a graph, as shown in Figure 11. The x-axis represented the number of nodes, while the y-axis represented the erosion rate. The graph indicated that the maximum wear rate increased with the number of nodes increased, but the increase diminished as the mesh became finer.
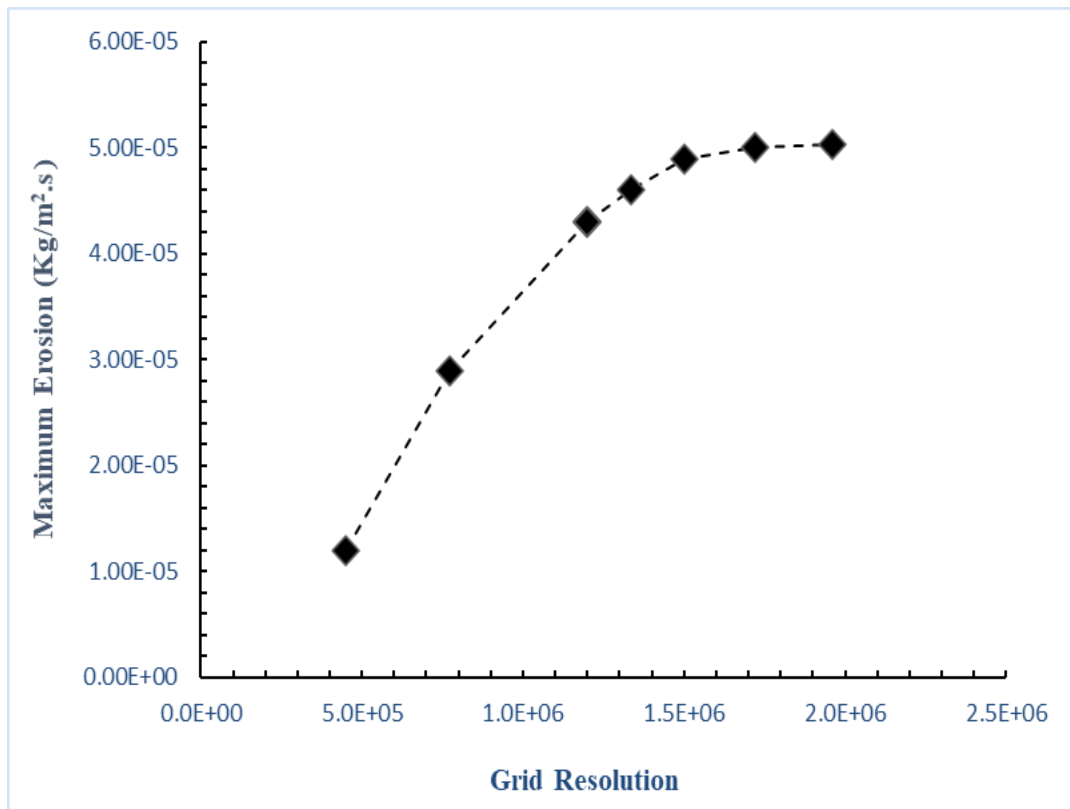


**Figure 11:** Grid independent study: maximum erosion rate vs. node count

To generate the meshes for the different elbow geometries, ANSYS Meshing was used to construct hexahedral structured elements. The mesh size and quality were controlled by adjusting the number of divisions and the smoothing parameters. The resulting meshes are shown in Figures 12 and 13, respectively. Figure 12 shows the mesh for the conventional 90° elbow and the gored elbow with five 18° segments. Figure 13 shows the mesh for the gored elbow with four 22.5° segments and the gored elbow with three 30° segments. The zoomed-in view of the meshes illustrates the uniformity and orthogonality of the elements in the region of interest.
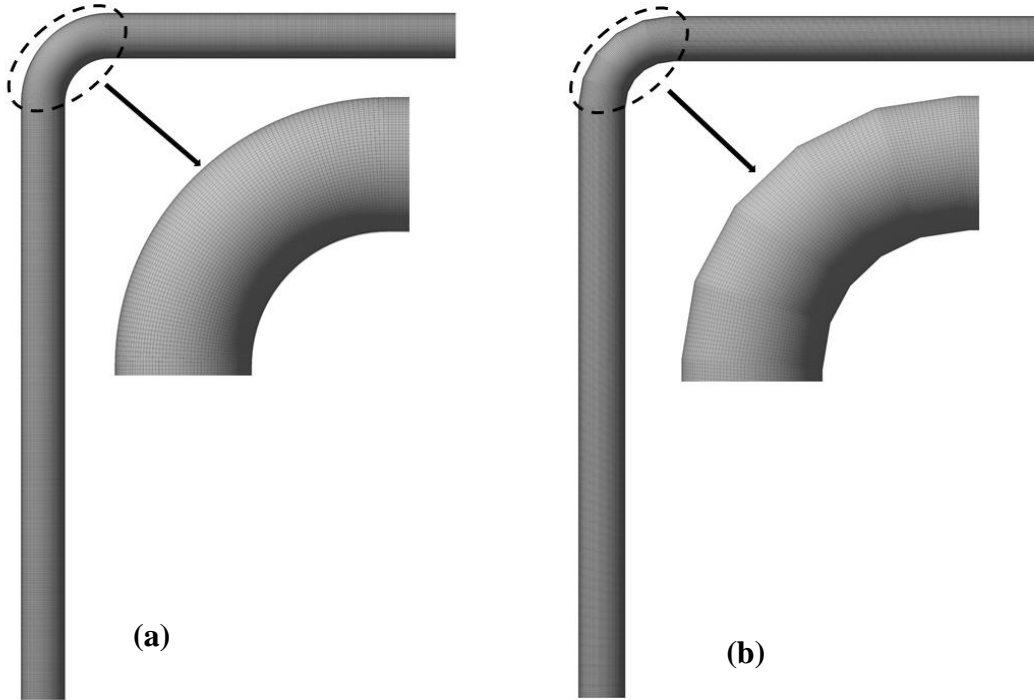
**Figure 12:** (a) Mesh generated for the standard 90° elbow (b) Mesh generated for the gored elbow with five 18° segments.
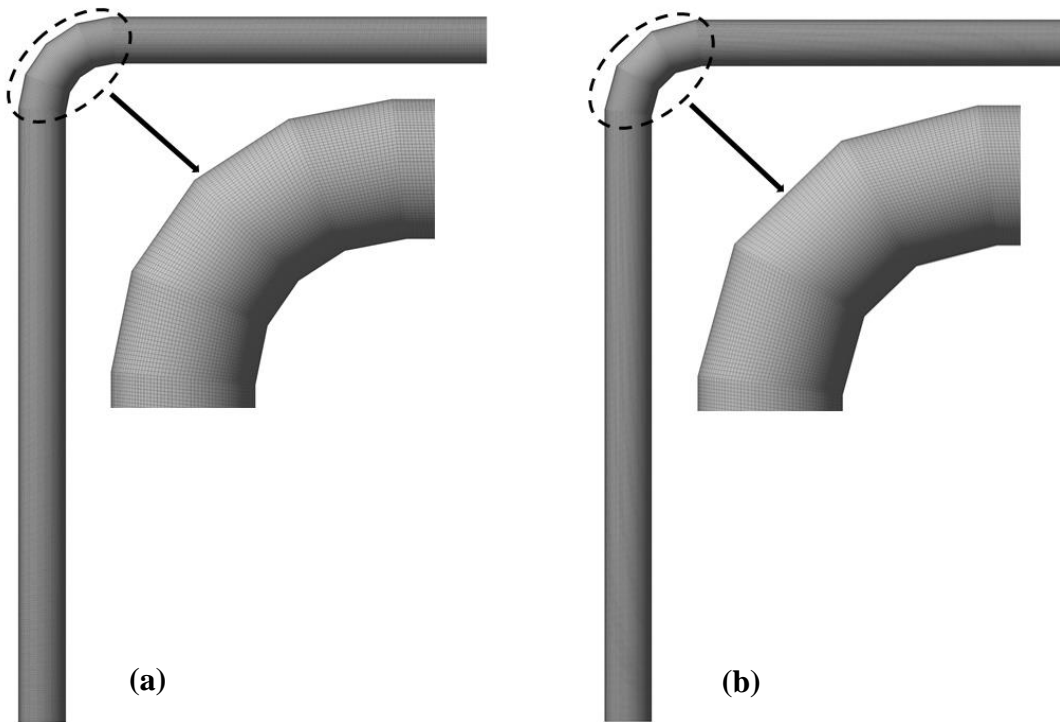


**Figure 13:** (a) Mesh generated for the gored elbow with four 22.5° segments (b) Mesh generated for the gored elbow with three 30° segments.

## 3.4 Operating Conditions

The fluid flow problem was solved using the finite volume method. The pressure-velocity coupling was handled by the SIMPLE (Semi-Implicit Method for Pressure-Linked Equations) scheme, which is an iterative algorithm that alternates between guessing the pressure field and correcting the velocity field until convergence is achieved. The second-order upwind scheme was utilized for the discretization of the pressure, momentum, and turbulent kinetic energy equations. This scheme is more accurate and stable than the first-order upwind scheme, as it uses a higher-order polynomial interpolation.

The numerical method involved two different scenarios: one with air and the other with water as the continuous phases, both interacting with a discrete phase of sand particles.

For the continuous air phase, which had an air density of 1.225 kg/m³ and an air viscosity of $1.78 \times 10\text{-}5$ kg/m-s, the boundary conditions were set as a velocity inlet and a pressure outlet. The simulation also adopted a standard wall function with no-slip conditions to model the interaction between the air and the pipe wall. The pipe wall material was stainless steel 316, with a density of 7990 kg/m³.

Similarly, water was considered as the continuous phase in another scenario, with properties different from air. In addition to the conditions stated above, the water phase was specified by its density, which was 998.2 kg/m³, and its viscosity, which was 0.001003 kg/m-s. This enabled a comparison of how the density and viscosity differences between water and air affected the behaviour of the sand particles inside the pipe, which in turn influenced the erosion rate of the pipe. This is an important factor to consider for the design and maintenance of pipelines that transport sand-water mixtures.

In both cases, spherical sand particles composed primarily of angular SiO2-1 were introduced into the pipeline through the inlet. Different sand diameters were examined to understand the effect of particle size on transport and behaviour within the respective continuous phases. The sand itself had a density of 2650 kg/m³, providing a wide range of properties for the analysis.

Various parameters of the continuous and discrete phases were employed to investigate the erosion rate in different conditions, The parameters that were varied included velocity, particle size and the sand flow rate. The velocity of the continuous phase ranged from 10 to 40 m/s, the particle size of the sand ranged from 200 to 500 microns, and the sand flow rate ranged from 0.05 to 0.4 kg/s. The erosion rate was also compared for each geometry under different conditions to detect the optimal geometry that minimized the erosion rate. These parameters were selected based on the typical and common conditions encountered in oil and gas pipelines. The velocity range covered the expected flow regimes and Reynolds numbers in the elbows, which affect the fluid dynamics and turbulence. The particle size range represented the sand particle sizes that are usually present in the produced fluids, which affect the impact force and abrasion of the elbows. The sand flow rate range varied the mass flow rate and concentration and the erosion intensity in the elbow pipes, which affected the material loss and degradation of the elbows.

The operating conditions for the simulations are summarized in Table 2. The table shows the properties of the continuous and discrete phases, as well as the material of the pipe wall. The table also includes the range of parameters that were varied to study the effect of velocity, particle size, and sand flow rate on the erosion rate.

**Table 2:** Operating conditions and parameters for air-sand and water-sand simulations

| Fluid | Air | Water |
|---|---|---|
| **Density (kg/m3)** | 1.225 | 998.2 |
| **Viscosity** | 1.78E-05 | 0.001003 |
| **Sand type** | Angular SiO2-1 | Angular SiO2-1 |
| **Sand density (kg/m3)** | 2650 | 2650 |
| **Material of wall** | Stainless steel 316 | Stainless steel 316 |
| **Steel density (kg/m3)** | 7990 | 7990 |
| **Velocity (m/s)** | 10-40 | 10-40 |
| **Particle size (microns)** | 200-500 | 200-500 |
| **Sand flow rate (kg/s)** | 0.05-0.4 | 0.05-0.4 |

The dual approach of studying both air-sand and water-sand interactions enables a thorough investigation of the erosion rate for various geometries. By incorporating water along the existing parameters, a more complete insight was gained into the different factors involved in this complex system. This allows us to optimize the best geometry among the others for both air-sand and water-sand conditions.

Five CFD cases with different influencing parameters were set up for each design to investigate the effects of air-sand and water-sand erosion on different elbow designs. The influencing parameters included air speed, sand diameter, and sand mass flow rate. Table 3 shows the CFD cases and their corresponding values for these parameters.

**Table 3:** CFD cases and influencing parameter for air-sand and water-sand analysis

| Case | Velocity (m/s) | Particle Size (µm) | Sand Flow rate (kg/s) |
|------|----------------|--------------------|------------------------|
| 1 | 10 | 200 | 0.05 |
| 2 | 12 | 225 | 0.065 |
| 3 | 15 | 250 | 0.08 |
| 4 | 18 | 275 | 0.095 |
| 5 | 20 | 300 | 0.1 |

For further analysis, two additional cases with higher values of the influencing parameters were created for each design to simulate the worst-case scenarios. The values for these two cases are shown in Table 4.

**Table 4:** Additional CFD cases with higher values of influencing parameters.

| Case | Velocity (m/s) | Particle Size (µm) | Sand Flow rate (kg/s) |
|------|----------------|--------------------|------------------------|
| 1 | 30 | 400 | 0.2 |
| 2 | 40 | 500 | 0.4 |

## 3.5 Numerical Modeling

Numerical modelling is a crucial tool for the in-depth study of the erosion phenomena, which involves the complex processes of fluid flow, particle tracking and erosion calculations. To simulate the interaction between air-sand and water-sand mixtures, the Eulerian-Lagrangian method is used. This method consists of the following components:

### 3.5.1    *Euler-Lagrange Approach*

This is the general framework that combines the Eulerian and Lagrangian descriptions of fluid and particle motion. The Eulerian description focuses on the properties of the fluid at fixed points in space, while the Lagrangian description follows the trajectories of individual particles as they move through the fluid. The Euler-Lagrange approach solves the fluid equations on a fixed grid or mesh and tracks the particles using a discrete phase model (DPM). The advantage of this approach is that it can capture the complex interaction between fluid and particles, such as drag, lift, heat transfer, and collision. The drawback is that it requires more computational resources and memory than other methods.

### 3.5.2    *Continuous Phase Model*

This is the part that deals with the modelling of the airflow or water flow as a continuous phase characterized by a fixed grid or mesh system that spans the entire computational domain. Various fluid properties, such as velocity, pressure, and density, are tracked over time on this grid, and the governing fluid motion equations, including the Navier-Stokes equations, are solved. The continuous phase model also accounts for the turbulence effects using a k-epsilon ((k- ε)) model, which is a two-equation model that describes the turbulence kinetic energy and dissipation rate. The continuous phase model provides the background fluid flow field within which particles move. In the continuous phase model, governing equations for multiphase flow (air-sand or water-sand) are expressed through the Navier-Stokes equations for fluid motion. The flow characteristics of the continuous phase are determined by the continuity and momentum equations, which are

$$\frac{\partial \rho}{\partial t} + \nabla(\rho \vec{u}) = 0 \qquad\qquad (3.1)$$

$$\frac{\partial(\rho\vec{u})}{\partial t} + \nabla(\rho\vec{u}\vec{u}) = -\nabla p + \nabla(\bar{\bar{\tau}}) + \rho g_i + S_D \tag{3.2}$$

In equations (3.1) and (3.2) $\rho$ is the density of the fluid, and $\vec{u}$ is the velocity vector of the fluid, p is the static pressure, $\bar{\bar{\tau}}$ is the stress tensor, $\mu$ is the fluid viscosity, $g_i$ is the gravitational acceleration, $S_D$ is the additional source term due to interaction with the other phase.

*3.5.3    Discrete Phase Model*

This is the part that deals with the modelling of the sand particles as a discrete phase characterized by individual particle properties and trajectories. Each particle's position, velocity, and other relevant properties are explicitly followed as it moves through the fluid domain, using Newton's second law to calculate its acceleration and trajectory based on the forces acting on it. The forces include gravity, buoyancy, drag, lift, virtual mass, pressure, gradient, thermophoretic, Brownian, Saffman lift, and Magnus forces. The discrete phase model also considers the particle-particle and particle-wall collision using different models, such as hard sphere, soft sphere, or stochastic models. The discrete phase model updates the position and properties of particles at each time step, considering their dynamic interaction with the fluid as determined by the continuous phase model. The equation of motion for a particle in a multiphase flow is expressed by the force balance:

$$m_p \frac{d\vec{u}_p}{dt} = \vec{F}_D + \vec{F}_G + \vec{F}_{VM} + \vec{F}_P \tag{3.3}$$

The equation in (3.2) includes the mass of the particles $m_p$, the drag force $\vec{F}_D$, the buoyancy force $\vec{F}_G$, the virtual mass force $\vec{F}_{VM}$, and the pressure gradient force $\vec{F}_P$.

*3.5.4    K-Epsilon (K- ε) Model*

This section deals with the aspect that addresses the turbulence effects at the interface between continuous and discontinuous phases, using a two-equation model that describes the turbulent kinetic energy and dissipation rate. Turbulence is a phenomenon that occurs when fluid flow becomes irregular and chaotic because of a high Reynolds number or large velocity gradients. Turbulence affects the transport of momentum, heat, mass, and energy in fluid flows. The k-

epsilon (k-ε) model gives a general description of turbulence by means of two transport equations: one for the turbulent kinetic energy (k), which represents the intensity of the turbulence, and one for the turbulent dissipation rate (ε), which represents the rate of energy loss due to viscosity. The equations are expressed as

$$\frac{\partial(\rho k)}{\partial t} + \nabla \cdot (\rho k \mathbf{v}) = \nabla \cdot [(\mu + \frac{\mu_t}{\sigma_k})\nabla k] - \rho k \omega + 2\mu_t S_{ij} S_{ij} - \frac{\rho}{2} u_i u_j E_{ij} \qquad (3.4)$$

$$\frac{\partial(\rho \epsilon)}{\partial t} + \nabla \cdot (\rho \epsilon \mathbf{v}) = \nabla \cdot [(\mu + \frac{\mu_t}{\sigma_\epsilon})\nabla \epsilon] - C_1 \rho \epsilon \omega + C_2 \rho \epsilon \omega^2 \qquad (3.5)$$

In equation (3.4) $k$ is the turbulent kinetic energy, $S_{ij}$ is mean strain rate tensor, and $E_{ij}$ is the mean rotation rate tensor. In equation (3.5) $\epsilon$ denote the turbulent dissipation rate and $\omega$ is the specific dissipation rate.

The k-epsilon (k-ε) model is integrated into the continuous phase model to account for the effects of turbulence on the fluid flow and fluid-particle interaction. This model was employed as the turbulence model for the erosion simulation in accordance with the literature findings and suggestions.

### 3.5.5    *Erosion Modelling*

Erosion modelling is important for the design and maintenance of pipelines, valves, chokes, pumps, and other equipment that are exposed to abrasive flows. Numerous erosion models have been proposed by researchers to investigate and comprehend the impact of erosion in a numerical context. Notable models by Oka [37],[38], Finnie [39], McLaury [40], and Generic models serve as valuable blueprints for exploring erosion phenomena. However, it is important to understand that no model can guarantee absolute precision and dependability, making it essential to choose wisely based on the specific use case and available experimental data.

The Oka erosion model was chosen for both the air-sand and water-sand analysis in this research endeavour. This selection was motivated by the widespread adoption of this model within the research community and its notable alignment with empirical data. The Oka model is a semi-empirical model that accounts for particle impact velocity, impact angle, particle size, and material properties when predicting erosion rates. It offers a reasonable and effective method for

quantitatively calculating erosion phenomena across a range of scenarios. The Oka erosion model is a widely used model for predicting erosion rates. It is a relatively simplified but accurate model in many cases. The following equation represents the Oka erosion model

$$E = E_0 \left(\frac{v_p}{v_{ref}}\right)^{k_2} \left(\frac{D_p}{D_{ref}}\right)^{k_3} f(\theta) \tag{3.6}$$

In equation (3.6) E is the erosion rate, E0 is the reference erosion rate at 90° impact angle, vp is the particle impact velocity, vref is the reference impact velocity, Dp is the particle diameter, Dref is the reference particle diameter, k2 and k3 are constant, and f $(\theta)$ is the impact angle function.

In addition to this model, the Generic erosion model was also employed for the purpose of comparing the erosion rates in the regression analysis and examining their trends with the Oka model. Although there is a significant difference in the values of the two models, their results can still be used for the design evaluation process. The Generic model is a general and flexible model that does not depend on specific parameters or assumptions for different situations and conditions. It can provide reasonable predictions for erosion in fluid flows, even in complex geometries such as elbows.

## 3.6 Validation of Experimental Results

This section presents the validation of the erosion rate in a conventional 90-degree elbow using numerical simulations. The Oka erosion model, which is suitable for this validation context, was used to perform the calculations for the numerical results. The experimental data obtained by Vieira et al. [41] were used as a benchmark to evaluate the accuracy of the numerical model. Four cases were selected from the experimental study, each considering different air speeds of 15 m/s and 23 m/s, sand sizes of 150 µm and 300 µm, and sand rates of 0.00222 kg/s, 0.00263 kg/s, 0.00274 kg/s and 0.00297 kg/s as input parameters. Table 5 shows the values of these parameters, along with the experimental erosion rates reported by Vieira et al. [41] and the numerical erosion rates obtained in this study. The percentage error between the numerical and experimental results is also listed in the Table 5.

**Table 5:** Numerical and Experimental evaluation of erosion rates in 90-degree elbow

| Case | Air Speed (m/s) | Sand Size (μm) | Sand Rate (kg/s) | Experimental Erosion Rate(mm/year) | Numerical Erosion Rate (mm/year) | % Error |
|------|-----------------|----------------|------------------|-------------------------------------|-----------------------------------|---------|
| 1 | 15 | 150 | 0.00274 | 13.2 | 14.8 | 12.1 |
| 2 | 15 | 300 | 0.00222 | 19.3 | 21.9 | 13.5 |
| 3 | 23 | 150 | 0.00297 | 36.2 | 41.5 | 14.6 |
| 4 | 23 | 300 | 0.00263 | 80.3 | 94.7 | 17.9 |

The results show that the numerical model is able to capture the trends of erosion rate with respect to the input parameters, and a good agreement was found between the numerical and experimental results. The percentage error was slightly higher for cases 3 and 4, where the air velocity and sand rate were higher. A possible reason for this is the increased complexity of the erosion model in these conditions, which makes it harder to account for all the variables that affect erosion. Moreover, the experimental data may have lower accuracy in these conditions because of the challenges of measuring erosion rates at high velocities. However, it is noteworthy that the numerical results obtained by this study are significantly lower and closer to the experimental results of Vieira et al.'s own numerical results, indicating an improvement in the accuracy of the erosion rate predictions. The percentage error, which remained below 20%, is still considered acceptable for this type of study. This confirms the validity and accuracy of the numerical model for predicting the erosion rate in a conventional 90-degree elbow. Figure 14 demonstrates the graphical representation of the experimental and numerical erosion rates for each case, indicating a strong agreement between the two sets of results.
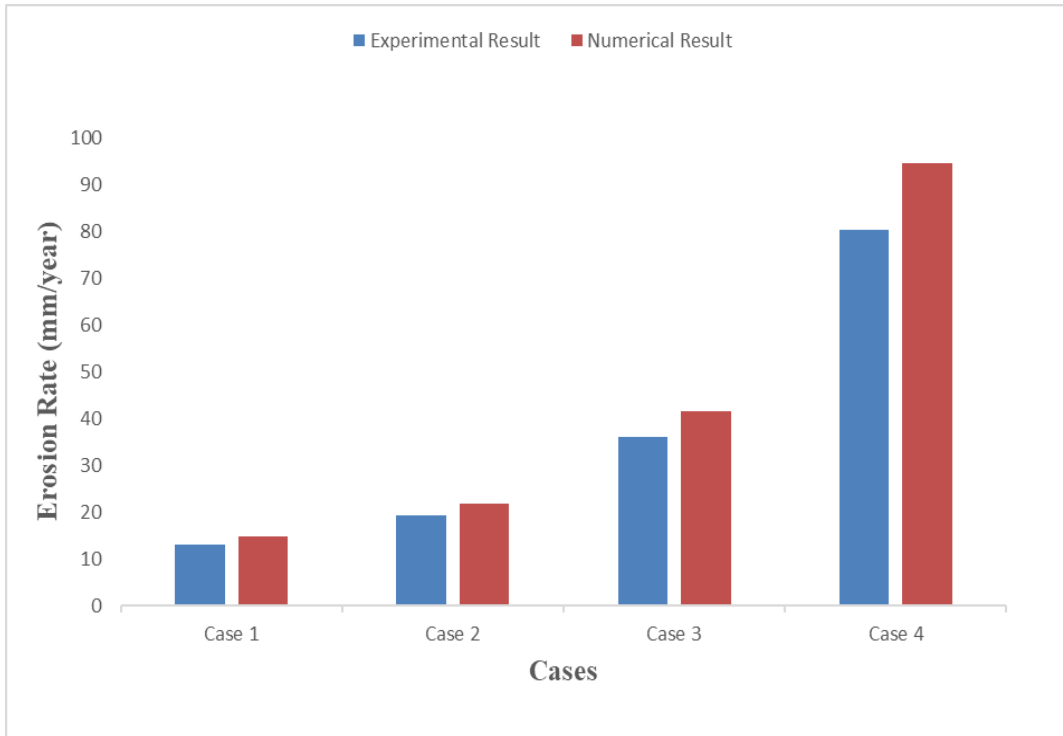
**Figure 14:** Comparison of the experimental and numerical erosion rates in various conditions

The data in the table reveals the relationship between specific parameters and erosion rates. It shows that erosion rates increase with increasing air velocity. This indicates the significant effect of air velocity on erosion phenomena under the studied conditions. Likewise, sand size also influences erosion rates, with larger sand particles causing more erosion than smaller ones. This trend is illustrated in Table 3, which shows the erosion rates for two different sand sizes, specifically 150 and 300 micrometres, at an air velocity of 23 m/s. These results demonstrate the sensitivity of erosion rates to changes in air velocity and sand size, providing a useful reference for further analysis and design considerations in related applications.

The characteristic Elliptical and V-shaped erosion marks observed on the outer surface of the 90° elbow (Figure 4(a)) closely match those reported by Vieira et al. [41] (Figure 4(b)), strongly validating the accuracy of the present analysis. The thickness loss in mm/year or mm/day is calculated by dividing the erosion rate in Kg/m2-s by the density, as follows:

$$\text{Thickness Loss} = \text{Erosion Rate/density} \tag{3.7}$$

36
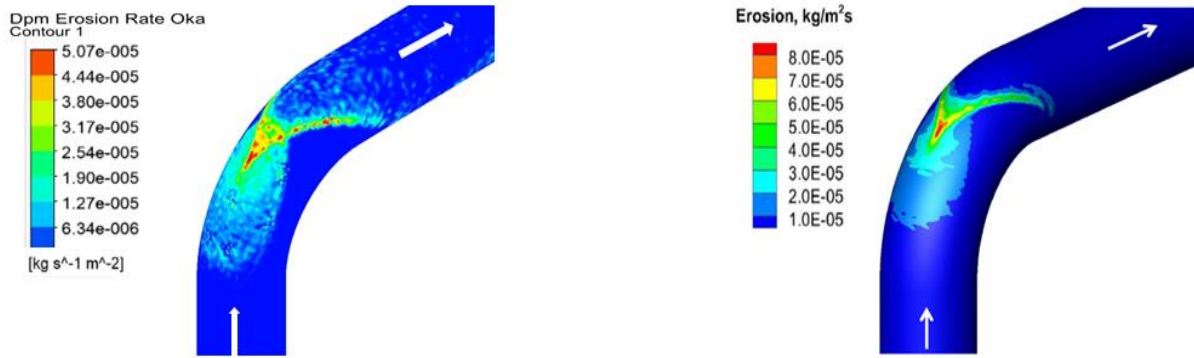
**Figure 15:** Erosion rates for (a) 300 µm and (b)150 µm sand sizes at 23 m/s air velocity

## 3.7 Summary

This chapter presents the overall research methodology and numerical techniques used for predicting erosion rates in elbow pipes. It starts with a discussion of the elbow pipe geometry and mesh generation techniques. It then provides a detailed overview of the operating conditions for simulations involving air and water as continuous phases interacting with discrete sand particles. The simulations change the velocity, particle size, and sand flow rate of the sand particles. It also explains the numerical modelling approach that combines the Eulerian-Lagrangian method, continuous and discrete phase models, and the K-Epsilon turbulence model. The chapter describes erosion modelling using the Oka and a Generic model. The chapter ends with a validation of the numerical model against experimental data for standard 90-degree elbows, showing good agreement and offering insight into the influence of parameters like air velocity and sand size on erosion rates.

# CHAPTER 4: RESULTS AND DISCUSSION

## 4.1 Introduction

This chapter discusses and analyses the numerical results obtained from this study through CFD simulations. The starting section (4.2) performs a comprehensive analysis of erosion rates in air-sand flow. By examining the behaviour of various elbow designs under varying operating conditions, this section aims to understand their erosion resistance and performance. The succeeding section (4.3) highlights the thorough analysis of the erosion rate in water-sand flows. Through a systematic examination of diverse elbow configurations subjected to a range of influencing factors, the study of erosion performance is carried out.

The next section (4.4) focuses on the complex pressure distribution analysis of elbow designs in air-sand as well as water-sand flows. The objective is to evaluate factors that influence the pressure within the various elbow designs and to identify the high and low-pressure zones. Section (4.5) examines the velocity distribution in different elbow configurations within both air-sand and water-sand flows. This analysis provides valuable insight into the fluid dynamics and its interactions with different designs.

The following section (4.6) investigates particle tracking and analyzes the trajectory and impact patterns of the sand particles in both air-sand and water-sand flows. The points of high and low-impact zones in various elbow designs are highlighted. Understanding particle behaviour is essential for evaluating elbow performance and stability.

The ending sections (4.7) explore the regression analysis and the generation of regression equations for both the air-sand and water-sand flows from the CFD simulation data. This section also highlights the standardized effect of the influencing parameters on the elbow design. This analytical approach reveals the relationship between the variables and understands how various factors influence the erosion rates of elbow designs. The main effect plots in this section examine the performance of the elbow configurations and show the resistance against erosion.

## 4.2 Erosion Rates Analysis in Air-Sand Flows.

The numerical analysis of the erosion rate in air-sand flow in normal conditions and worst-case scenarios is presented in the following section.

### *4.2.1 Erosion Rates Analysis of Air-Sand Flows in Normal Conditions.*

Table 6 shows the results of the air-sand erosion simulations by ANSYS software on four elbow designs: a standard 90-degree elbow (Design 1), an 18-degree gored elbow (Design 2), a 22.5-degree gored elbow (Design 3), and a 30-degree gored elbow (Design 4). The simulations varied velocity, particle size, and sand flow rate to assess erosion phenomena. The Oka model estimated the maximum erosion rates to compare erosion susceptibility across the designs. This paragraph shows the design details using descriptive and consistent names for each design.

**Table 6:** Maximum erosion rates for different elbow designs and factors in air-sand flow

| | Velocity | Sand Size | Flow Rate | Maximum Erosion Rate Oka (Kg/m2-s) | | | |
|---|---|---|---|---|---|---|---|
| Case | (m/s) | (µm) | (Kg/s) | Design 1 | Design 2 | Design 3 | Design 4 |
| 1 | 10 | 200 | 0.05 | 6.865E-05 | 9.070E-05 | 6.510E-05 | 7.269E-05 |
| 2 | 12 | 225 | 0.065 | 1.875E-04 | 1.787E-04 | 1.322E-04 | 1.632E-04 |
| 3 | 15 | 250 | 0.08 | 4.362E-04 | 4.358E-04 | 2.948E-04 | 4.244E-04 |
| 4 | 18 | 275 | 0.095 | 8.134E-04 | 7.533E-04 | 5.885E-04 | 7.805E-04 |
| 5 | 20 | 300 | 0.1 | 1.149E-03 | 1.151E-03 | 8.053E-04 | 1.029E-03 |

The table shows that for the first case, the 18-degree gored elbow (Design 2) has the highest erosion rate, while the 22.5-degree gored elbow (Design 3) has the lowest erosion rate. This suggests that Design 2 is the most susceptible to erosion and Design 3 is the most resistant. Design 1 and 4 have comparable erosion rate values, with Design 4 slightly higher than Design 1. The results for case 2, as shown in Table 6 indicate that the 22.5-degree gored elbow (Design 3) has the lowest erosion rate in all designs. On the other hand, the standard 90-degree elbow (Design 1) has the highest erosion rate in all configurations. The erosion rate values of the 18-degree gored

39

elbow (Design 2) and the 30-degree gored elbow (Design 4) are almost the same, but Design 2 is somewhat higher than Design 4. The results for cases 3 to 5, as presented in Table 6, confirm the outstanding erosion resistance of the 22.5-degree gored elbow (Design 3) in different conditions. This supports the idea that Design 3 is suitable for a wide range of operation conditions. The other designs have varying erosion rates, depending on bend angle and flow properties. Figure 16 illustrates the erosion rates for each case and design in a graphical way.
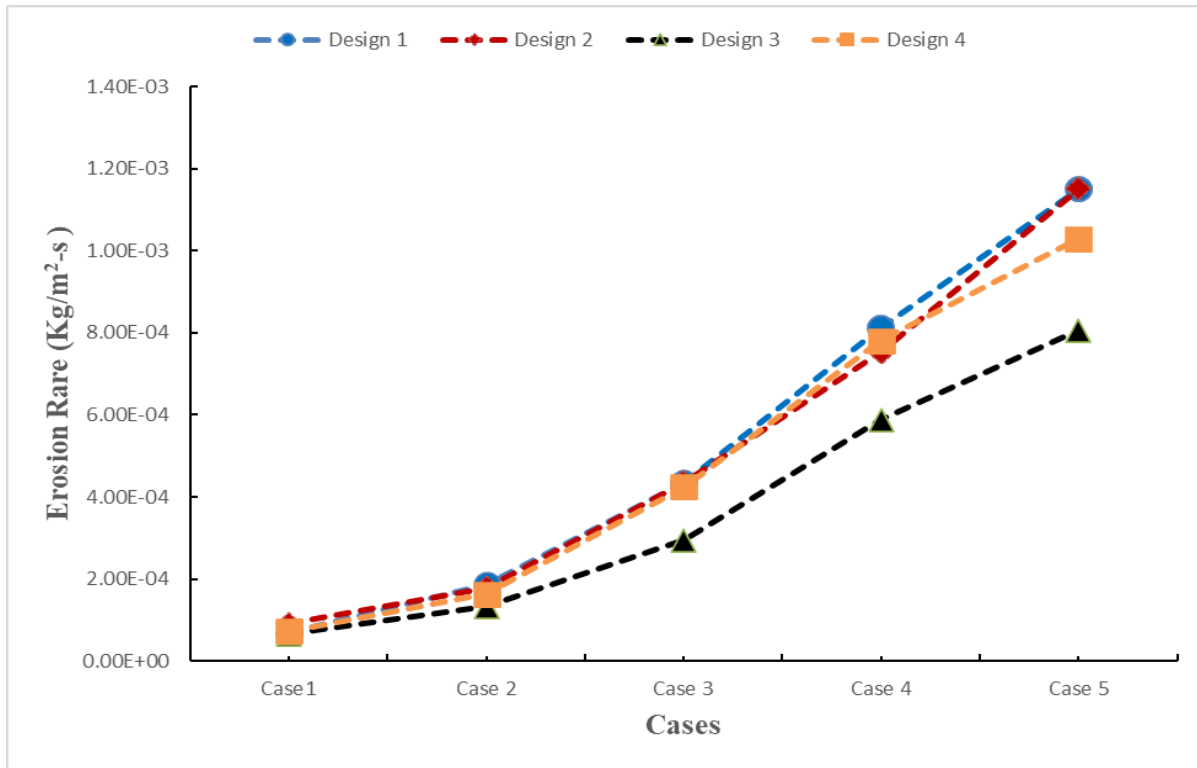


**Figure 16:** Erosion rate trends for different elbow designs and air-sand operating conditions

    The graph clearly displays the different erosion rate patterns for distinct elbow designs. Compared to the conventional 90-degree elbow (Design 1), represented by the blue curve, the 22.5-degree gored elbow (Design 3), indicated by the black curve, exhibits a higher erosion resistance. The other two designs, the 18-degree gored elbow (Design 2) and the 30-degree gored elbow (Design 4), have varying erosion rates compared to the conventional 90-degree elbow (Design 1). Depending on the conditions, they demonstrate slightly higher or lower erosion rates. As the value of the influencing parameters increases, the 22.5-degree gored elbow maintains its erosion resistance better than other configurations. This indicates that the 22.5-degree gored elbow is a more effective design choice with outstanding erosion-resistant properties in air-sand flows.

The erosion rates of the conventional 90-degree elbow (Design 1) and the 18-degree gored elbow (Design 2) for the first case in air-sand flows are illustrated in Figure 17. In contrast, the erosion rates of the 22.5-degree gored elbow (Design 3) and the 30-degree gored elbow (Design 4) for the same case are shown in Figure 18.
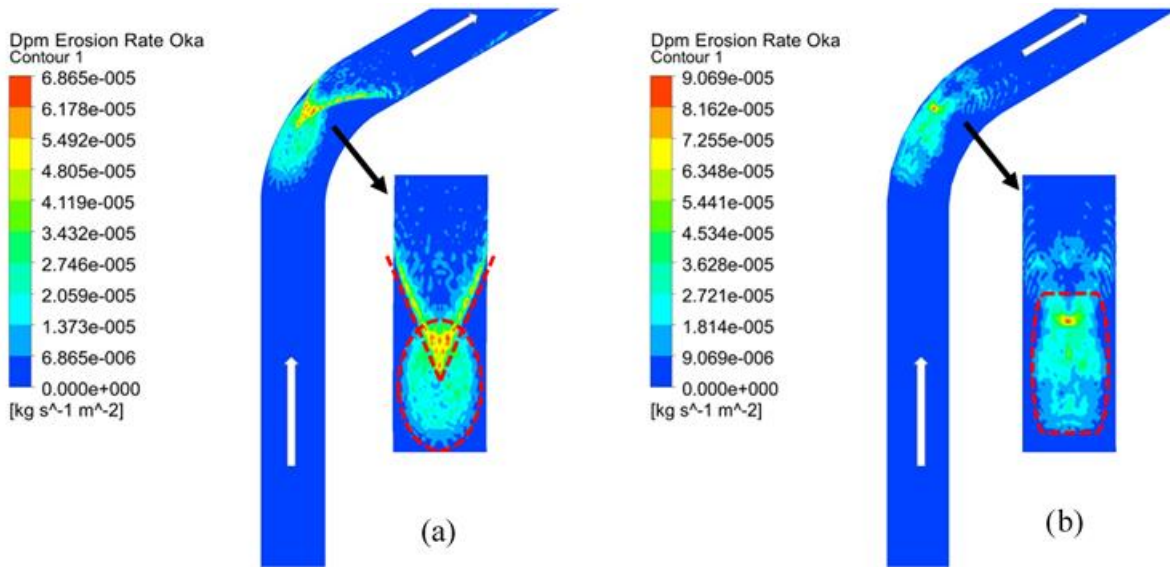


**Figure 17:** Erosion rate of (a) standard 90-degree elbow (b) 18-degree gored elbow in air-sand flow for the first case (velocity=10 m/s, sand size=200μm, flow rate=0.05 kg/s)
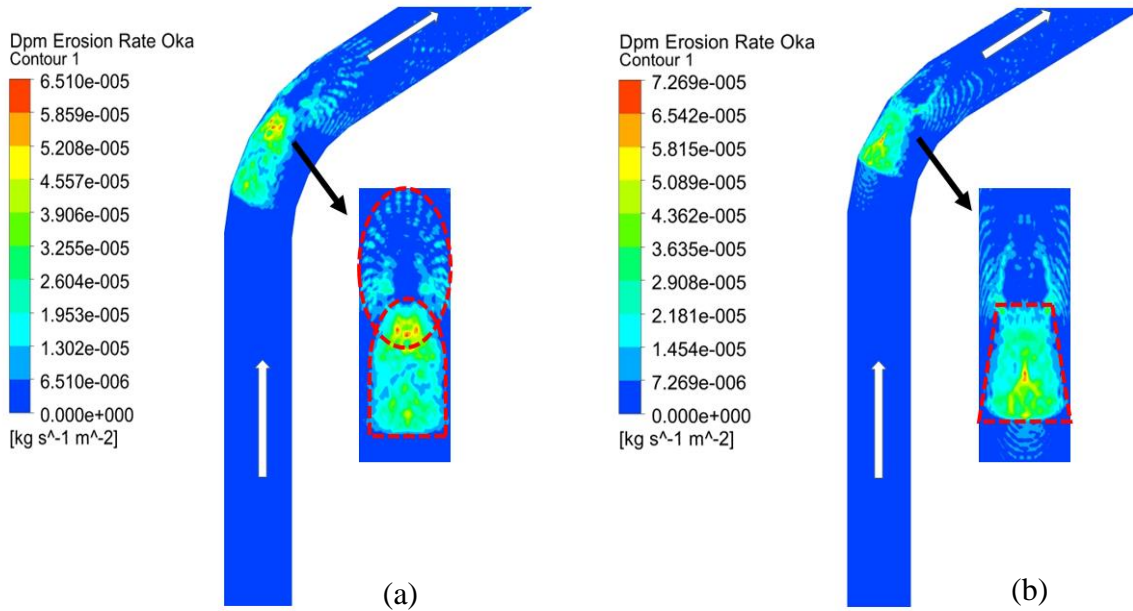


**Figure 18:** Erosion rate of (a) 22.5-degree gored elbow, (b) 30-degree gored elbow in air-sand flow for the first case (velocity=10 m/s, sand size=200μm, flow rate=0.05 kg/s)

The erosion pattern observed in the standard 90-degree elbow, as shown in Figure 17 (a), reveals elliptical and V-shaped erosion scars. This pattern is typically evident in situations involving air-sand flows, as supported by the literature. A comparison of the erosion pattern of the 18-degree gored elbow and the standard 90-degree elbow shows significant differences. The erosion scar in the 18-degree gored elbow is not elliptical; instead, it has a rectangular shape, with the larger sides slightly curved. Furthermore, in the case of the 18-degree gored elbow, as demonstrated in Figure 17 (b), a unique pattern of scattered and dispersed erosion points, which lack a clear shape, replaces the V-shaped scars of the standard 90-degree elbow. In contrast, the 22.5-degree gored elbow shows a cylindrical erosion scar with one straight side and one gently curved side, similar to a semi-circular closed arch. Moreover, the upper surface of the elbow pipe exhibits an elliptical erosion scar, characterized by a hollow interior and formed by the dispersion of erosion points. These two distinct erosion patterns are illustrated in Figure 18(a). Finally, the 30-degree gored elbow demonstrates a trapezium-shaped erosion scar with a slightly rounded lower side and dispersed erosion points on the upper sections that do not form a specific shape, as shown in Figure 18 (b). The varying impact points of sand particles result in different erosion scar characteristics in each design. Moreover, the erosion scars indicate that areas more severe erosion occurs in areas with higher concentrations of sand particles.

*4.2.2      Numerical Analysis of Erosion Rates in Air-Sand Flows in Worst-Case Scenario*

To determine the performance of each design under the worst-case scenario, the erosion rate was further examined by significantly increasing the influencing parameters. Table 7 lists the operating conditions and the maximum erosion rate for the two cases.

**Table 7:** Maximum erosion rates in worst-case scenarios for different elbow designs and factors in air-sand flow

| Case | Velocity (m/s) | Sand Size (μm) | Flow Rate (Kg/s) | Maximum Erosion Rate Oka (Kg/m2-s) | | | |
|------|----------|-----------|-----------|-----------|-----------|-----------|-----------|
| | | | | Design 1 | Design 2 | Design 3 | Design 4 |
| 1 | 30 | 400 | 0.2 | 6.383E-03 | 7.041E-03 | 4.659E-03 | 5.971E-03 |
| 2 | 40 | 500 | 0.4 | 2.485E-02 | 2.906E-02 | 1.935E-02 | 2.615E-02 |

As Table 7 illustrates, the maximum erosion rate among varies elbow designs. For case 1, Design 2, the 18-degree gored elbow, shows the highest maximum erosion, revealing its weakness to erosion compared to Design 1, the standard 90-degree elbow. In contrast, Design 3, the 22.5-degree gored elbow, has the least maximum erosion in all cases, showing its strength against erosion. Design 1 and Design 4, the 30-degree gored elbow have comparable erosion rates, with Design 1 slightly exceeding Design 4. For case 2, as Table 7 demonstrates, Design 3 keeps its low erosion rate among all designs. However, Design 2 has the most erosion in all cases. The erosion rates of Design 1 and Design 4 are nearly the same, with Design 4 slightly surpassing Design 1. Design 3, the 22.5-degree gored elbow, exhibits the lowest erosion rate in both cases, demonstrating its erosion mitigation in the worst-case scenarios. Design 2, the 18-degree gored elbow, displays the highest erosion rate in both cases, indicating its susceptibility to erosion. The graphical comparison of the erosion rate across various cases and designs, illustrating the performance of each design, is presented in Figure 19.
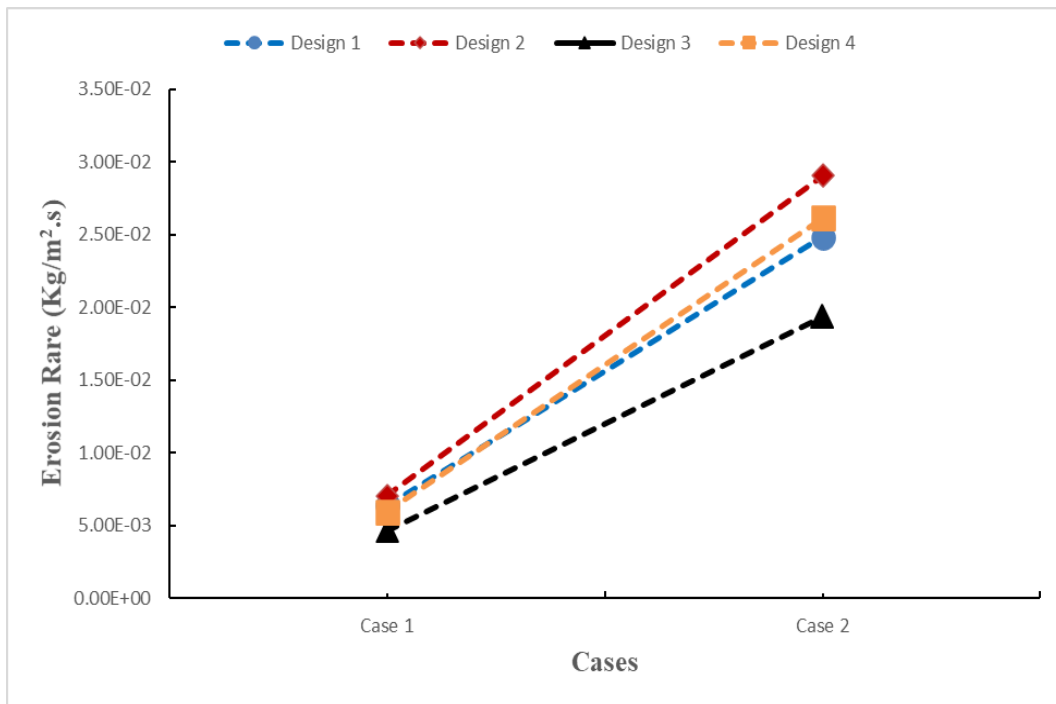


**Figure 19:** Effect of elbow design on erosion rate in worst case-scenario air-sand flow

Figure 20 shows the erosion rates for the standard 90-degree elbow and 18-degree gored elbow in the worst-case scenario for case 2. Similarly, Figure 21 represents the erosion rate for the 22.5-degree gored elbow and 30-degree gored elbow in the same case.
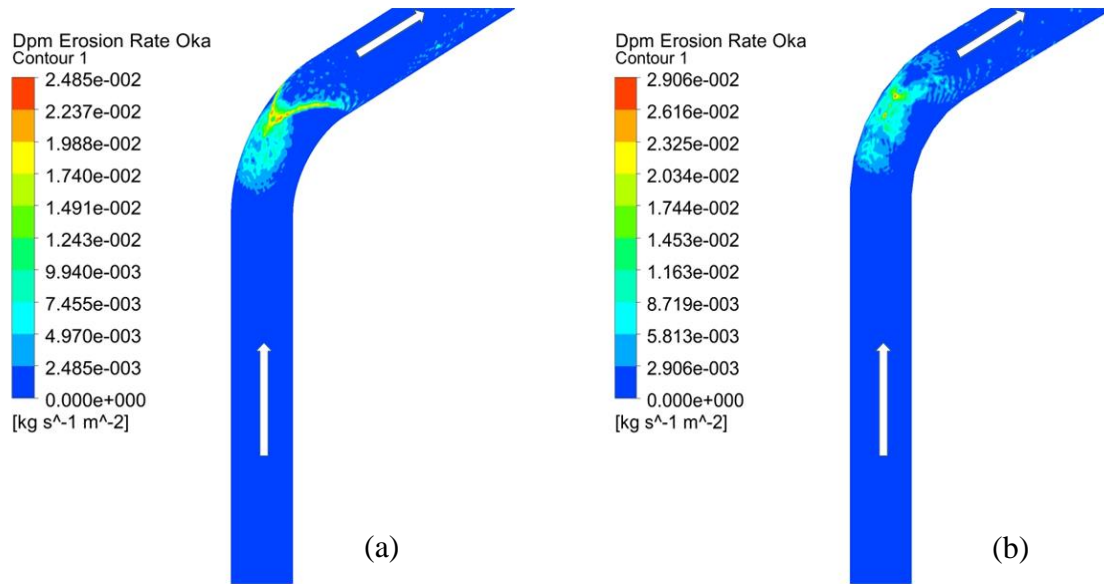
**Figure 20:** Erosion rate of (a) standard 90-degree elbow, (b) 18-degree gored elbow in the worst-case scenario, in air-sand flow (velocity=40 m/s, sand size=500μm, flow rate=0.4 kg/s)
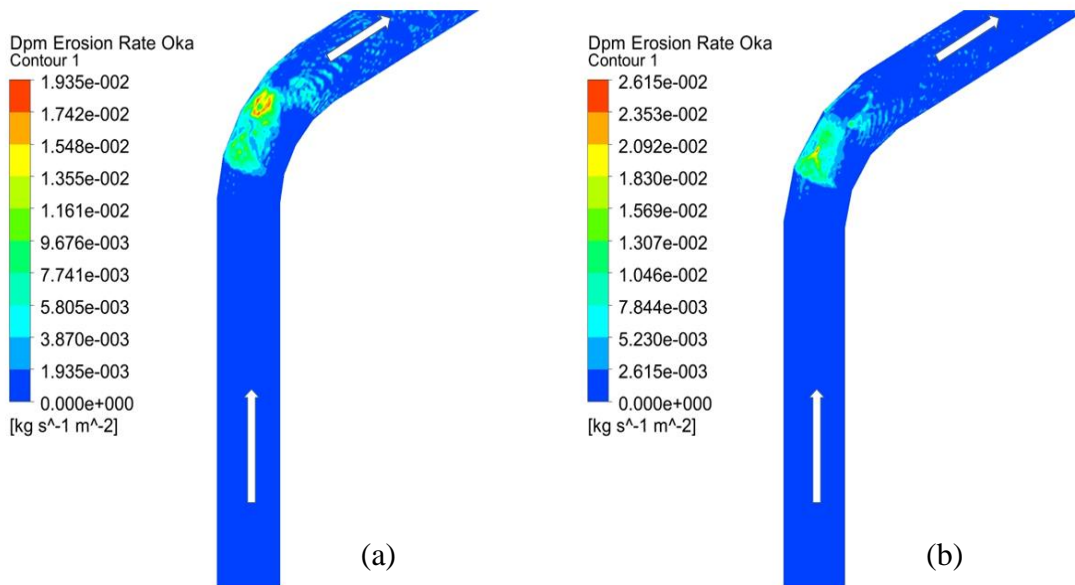


**Figure 21:** Erosion rate of (a) 22.5-degree gored elbow, (b) 30-degree gored elbow in the worst-case scenario, in air-sand flow (velocity=40 m/s, sand size=500μm, flow rate=0.4 kg/s)

Gored elbows, with their gentle curvature, offer a promising solution for mitigating erosion in air-sand flows compared to their sharp-angled 90-degree elbow. This improvement originates from several key factors. Firstly, the gored elbow design acts as a gradual transition, easing the flow direction change and reducing the harsh flow separation observed in 90-degree elbows. This transfer to smoother, more laminar flow with fewer eddies and vortices. Consequently, abrasive

particle interactions with the elbow wall are minimized, leading to less wear. Additionally, the expanded flow area within the gored elbow reduces localized high-velocity zones near the inner surface, which is the main cause of severe erosion from sand particles. Secondly, the curved surface of gored elbows alters the impact angle of sand particles. Compared to the head-on collision with a 90-degree elbow, particles meet a lower angle of the gored elbow segments. This has two beneficial effects: the normal component of particle velocity decreases, meaning the impact force acting perpendicular to the surface is less intense. Additionally, the glancing angle increases the likelihood of particle rebound, preventing them from lingering on the surface and causing increasing erosive damage. Our data further suggest that the 22.5-degree gored elbow emerges as the superior in terms of erosion reduction. This angle appears to achieve the optimal balance between flow streamlining and reduced particle impact, outperforming both the 18-degree and 30-degree elbow designs.

The comparison of the gored elbows (Design 2,3 and 4) erosion rate with the standard 90-degree elbow (Design 1) in various air-sand flow conditions is shown in Table 8.

**Table 8:** Gored elbows erosion rate against the standard 90-degree elbow in various air-sand flows

| Case | Design 2 | Design 3 | Design 4 |
|------|----------|----------|----------|
| 1 | 1.32 times increase | 0.95 times decrease | 1.06 times increase |
| 2 | 0.95 times decrease | 0.71 times decrease | 0.87 times decrease |
| 3 | 0.99 times decrease | 0.68 times decrease | 0.97 times decrease |
| 4 | 0.93 times decrease | 0.72 times decrease | 0.96 times decrease |
| 5 | 1.01 times increase | 0.70 times decrease | 0.89 times decrease |

The air-sand results show that the erosion rate in the gored elbows varies significantly depending on the case and the angle. The 18-degree gored elbow (Design 2) has the most erratic behaviour, with erosion ranging from 0.95 to 1.32 times the standard 90-degree elbow. The 22.5-degree gored elbow (Design 30) exhibits the most consistent performance, with erosion decreasing in all cases, reaching up to 0.68 times the baseline. The 30-degree gored elbow (Design 4) has a moderate performance, with erosion mostly decreasing (0.87 to 0.97 times), except for one case

where it slightly increases (1.06 times). The data demonstrate that the gored elbows have the potential to substantially reduce erosion (as in Design 3) but also the risk of unpredictable performance (as in Design 2) and, in some cases, even erosion enhancement (as in Design 4). Therefore, further investigations are required to optimize the angle performance of the gored elbows under different flow conditions and case scenarios.

The performance of the gored elbows in comparison to the standard 90-degree elbow (Design 1) in worst-case scenarios, where the influential parameters have the highest values, is presented in Table 9.

**Table 9:** Gored elbows erosion rate against the standard 90-degree elbow in worst-case scenarios in air-sand flows

| Case | Design 2 | Design 3 | Design 4 |
|------|----------|----------|----------|
| 1 | 1.10 times increase | 0.73 times decrease | 0.94 times decrease |
| 2 | 1.17 times increase | 0.78 times decrease | 1.05 times increase |

The table shows that the 18-degree gored elbow (Design 2) has the highest increase in erosion depth in both cases, suggesting that it is the most vulnerable to the worst-case scenarios. The 22.5-degree gored elbow (Design 3) has the highest decrease in erosion in both cases, indicating that it is the most resistant to the worst-case scenarios. The 30-degree gored elbow (Design 4) has mixed performance, with an increase in one case and a decrease in another, indicating that it is moderately affected by the worst-case conditions. The table suggests that the angle of the gored elbows plays a significant role in determining the erosion under the worst-case scenarios.

### 4.3 Erosion Rates Analysis in Water-Sand Flows.

The numerical analysis of the erosion rate in water-sand flow in normal conditions and worst-case scenarios is presented in the following section.

The results for the water-sand erosion simulation for the four distinct elbow designs, each subjected to various influencing parameters, are represented in Table 10. The values of velocity, sand size, and flow rate and their effect on the maximum erosion rate of each design are displayed in Table 10.

**Table 10:** Maximum erosion rates for different elbow designs and factors in water-sand flow

| | Velocity | Sand Size | Flow Rate | Maximum Erosion Rate Oka (Kg/s.m2) | | | |
|:---:|:---:|:---:|:---:|:---:|:---:|:---:|:---:|
| Case | (m/s) | (μm) | (Kg/s) | Design 1 | Design 2 | Design 3 | Design 4 |
| 1 | 10 | 200 | 0.05 | 8.273E-06 | 1.772E-05 | 1.858E-05 | 1.634E-05 |
| 2 | 12 | 225 | 0.065 | 1.884E-05 | 4.926E-05 | 4.514E-05 | 4.374E-05 |
| 3 | 15 | 250 | 0.08 | 3.378E-05 | 9.081E-05 | 1.181E-04 | 1.312E-04 |
| 4 | 18 | 275 | 0.095 | 7.069E-05 | 1.874E-04 | 2.224E-04 | 2.494E-04 |
| 5 | 20 | 300 | 0.1 | 8.972E-05 | 2.125E-04 | 3.458E-04 | 3.923E-04 |

The table shows that in the first case, the conventional 90-degree elbow (Design 1) has the lowest erosion rate, while the 22.5-degree gored elbow (Design 3) has the highest erosion rate. This means that Design 3 is more prone to erosion, while Design 1 is more resistant to erosion effect in the water-sand flows. The table also shows that the 18-degree gored elbow (Design 2) and the 30-degree gored elbow (Design 4) have higher erosion rates than the standard 90-degree elbow. The erosion rates of Design 2 and Design 4 are similar, but Design 2 is lightly higher than Design 4 in terms of erosion susceptibility.

As shown in Table 10, the conventional 90-degree elbow (Design 1) has the lowest erosion rate among all the designs for case 2. In contrast, the 18-degree gored elbow (Design 2) has the highest erosion rate, followed by the 22.5-degree gored elbow (Design 3) and the 30-degree gored elbow (Design 4). These results indicate that the conventional 90-degree elbow is more resistant to erosion than the gored elbows with different angles in the water-sand flows.

For cases 3 to 5, all three cases show a similar trend in the erosion rates of different elbow designs. The conventional 90-degree elbow (Design 1) has the lowest erosion rate, while the 30-degree gored elbow (Design 4) has the highest erosion rate. The 18-degree gored elbow (Design 2) and the 22.5-degree gored elbow (Design 3) have intermediate erosion rates, with Design 2 being lower than Design 3. Figure 22 shows the graphical representation of how the erosion rate varies in different designs under different operating conditions.
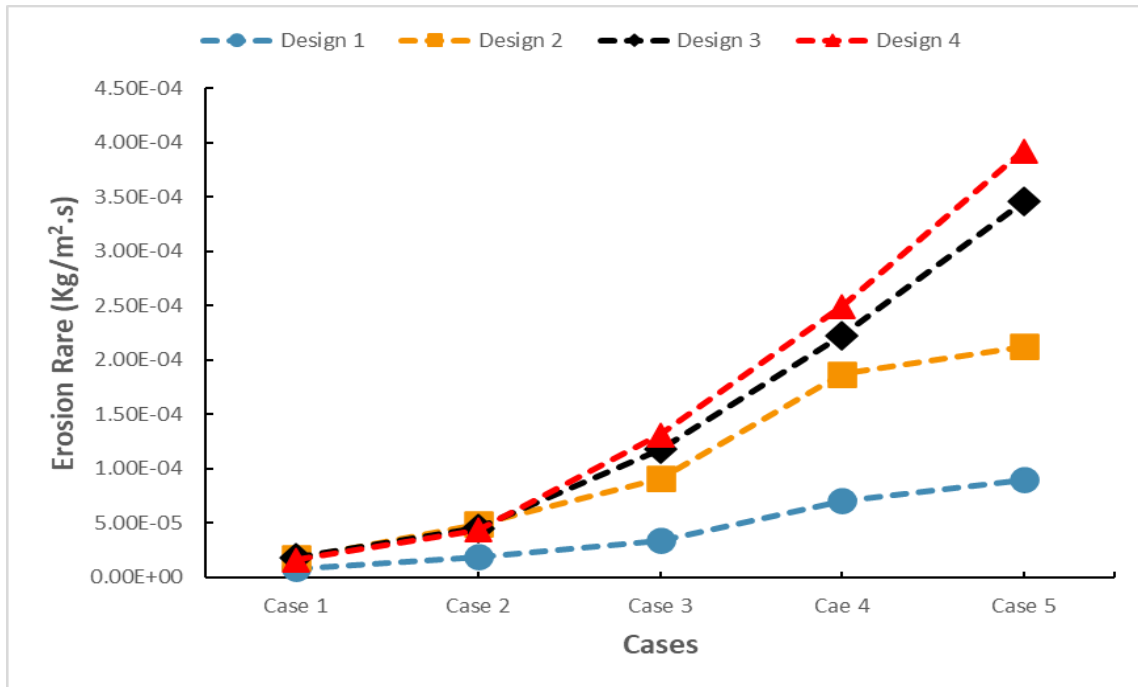


**Figure 22:** Erosion rate trends for different elbow designs and water-sand operating conditions

The graph shows how the erosion rate varies for different elbow designs in water-sand flows. The conventional 90-degree elbow (Design 1), shown by the blue curve, has the lowest erosion rate in all cases. The other three designs, the 18-degree gored elbow (Design 2), shown by the orange curve; the 22.5-degree gored elbow (Design 3), shown by the black curve; and the 30-degree gored elbow (Design 4), shown by the red curve, have higher erosion rates than the standard 90-degree elbow. The gored elbows have similar erosion rates, with minor fluctuations, in the first two cases. However, from cases 3 to 5, the 30-degree gored elbow (Design 4) has the highest erosion rate, followed by the 22.5-degree gored elbow (Design 3) and the 18-degree gored elbow (Design 2). This indicates that gored elbows are less effective in reducing erosion in water-sand flow. Compared to other designs, the standard 90-degree elbow shows better performance in resisting erosion, even under high-influencing conditions. Hence, the conventional 90-degree

48

elbow is a suitable design for water-sand flows that require high erosion resistance. Figures 23 and 24 show the erosion rates of the four elbow designs in water-sand flows for the first case. The figures also include a top view of the elbow geometry for each design.



(a)                                                      (b)
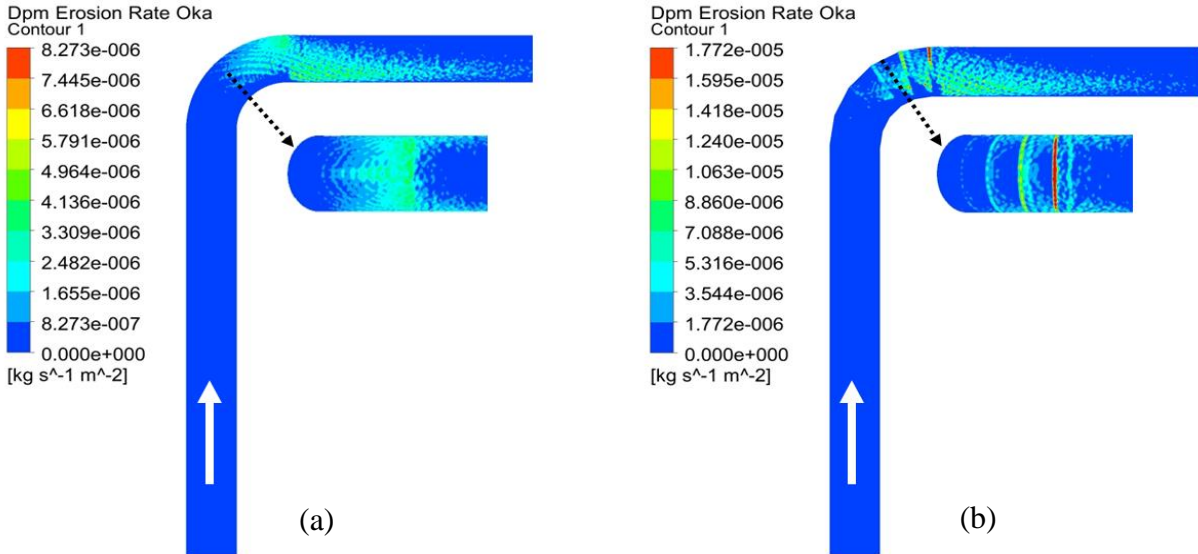
**Figure 23:** Erosion rate of (a) standard 90-degree elbow, (b) 18-degree gored elbow in water-sand flow for the first case (velocity=10 m/s, sand size=200μm, flow rate=0.05 kg/s)



(a)                                                      (b)
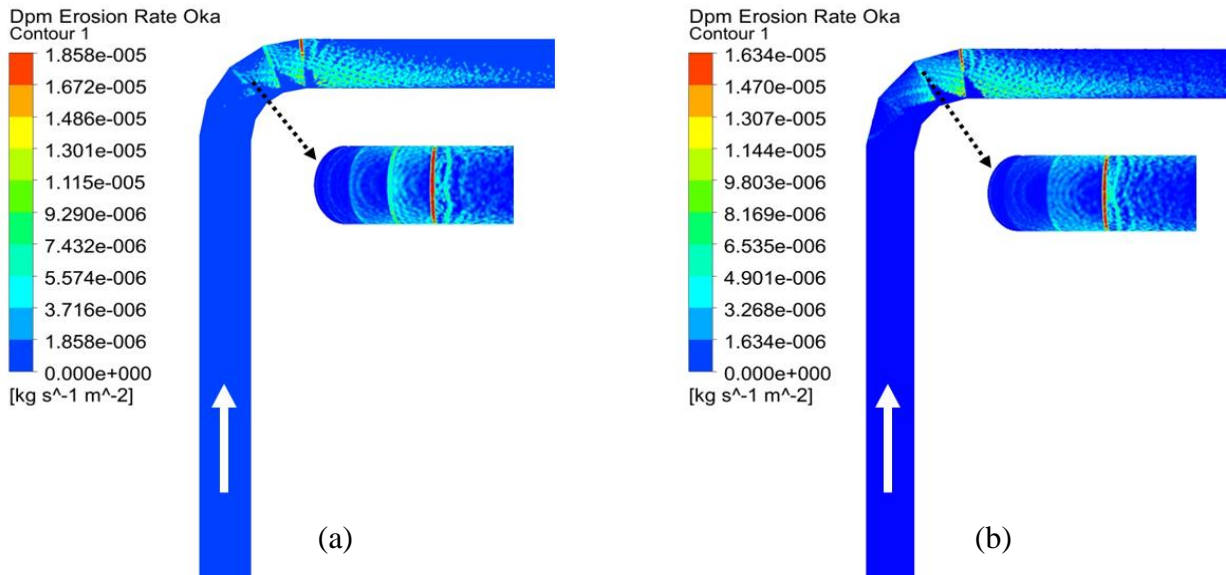
**Figure 24:** Erosion rate of (a) 22.5-degree gored elbow, (b) 30-degree gored elbow in water-sand flow for the first case (velocity=10 m/s, sand size=200μm, flow rate=0.05 kg/s)

The contour plot in Figure 23 (a) indicates that the erosion rate is highest at the downstream end of the standard 90-degree elbow. The sides of the pipe experience significant erosion, and the elbow experiences the most severe erosion at the point of flow impact, as illustrated by the top

view. The erosion pattern in all three gored elbows is identical to the standard 90-degree elbow. However, the gored elbows experience significantly higher erosion at the flow impact. This region is evident in all the gored elbows by the red lines, indicating a severe erosion rate at this point. The edges of the gored elbows, where the segments meet, are the most critical erosion points. In water-sand flow, the sand particles directly impact the edges of the gored elbows, causing significant wear and tear at these locations. The top view of gored elbows, as shown in Figures 23 (a) and 24 (a) and (b), reveals dispersed erosion points, in contrast to the conventional 90-degree elbow. This difference may be due to the varying impact angles caused by the segments in gored elbows. However, it is clear that gored elbows experience significantly higher erosion rates than the standard 90-degree elbow in water-sand flows.

*4.3.2      Numerical Analysis of Erosion Rates in Water-Sand Flows in Worst-Case Scenario*

The influencing parameters for the water-sand flow were significantly increased to simulate the worst-case scenario, similar to the air-sand flow. Table 11 shows the maximum erosion rate and the influencing parameters for the two additional cases.

**Table 11:**Maximum erosion rates in worst-case scenarios for different elbow designs and factors in water-sand flow

| | **Velocity** | **Sand Size** | **Flow Rate** | **Maximum Erosion Rate Oka (Kg/s.m2)** | | | |
|---|---|---|---|---|---|---|---|
| **Case** | **(m/s)** | **(µm)** | **(Kg/s)** | **Design 1** | **Design 2** | **Design 3** | **Design 4** |
| 1 | 30 | 400 | 0.2 | 6.649E-04 | 1.669E-03 | 1.903E-03 | 1.791E-03 |
| 2 | 40 | 500 | 0.4 | 2.584E-03 | 6.746E-03 | 8.551E-03 | 8.932E-03 |

As shown in Table 11, the standard 90-degree elbow (Design 1) exhibits the best erosion resistance in water-sand flows among all the designs, having minimum erosion in both cases. For the first case, the 22.5-degree gored elbow (Design 3) suffers the most from erosion, followed by the 30-degree gored elbow (Design 4) and the 18-degree gored elbow (Design 2). For the second case, however, the erosion rate is worst for the 30-degree gored elbow (Design 4), followed by the 22.5-degree gored elbow (Design 3) and the 18-degree gored elbow (Design 2). This shows that gored elbows are not valuable for mitigating erosion rate in water-sand flow. Based on this

discussion, it can be concluded that gored elbows are ineffective in reducing the erosion rate in water-sand flows. A graphical representation of the worst-case scenario performance of each design is given in Figure 25.
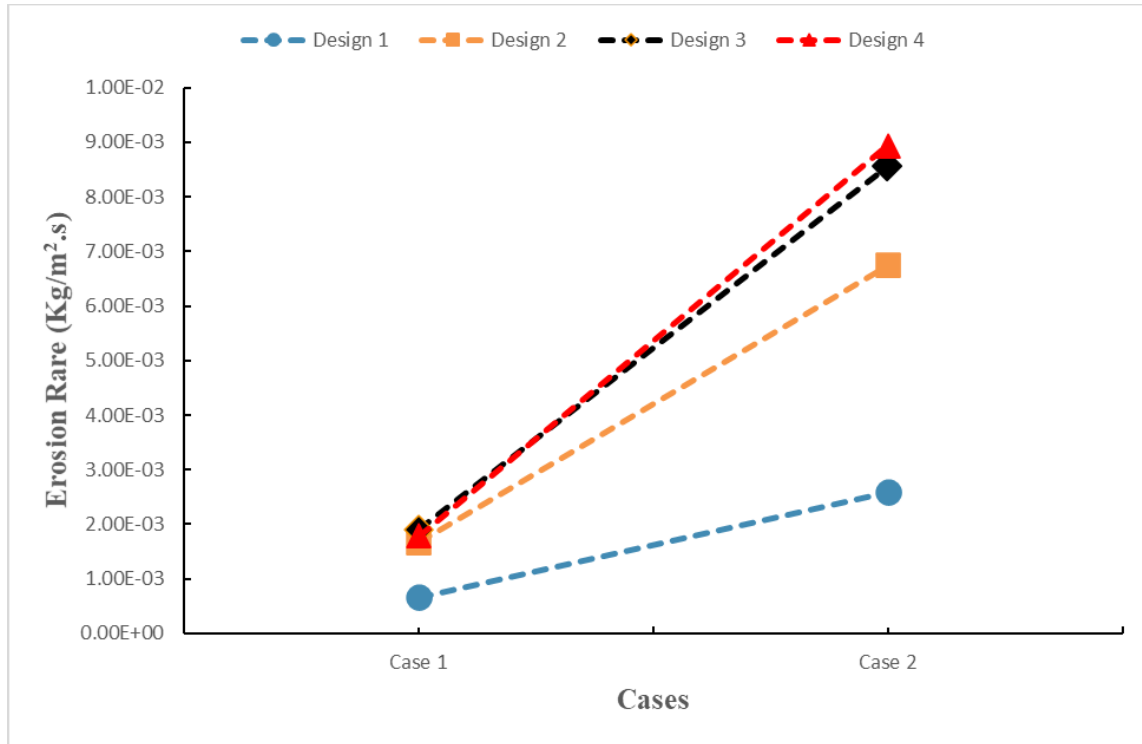


**Figure 25:** Effect of elbow design on erosion rate in the worst case-scenario water-sand flow

Figure 25 shows that the 90-degree elbow has significantly lower erosion rates than the gored elbows, even in the worst-case scenario of water-sand flow. This is probably due to its streamlined shape, which reduces the impact of solid particles. In contrast, the edges in the gored elbows make erosion worse, particularly in worst-case scenarios. Therefore, the 90-degree elbow is a better option in water-sand flow applications.

The erosion rate rises sharply as the influencing parameters increase, as Figures 26 and 27 demonstrate. This is evident in the erosion spots, especially on the outer surface of the 90-degree elbow, and the gored elbow corners are more prone to erosion, as indicated by the red marks. This finding reveals how these components react to different parameters and show the areas where erosion is more intense. The worst-case scenario for case 2 is illustrated in Figures 26 and 27, which compare the erosion rates of the standard 90-degree elbow and the gored elbows with 18, 22.5 and 30 degrees.
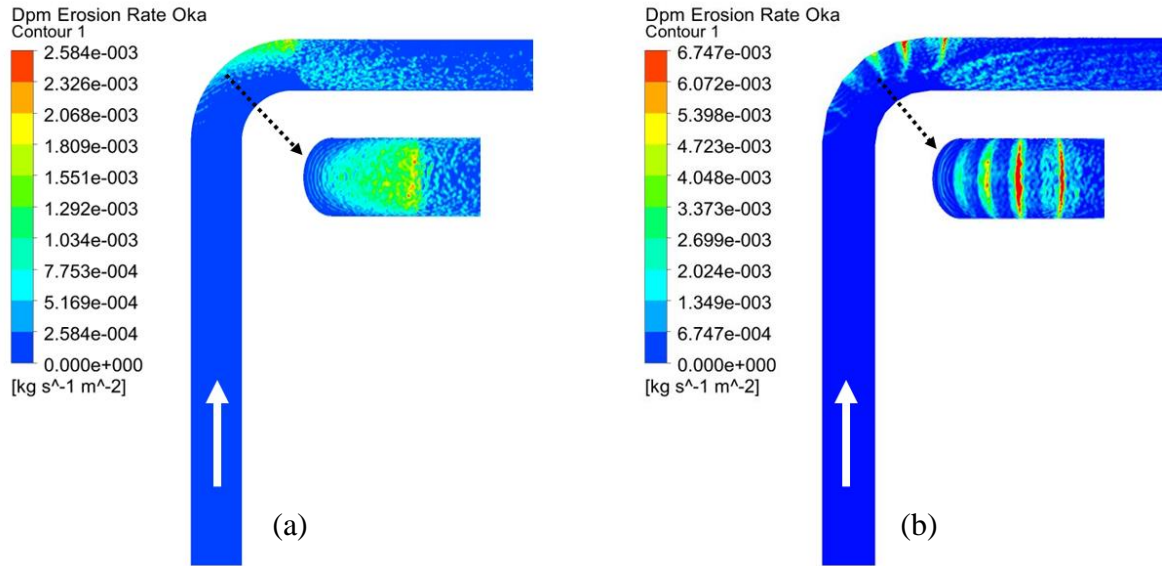
**Figure 26:** Erosion rate of (a) standard 90-degree elbow, (b) 18-degree gored elbow in the worst-case scenario, in water-sand flow (velocity=40 m/s, sand size=500μm, flow rate=0.4 kg/s)
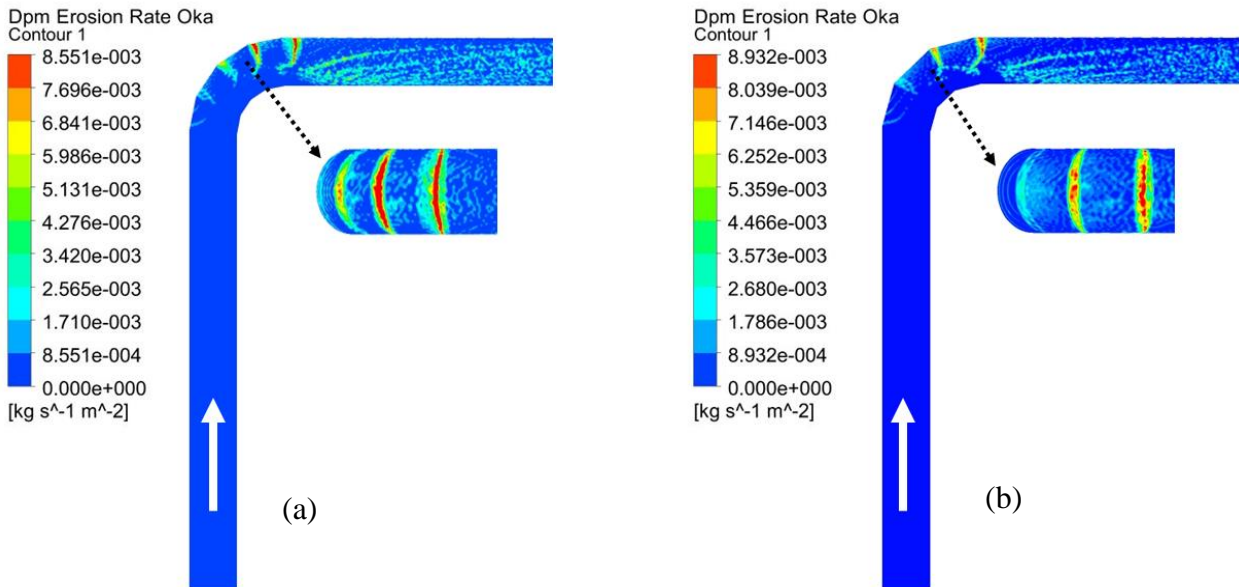


**Figure 27:** Erosion rate of (a) 22.5-degree gored elbow, (b) 30-degree gored elbow in the worst-case scenario, in water-sand flow (velocity=40 m/s, sand size=500μm, flow rate=0.4 kg/s)

Water-sand flows turn gored elbows from erosion protectors to erosion causers. Their curved shapes, which work well in air-sand flows, cause a lot of damage in water-sand flows. The gored elbow shape makes the flow more chaotic, and sand particles spin around and scratch the elbow surface. Vortices and recirculation zones keep these sand particles in place, making some areas more eroded than others.

The gored elbow shape reduces the overall flow rate but increases the flow velocity in some regions. Near the inner wall and the transitions, the flow is constricted, giving more energy to the sand particles. These regions have high erosion rates, where sand particles create deep groves and marks on the elbow surface. At the edges, where the segments meet, the flow makes a sharp turn, creating a vortex and a velocity spike. This region also has high erosion rates, where sand particles abrade the elbow surface. Our results show that the 30-degree design, with its large curve, has the highest erosion rate, followed by the 22.5-degree and 18-degree designs. The 90-degree elbow, with its simple geometry, has the lowest erosion rate.

Table 12 shows how the erosion rate in the gored elbows (Designs 2,3 and 4) differs from the standard 90-degree elbow (Design 1) under various water-sand flow conditions.

**Table 12:** Gored elbows erosion rate against the standard 90-degree elbow in various water-sand flows

| Case | Design 2 | Design 3 | Design 4 |
|------|----------|----------|----------|
| 1 | 2.14 times increase | 2.25 times increase | 1.97 times increase |
| 2 | 2.62 times increase | 2.40 times increase | 2.32 times increase |
| 3 | 2.69 times increase | 3.49 times increase | 3.88 times increase |
| 4 | 2.64 times increase | 3.14 times increase | 3.52 times increase |
| 5 | 2.37 times increase | 3.86 times increase | 4.37 times increase |

The table shows that the gored elbows have much higher erosion than the standard 90-degree elbow in all cases and that the erosion generally increases with the angle of the gored elbows. The table also suggests that the water-sand flows have different effects on erosion depending on each case. All the 18-degree elbow (Design 2), the 22.5-degree gored elbow (Design 3), and the 30-degree gored elbow (Design 4) have the lowest increase in erosion rate in case 1 with 2.14, 2.25 and 1.97 times, respectively, as the factor of erosion increase. Conversely, the 18-degree gored elbow (Design 2) in case 3 has the highest increase of 2.69 times, while the 22.5-degree gored elbow (Design 3) and the 30-degree gored elbow (Design 4) have an increase in erosion in case 5 with 3.49 and 4.37 times respectively.

The performance of the gored elbows in comparison to the standard 90-degree elbow (Design 1) in worst-case scenarios, is shown in Table 13.

**Table 13:** Gored elbows erosion rate against the standard 90-degree elbow in worst-case scenarios in water-sand flows

| Case | Design 2 | Design 3 | Design 4 |
|------|----------|----------|----------|
| 1 | 2.51 times increase | 2.86 times increase | 2.69 times increase |
| 2 | 2.61 times increase | 3.31 times increase | 3.46 times increase |

The 30-degree gored elbow (Design 4) has the highest increase in erosion in both cases, implying that it has the most erosion compared to the standard 90-degree elbow (Design 1). The 18-degree gored elbow (Design 2) has the lowest erosion in both cases, indicating the least erosion, while the 30-degree gored elbow (Design 3) has a moderate increase in erosion in both cases, representing a medium erosion increase compared to the standard 90-degree elbow. The increase in erosion demonstrates that the gored elbows are less effective than the standard 90-degree elbow for water-sand flows.

## 4.4 Pressure Distribution

This section explores how pressure varies in different elbow designs for air-sand and water-sand flows and how these designs influence the flow of fluids.

### 4.4.1 Pressure Distribution Analysis of Elbow Designs in Air-Sand Flow

The numerical results show that the pressure is highest at the extrados (outer surface of the elbow), and lowest at the intrados (inner surface of the elbow) of the elbow in the air-sand flow. The pressure decreases gradually from the extrados to the intrados. The extrados of the elbow has the highest pressure and the most particle impact, leading to the most erosion at that point. The opposite is true for the intrados of the elbow, where the pressure and the particle impact are lowest, and the erosion is minimal. The pressure distribution in the standard 90-degree elbow and the 18-degree gored elbow is illustrated in Figure 28.
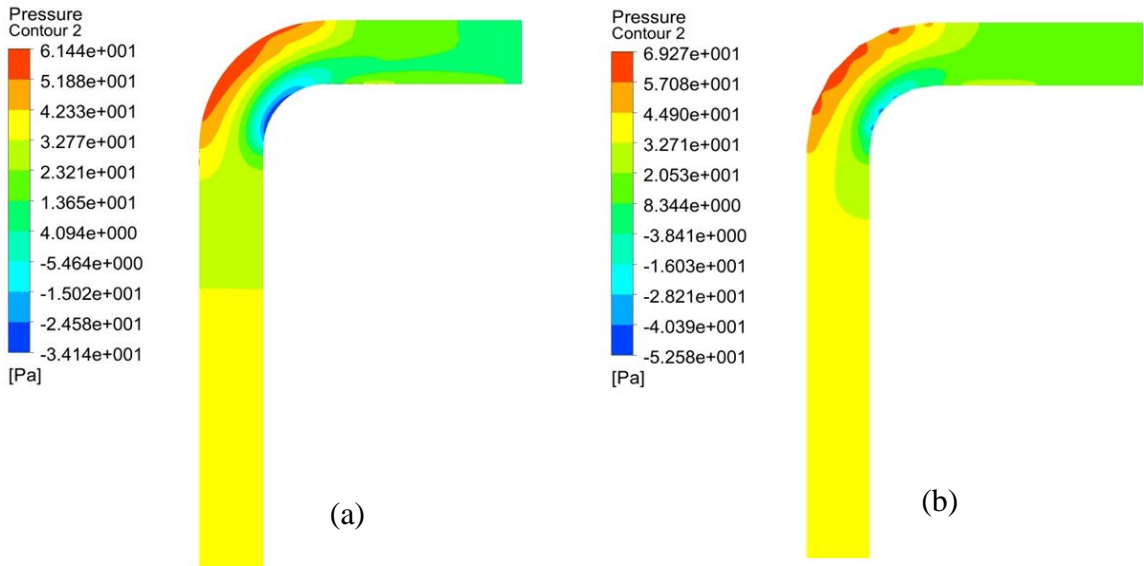
**Figure 28:** Pressure distribution in (a) standard 90-degree elbow, (b) 18-degree gored elbow for air-sand flow

The pressure distributions in the conventional 90-degree elbow and the 18-degree gored elbow are largely similar, with some minor variations. The most notable differences are in the extrados and intrados areas, where the contour patterns differ. Moreover, the 18-degree gored elbow has a slightly higher maximum pressure than the 90-degree elbow. The pressure distribution in the 22.5-degree gored elbow and the 30-degree gored elbow is displayed in Figure 29.
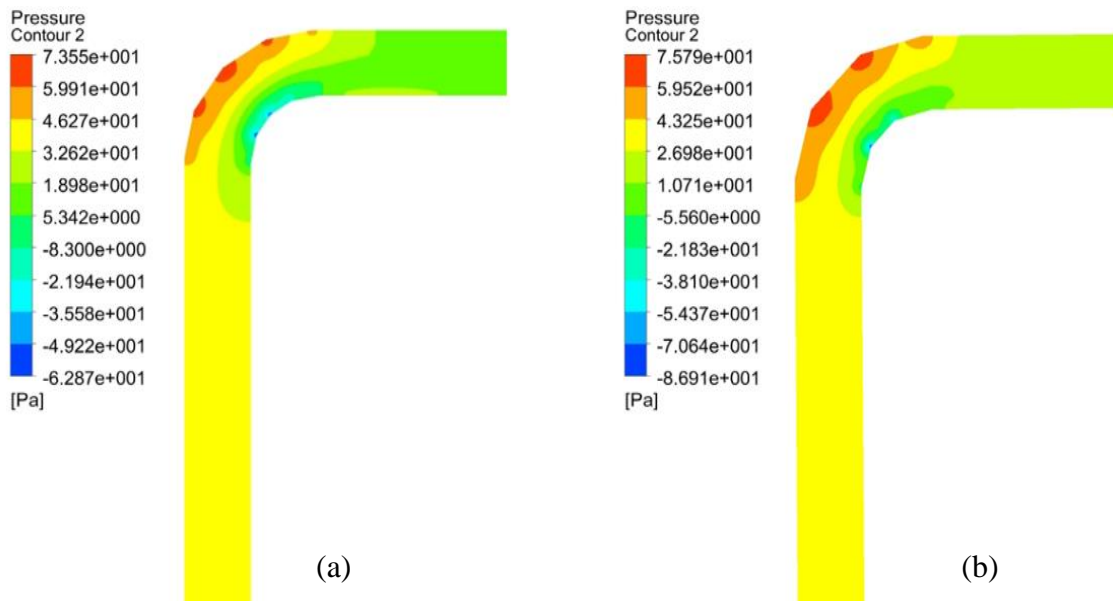


**Figure 29:** Pressure distribution in (a) 22.5-degree gored elbow, (b) 30-degree gored elbow for air-sand flow.

The pressure distribution varies notably between the 90-degree elbow and the 22.5 and 30-degree gored elbows. The gored elbows have red dots at the edges of the extrados, which contrast with the continuous lines of the 90-degree elbow, showing different patterns. The intrados of both the gored elbows also have so minor variations. The 22.5-degree gored elbow has a higher maximum pressure than the standard 90-degree elbow, and the 30-degree elbow has the highest pressure among all the elbows.

*4.4.2        Pressure Distribution Analysis of Elbow Designs in Water-Sand Flow*

The pressure variations in the conventional 90-degree elbow and the gored elbows with 18, 22.5 and 30-degree angles in water-sand flows are shown in Figures 30 and 31.



(a)                                                    (b)
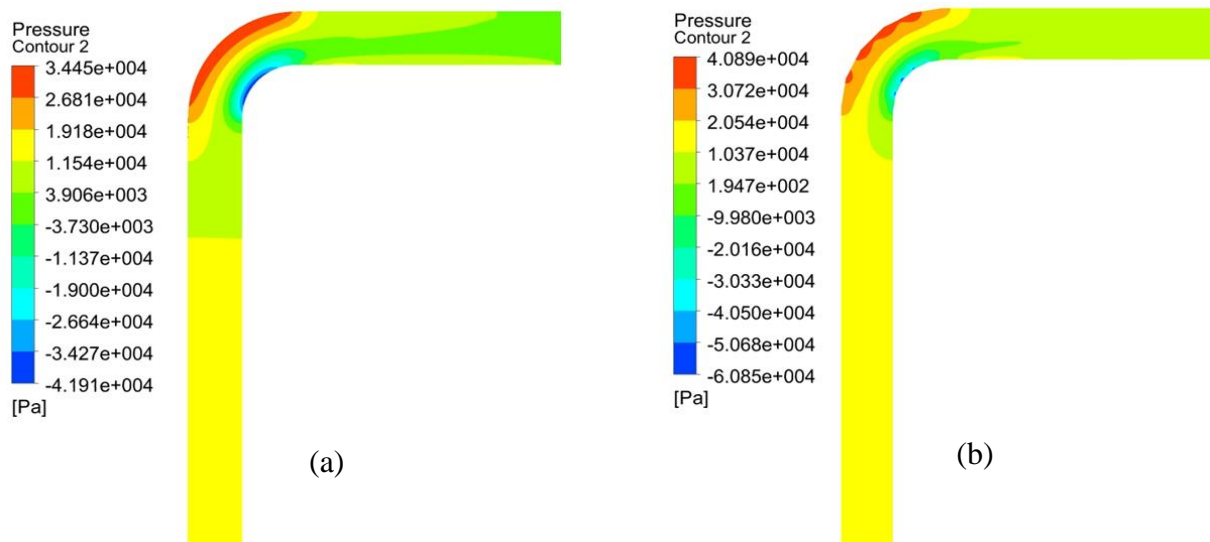
**Figure 30:** Pressure distribution in (a) standard 90-degree elbow, (b) 18-degree gored elbow for water-sand flow

The pressure distribution in water-sand flow is similar to that in air-sand flow. The extrados has the highest pressure, and the intrados has the lowest pressure. The main difference is that the pressure values are much higher in water-sand flow; this could be due to the greater density of water. The pressure patterns in the 90-degree elbow and the gored elbows are consistent with those in the air-sand flow. The corners of the gored elbows have red spots in water-sand flow, which show the highest pressure and imply a similar pressure pattern to air-sand flow.
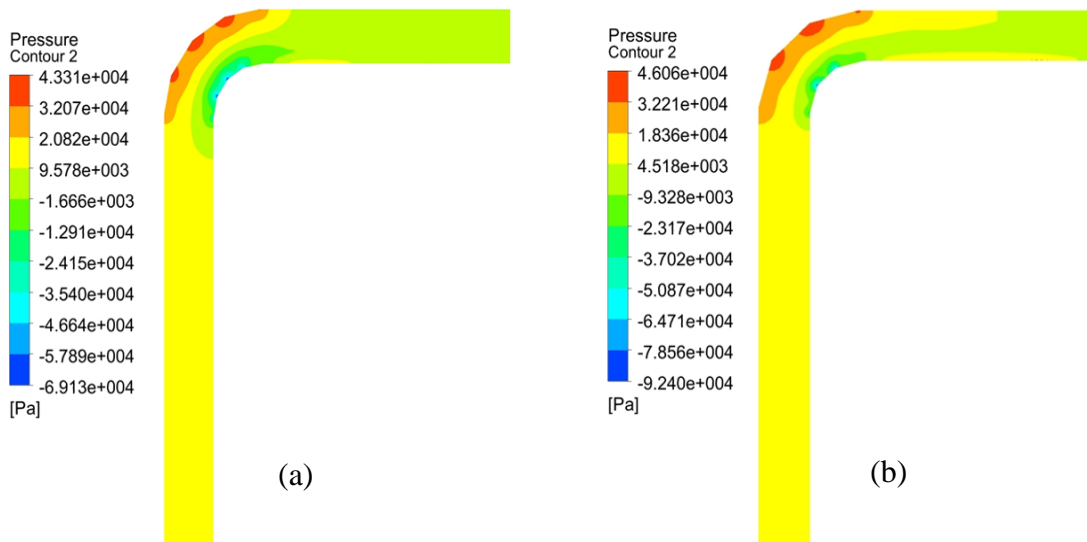
**Figure 31:** Pressure distribution in (a) 22.5-degree gored elbow, (b) 30-degree gored elbow for water-sand flow.

## 4.5 Velocity Distribution

This section examines how different elbow designs affect the velocity distribution and fluid flow dynamics in both air-sand and water-sand flows.

### 4.5.1     *Velocity Distribution Analysis of Elbow Designs in Air-Sand Flow*

CFD simulations revealed that the highest flow velocities occur at the intrados of the elbow, while the lowest flow velocities occur at the extrados. A gradual decline in velocity is observed from the intrados toward the extrados of the elbow. Furthermore, it is worth noting that the region immediately adjacent to the extrados, known as the boundary region, experiences a somewhat slower flow. This is followed by a subsequent increase in velocity and finally attains maximum speed at the intrados. Figure 32 shows the velocity distribution in both the standard 90-degree elbow and the 18-degree gored elbow, revealing a remarkable similarity between the two configurations. This could be attributed to the fact that the 18-degree gored elbow consists of five segments that form a smooth curve with slightly flattened sides, resembling the shape of the conventional 90-degree elbow.

57
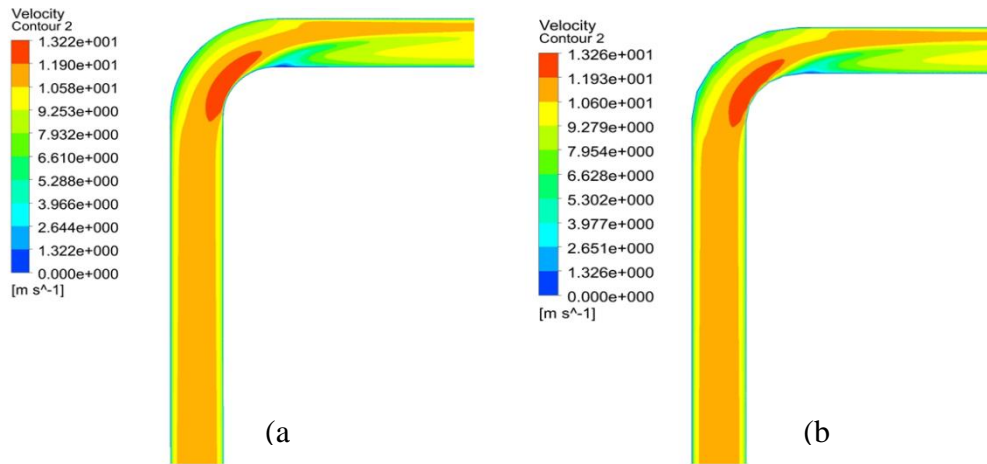
**Figure 32:** Velocity distribution in (a) standard 90-degree elbow, (b) 18-degree gored elbow for air-sand flow

The design of the elbow has a significant impact on the velocity distribution. The velocity distribution in the 22.5-degree and 30-degree gored elbows is shown in Figure 33.
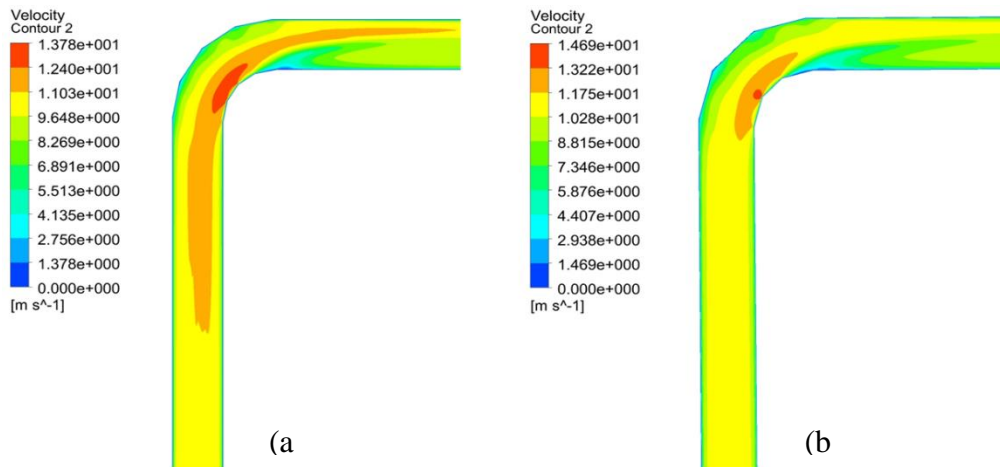


**Figure 33:** Velocity distribution in (a) 22.5-degree gored elbow, (b) 30-degree gored elbow for air-sand flow

The velocity variation in these elbows differs significantly from the standard 90-degree elbow. The 22.5-degree gored elbow has a larger region of low velocity near the extrados and a smaller region of high velocity in the middle than the standard 90-degree elbow. Furthermore, the high-velocity region near the intrados of the 22.5-degree gored elbow is also much smaller than

that of the standard 90-degree elbow. The velocity distribution in the 30-degree gored elbow is very similar to that of the 22.5-degree gored elbow, but there are some minor differences. In the 30-degree gored elbow, the region of low velocity near the extrados is larger than in the 22.5-degree gored elbow. Similarly, the region of high-velocity in the middle is smaller, and the high-velocity region near the intrados is somewhat less evident in the 30-degree gored elbow compared to the 22.5-degree gored elbow. The shape of the gored elbow, especially the edges, influences the streamlining of the elbow configuration and causes these variations.

*4.5.2        Velocity Distribution Analysis of Elbow Designs in Water-Sand Flow*

The velocity distribution in the water-sand flow in the 90-degree elbow and the 18, 22.5 and 30-degree gored elbow is shown in Figures 34 and 35. The velocity distribution of water-sand flow is similar to that of air-sand flow, with some small differences. In water-sand flow, the low-velocity region near the extrados is more noticeable, and the high-velocity region near the intrados is less prominent. These higher densities of water affect the velocity distributions in the boundary layer near the wall, resulting in different flow patterns between the conventional 90-degree elbow and the gored elbows. Moreover, in the gored elbows, the high-velocity and low-velocity regions are comparatively smaller than in the 90-degree elbow configuration. The shape of the elbow affects the velocity distribution of water-sand flow in the same way as it does for air-sand flow. The shaper edges of the 30-degree gored elbow case have more noticeable velocity distributions near the wall, which is consistent with what is observed in air-sand flow.
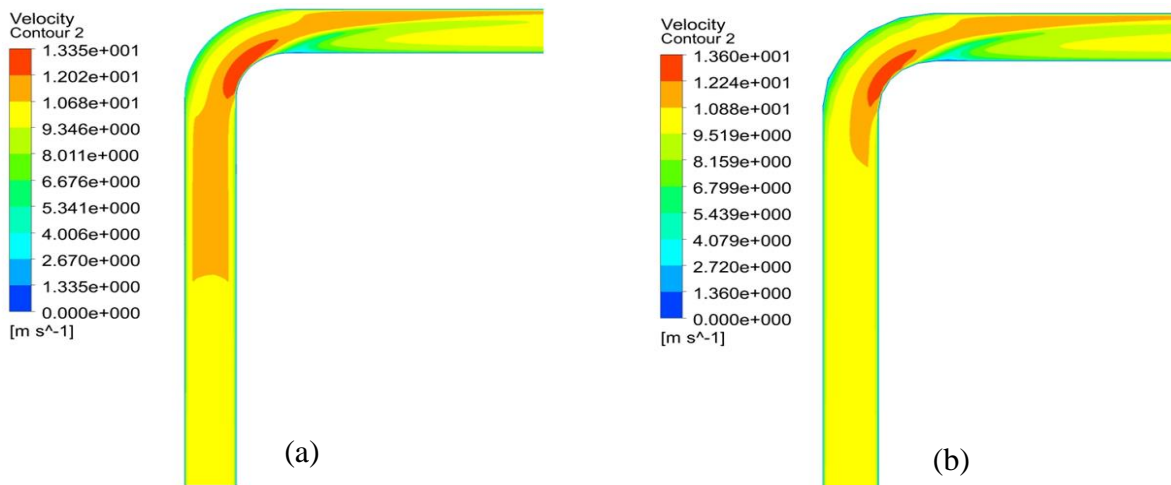


**Figure 34:** Velocity distribution in (a) standard 90-degree elbow, (b) 18-degree gored elbow for water-sand flow

59
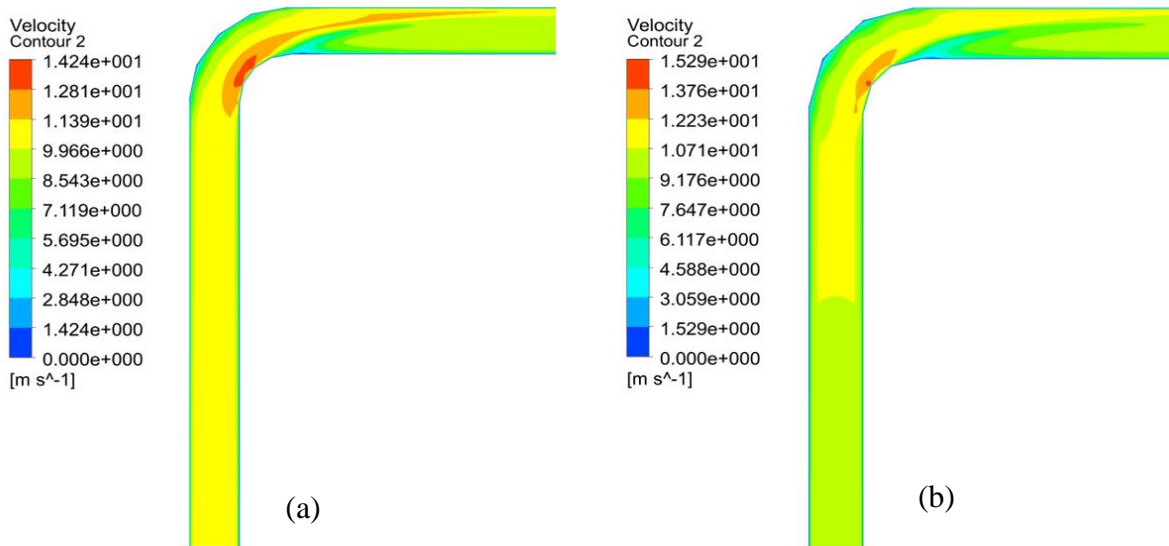
**Figure 35:** Velocity distribution in (a) 22.5-degree gored elbow, (b) 30-degree gored elbow for water-sand flow.

## 4.6 Particle Track

This section uses particle tracking to visualize the paths of particles and the region of the elbow that experiences different levels of erosion. This section will discuss the particle tracking analysis for each of the four designs: the standard 90-degree elbows and the three-gored elbows with 18, 22.5 and 30-degree segments.

### 4.6.1 Particle Track in Air-Sand Flow

Particle tracking is used in both air-sand and water-sand flows to identify the areas where particle impacts are more or less frequent. Particle tracking also reveals the paths that particles follow after impacting the elbow surface, providing insights into their post-impact trajectories. To comprehensively illustrate the diverse particle paths and behaviours within each design, two specific particles were tracked in detail. This in-depth analysis allowed for a subtle understanding of individual particle interactions with the elbow segments. Additionally, the trajectories of a larger number of particles were also tracked to provide a broader perspective on the overall flow patterns and collision frequency within each design.

Figure 36 (a) shows the particle trajectories within the standard 90-degree elbow in air-sand flow. The particle trajectory is shown by two particles which enter the inlet of a 90-degree

60

elbow pipe and follow a straight path until they collide with the elbow wall. The first point of impact for particles 1 and 2 are indicated by a1 and a2, respectively. After the first impact, their paths change and they collide with the elbow wall again at the second points of impact, as shown by b1 and b2, respectively. After impinging on the wall of the 90-degree elbow at a1, Particle 1 undergoes a slight deflection and subsequently strikes the upper wall of the elbow at the second point, b1. It then exits the elbow towards the outlet, following a straight path. Conversely, particle 2, upon impacting the elbow's upper wall at a2, undergoes a rebound at a shallower angle compared to particle 1. This deflection directs it towards the lower side of the pipe, where it strikes at point b2. Finally, it exits the pipe through a straight path. Although both particles exhibit high kinetic energy at their initial impact, leading to significant wall abrasion at points a1 and a2, the subsequent collisions, characterized by lower momentum and diverse angles, contribute less to the cumulative erosion rate.

The zoomed-in view of Figure 36 (a) reveals that particle-wall interactions continue beyond the elbow, as evidenced by the scattered points of impact on the lower pipe wall. The most prominent finding is a significantly higher concentration of particles impacting on the extrados, causing the most severe wear and tear. Conversely, the intrados experiences minimal impact, forming a region with markedly lower erosion. This is further visualized by the side view of the elbow pipe, where the dotted box highlights the area receiving the majority of particle strikes. These diverse impact points directly manifest as distinct erosion patterns. Some particles in the elbow strike the extrados, rebound and hit the lower wall, while the intrados remains largely untouched, highlighting a vast area with no particle impact.

Figure 36 (b) illustrates the distinct particle trajectories within the 18-degree gored elbow. The particle trajectories in the 18-degree gored elbow are initially similar to those in the standard 90-degree elbow, but the impact points and post-impact regions differ significantly. Particle 1 strikes the second segment of the 18-degree gored elbow at point a1, and due to the inclination of the segment, the particle experiences a deflection and hits the upper wall at point b1 at a slightly longer distance than in the 90-degree elbow. At point b1, the particle is again deflected from the last segment of the elbow and collides with the lower wall of the pipe at point c1 at a longer distance and then moves to the outlet of the elbow without further encounter with the wall. The path of particle 2 after the first collision with the wall at point a2 slightly bends in the upward

61

direction where it hits the side of the pipe at point b2. The rebound of particle 2 directs it to the lower wall at c2, similar to particle 1 before exiting.
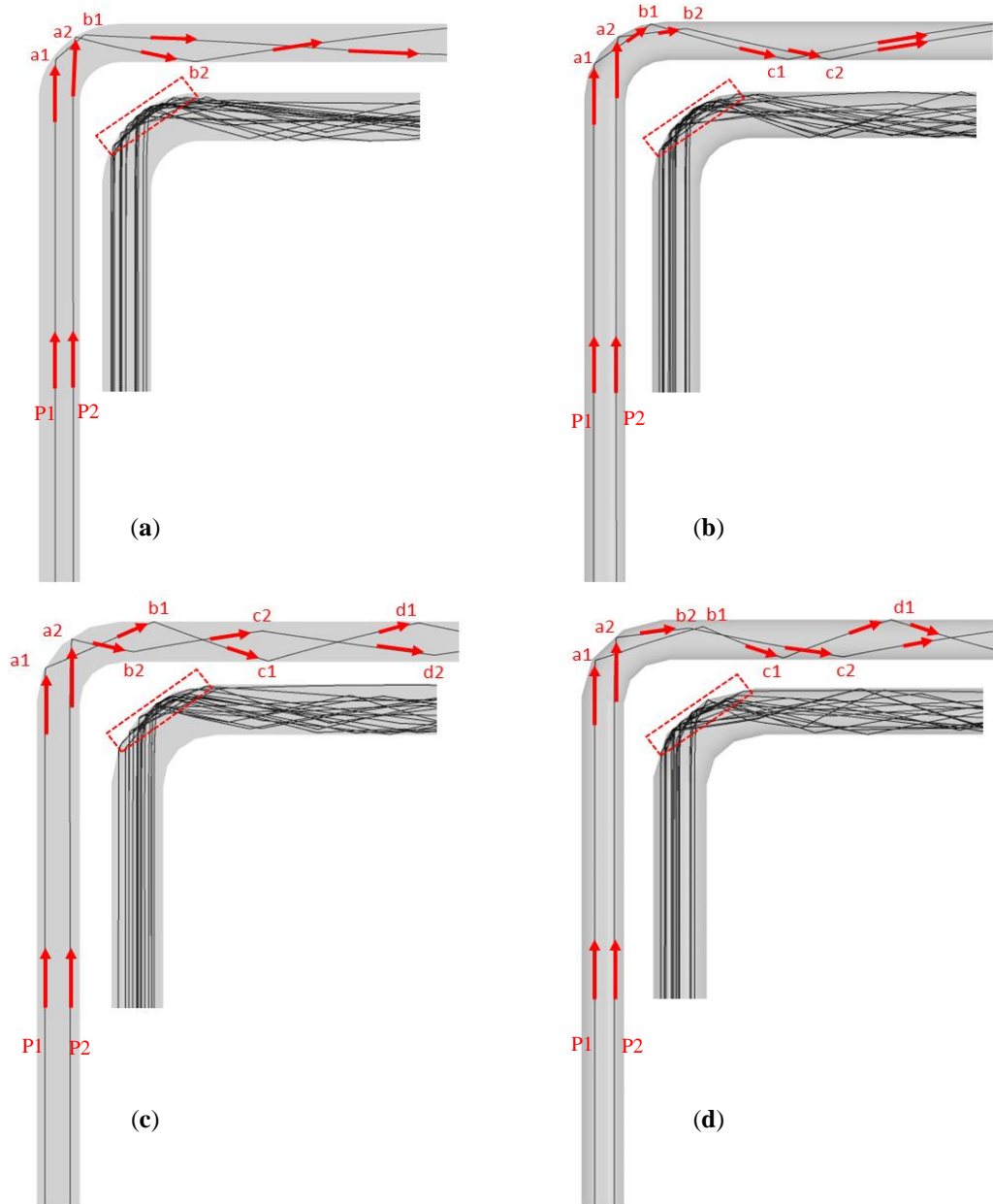


**Figure 36:** Particle track for air-sand flow in (a) standard 90-degree elbow, (b) 18-degree gored elbow, (c) 22.5-degree gored elbow, (d) 30-degree gored elbow

The zoomed-in view reveals that the extrados experience extreme particle impacts, contributing to higher erosion, while the intrados remain intact. The segment inclination significantly affects the paths of the particles, causing them to hit the lower wall at different locations, as shown in Figure 36 (b). Compared to the standard 90-degree elbow, the 18-degree

gored elbow experiences a higher number of particles colliding with the lower wall. Additionally, the segments in the 18-degree gored elbow distribute particle impacts instead of concentrating them in specific locations. This distribution also reduces the erosion rate and directs some particles towards the upper wall, receiving a portion of the particle impact.

Figure 36 (c) and (d) illustrate the contrasting particle trajectories within the 22.5-degree and 30-degree gored elbows. In the 22.5-degree case (Figure 36 (c)), particle paths become significantly more erratic after the initial collision. Particle 1, highlighted in Figure 36 (c), initially follows a straight path before hitting the lower part of the second segment of the elbow at point a1. It then deflects off the elbow surface, striking the upper wall at b1. Particle 1 then rebounds from this point, hitting the lower wall at c1. Another rebound guides it back to the upper wall, where it strikes at d1 before exiting the outlet. Particle 2 (Figure 36 (c)), takes a different path compared to particle 1. It initially strikes the third segment of the 22.5-degree gored elbow at a2. This segment angle guides particle 2 towards the lower portion of the pipe, causing it to collide with the wall at b2. It then rebounds from this point and strikes the pipe again at two distinct locations, c2 and d2. Both follow a zigzag pattern, colliding with the outlet pipe wall at multiple locations, unlike the 90-degree case where impacts are concentrated. This helps to reduce the erosion rate considerably in the 22.5-degree gored elbow due to the segment position in this design.

The 22.5-degree gored elbow causes particles to rebound from the extrados and hit the adjacent part of the lower wall of the elbow pipe. This behaviour is primarily due to the orientation of the third segment within the gored elbow design. Observing the side view (Figure 36 (c)), it is evident that many particles also impact the upper wall of the pipe. This can be attributed to the deflection of particles caused by the first and second segments. Overall, the 22.5-degree gored elbow's third segment orientation significantly alters the particle trajectories compared to the standard 90-degree elbow. This results in a more dispersed distribution of impacts on both the upper and lower walls of the pipe, potentially contributing to reduced erosion in specific areas.

The 30-degree gored elbow exhibits a broadly similar impact pattern as the 22.5-degree gored elbow, with subtle deviations after the first encounter. Particles 1 and 2 initially impact at points a1 and a2 (Figure 36 (d), as with the 22.5-degree case. However, their rebounds differ slightly. In the 30-degree case, particle 1 exhibits a near identical rebound angle to the 22.5-degree

case, striking the upper surface at b1. Particle 2, however, diverges significantly. Its rebound angle differs, propelling it towards the upper wall for impact at b2, unlike the lower wall impact seen in the 22.5-degree case. Following this, the trajectories diverge further. Particle 1 deflects again and hits the lower wall at c1 before striking the upper wall at d1. In contrast, particle 2 hits the lower wall at c2 but exits the pipe without further interactions. This highlights the dynamic interplay between segment angles and particle paths within the 30-degree gored elbow. Figure 36 (d) reveals dispersed particle impacts on the outlet pipe in the 30-degree elbow. This, driven by the gored elbow segment angle, spreads particle impact, potentially reducing concentrated wear compared to the standard 90-degree elbow.

It is worth noting that factors beyond the elbow geometry, such as fluid properties, mass flow rate and velocity, also influence the impact points and intensity. These aspects contribute to shaping the overall erosion patterns and particle transport within the fluid.

### 4.6.2    Particle Track in Water-Sand Flow

As Figure 37 shows, water properties have a significant influence on the trajectories of water-sand flows. When two particles enter a standard 90-degree elbow, they initially follow straight paths until they reach the bend, as Figure 37 (a) illustrates. At this point, their trajectories change. Particle 1 curves sharply and impacts the lower wall at some distance from the elbow before exiting directly. Particle 2, on the other hand, follows a gentler curve towards the upper wall, crossing the path of particle 1. Particle 1 keeps its slight curvature and exits without further collision. Figure 37 (a) also shows the trajectories of a large number of particles in the standard 90-degree elbow. The outer surface near the end of the elbow, which is highlighted by a dotted box, has the highest erosion rate in the water-sand flow. Some particles rebound from this surface and hit the lower wall of the pipe, while other particles move straighter and exit of the pipe. Some particles curve towards the sides of the pipe and collide with the wall, resulting in erosion.

The particle trajectories in the 18-degree gored elbow are illustrated in Figure 37 (b). The trajectories of the two particles resemble those in the standard 90-degree elbow, but particle 1 is closer to the bend in the 18-degree gored elbow. More particles hit the segment edges, causing severe erosion. Some particles rebound from the edges and hit the lower pipe wall at different

positions. The segments in the 18-degree gored elbow disturb the particle paths, which deviate from those in the 90-degree elbow. The 22.5-degree and 30-degree gored elbows have similar particle trajectories as the 18-degree ones, with more impacts on the segment edges, as shown in Figure 37 (c) and (d). Particles also collide with various positions along the pipe sides, with a relatively small number following a straight path to the outlet. The water properties affect the paths of the particles to vary from those in airflow.
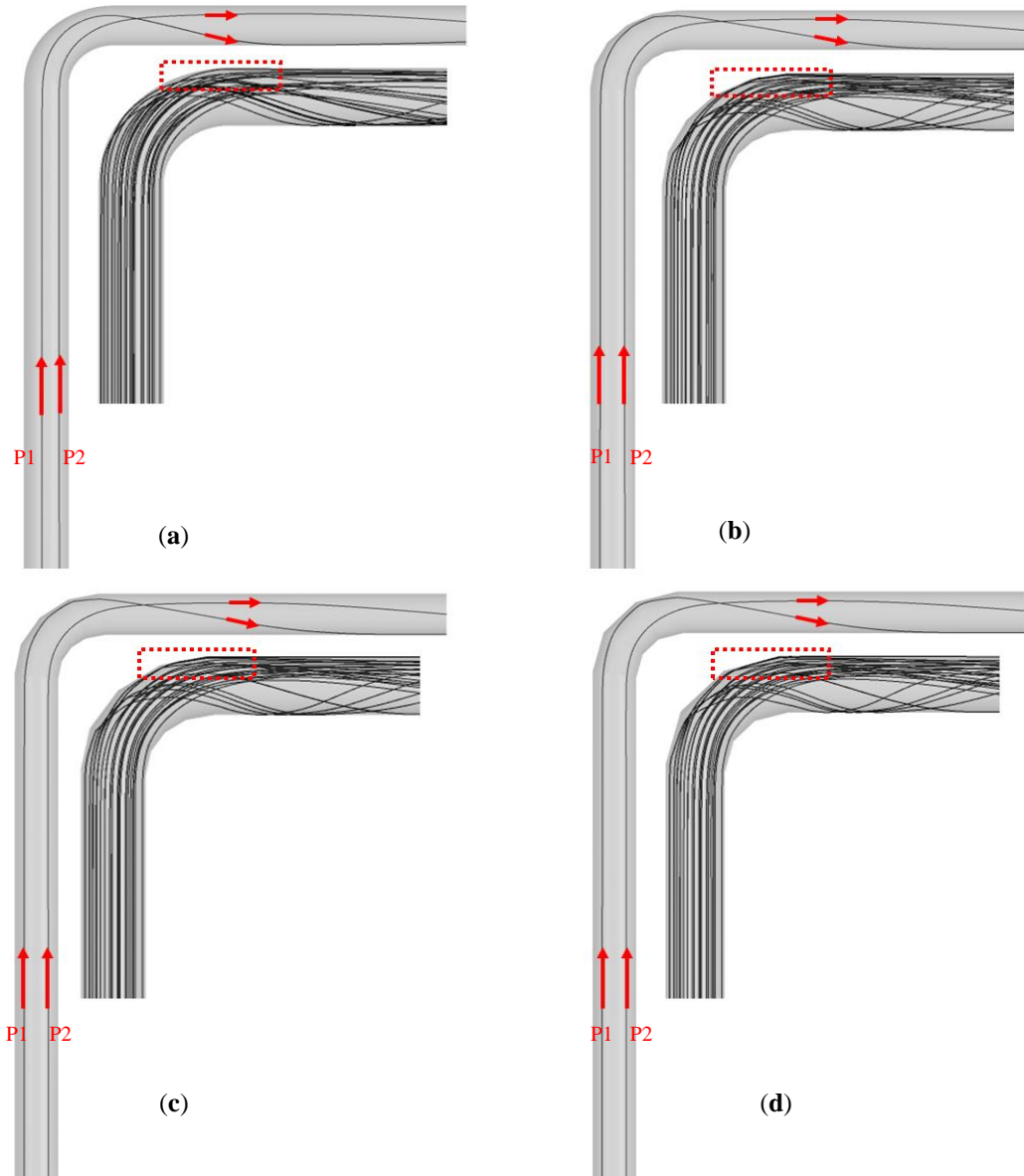


**Figure 37:** Particle track for water-sand flow in (a) standard 90-degree elbow, (b) 18-degree gored elbow, (c) 22.5-degree gored elbow, (d) 30-degree gored elbow.

## 4.7 Regression Analysis and Main Effect Plots

Regression analysis is a statistical method used to examine the relationship between a dependent variable and one or more independent variables. The goal is to understand how variations in the independent variables are associated with changes in the dependent variable. This analysis produces an equation that can be utilized for predicting and offers insight into the relationship's strengths and nature. The coefficients obtained from regression analysis represent the effect of each independent variable on the dependent variable. In contrast, a main effect plot is a graphical depiction of the relationship between an independent variable and the mean of the dependent variable. It aids in the identification of trends and patterns, simplifying the understanding of the variable's influence. Together, regression analysis and main effect plots provide a comprehensive method for understanding and interpreting intricate data sets. They serve as invaluable tools for decision-making and hypothesis testing in a variety of fields, including economics, social sciences, natural sciences etc.

This section examines the use of Minitab software for statistical analysis, with a focus on regression analysis and main effect plots. It also explores the effects of various factors on elbow designs, providing a comprehensive analysis of their impact. Regression analysis was performed using the Oka erosion model only due to its higher accuracy in predicting the erosion rate. Main Effect plots were generated using both the Oka and Generic erosion models to select the optimal design.

### 4.7.1    Regression Analysis in Air-Sand Flow

The regression equation has the advantage of being able to forecast future results and also show how the result changes when the influencing parameters are altered. Regression prediction involves estimating the value of a dependent variable using the presumed values of related independent variables. A regression analysis of air-sand flow was performed in Minitab, using the Oka erosion model as the dependent variable and the air velocity (AV), sand size (SS), and flow rate (FR) as the independent variable. For each design, a regression equation was fitted using the first five cases from the CFD simulations. In the conducting regression analysis, binary coding (1 for presence, 0 for absence) was employed to represent the categorical predictor of the Design

method. The derived regression equation pertinent to each design configuration, numbered from Design 1 through Design 4, is presented subsequently. In the equations, ER(Oka) represents the erosion rate predicted by the Oka erosion model.

**Design**

1      ER(Oka)    =    -0.000906 + 0.000210 AV + 0.000001 SS - 0.02431 FR    (4.1)

2      ER(Oka)    =    -0.000915 + 0.000210 AV + 0.000001 SS - 0.02431 FR    (4.2)

3      ER(Oka)    =    -0.001059 + 0.000210 AV + 0.000001 SS - 0.02431 FR    (4.3)

4      ER(Oka)    =    -0.000943 + 0.000210 AV + 0.000001 SS - 0.02431 FR    (4.4)

The regression equation coefficients can be obtained from Minitab, providing an extensive overview of all statistical parameters. Table 14 shows the regression coefficients for each term in the regression equation.

**Table 14:** Coefficients of the regression equations for air-sand flow

| Term | Coef | SE Coef | T-Value | P-Value | VIF |
|---|---|---|---|---|---|
| Constant | -0.000906 | 0.000588 | -1.54 | 0.147 | |
| Air Velocity | 0.000210 | 0.000061 | 3.47 | 0.004 | 226.67 |
| Sand Size | 0.000001 | 0.000005 | 0.13 | 0.899 | 170.00 |
| Flow Rate | -0.02431 | 0.00606 | -4.01 | 0.001 | 57.67 |
| Design | | | | | |
| 2 | -0.000009 | 0.000042 | -0.22 | 0.833 | 1.50 |
| 3 | -0.000154 | 0.000042 | -3.66 | 0.003 | 1.50 |
| 4 | -0.000037 | 0.000042 | -0.88 | 0.394 | 1.50 |

The statistics that measure the fit of the regression model are shown in Table 15. This model summary includes the standard error, the coefficient of determination, and the adjusted and

predicted R-squared values. In Table 15, S represents the standard error of the regression. In this particular case, it is very small, which means that this model fits the data very well. The term R-sq is the coefficient of determination. It is very high in this case, which means that this model explains most of the variations in the response variable. R-sq (adj) shows the adjusted R-squared, which is slightly lower than the R-sq. This means that the model has a good balance between complexity and fit. Finally, the R-sq (pred) indicates the predicted R-squared. In this case, it is slightly lower than R-sq (adj), which means that this model has a good predictive power.

**Table 15:** Model summary

| S | R-sq | R-sq(adj) | R-sq(pred) |
|---|---|---|---|
| 0.0000664 | 97.87% | 96.89% | 94.47% |

To test the effects of air velocity, sand size, flow rate, and design on the Oka erosion model, an analysis of variance (ANOVA) was conducted. Table 16 displays the results obtained in this analysis. The ANOVA showed that air velocity ($F_{(1,13)} = 12.07$, $p = 0.004$), flow rate ($F_{(1,13)} = 16.11$, $p = 0.001$) and design ($F_{(3,13)} = 5.72$, $p = 0.01$) had significant influences on the erosion rate, while sand size ($F_{(1,13)} = 0.02$, $p = 0.899$) did not have a significant impact.

**Table 16:** Analysis of variance (ANOVA) for regression model

| Source | DF | Adj SS | Adj MS | F-Value | P-Value |
|---|---|---|---|---|---|
| Regression | 6 | 0.000003 | 0.000000 | 99.67 | 0.000 |
| Air Velocity | 1 | 0.000000 | 0.000000 | 12.07 | 0.004 |
| Sand Size | 1 | 0.000000 | 0.000000 | 0.02 | 0.899 |
| Flow Rate | 1 | 0.000000 | 0.000000 | 16.11 | 0.001 |
| Design | 3 | 0.000000 | 0.000000 | 5.72 | 0.010 |
| Error | 13 | 0.000000 | 0.000000 | | |
| Total | 19 | 0.000003 | | | |

As shown in Table 17, the large negative value of the standard residual shows that observation 15 significantly differs from the fitted model. This indicates that the model may not accurately estimate the erosion rate for the particular observation. Further investigation is required to determine whether other observations also show deviations from the model.

**Table 17:** Fits and diagnostics for unusual observations

| Obs | ER(Oka) | Fit | Resid | Std Resid | |
|-----|---------|-----|-------|-----------|---|
| 15 | 0.000805 | 0.000930 | -0.000124 | -2.42 | R |

The Pareto chart in Figure 38 shows the standardized effects and reveals that the erosion rate is most affected by the flow rate. The velocity of air and design also have significant effects, while sand size has the smallest effect on the erosion rate among the factors and tested conditions.
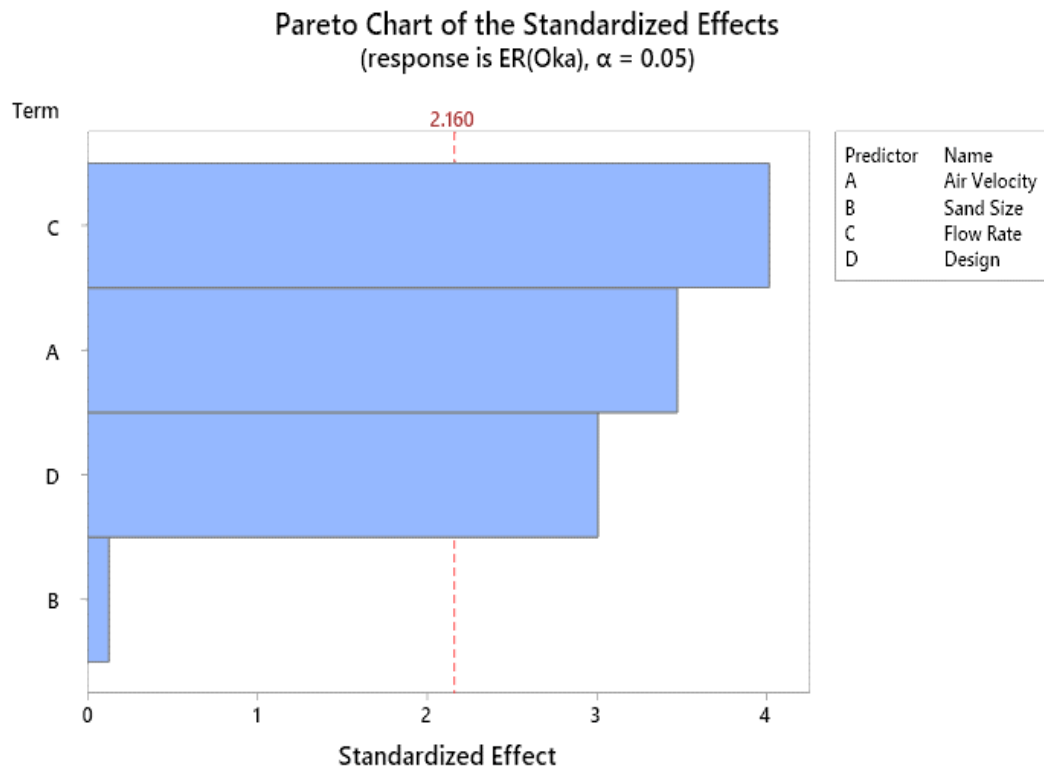


**Figure 38:** Standardized effects of various parameters on erosion rate in air-sand flow

### 4.7.2    *Regression Analysis in Water-Sand Flow*

The Oka erosion model was used as the dependent variable in a regression analysis to predict the erosion rate in water-sand flow. The independent variables were water velocity (WV), sand size (SS), and flow rate (FR). The regression equations for different designs were obtained using categorical predictors (1 or 0). A regression equation was fitted for water-sand flow using the first five CFD simulation cases to predict the erosion rate. The regression equations are presented in the following section.

**Design**

1    ER(Oka)    =    -0.000340 + 0.000053 WV + 0.000000 SS - 0.00652 FR    (4.5)

2    ER(Oka)    =    -0.000273 + 0.000053 WV + 0.000000 SS - 0.00652 FR    (4.6)

3    ER(Oka)    =    -0.000235 + 0.000053 WV + 0.000000 SS - 0.00652 FR    (4.7)

4    ER(Oka)    =    -0.000218 + 0.000053 WV + 0.000000 SS - 0.00652 FR    (4.8)

**Table 18:** Coefficients of the regression equations for water-sand flow

| Term | Coef | SE Coef | T-Value | P-Value | VIF |
|---|---|---|---|---|---|
| Constant | -0.000340 | 0.000475 | -0.72 | 0.487 | |
| Water Velocity | 0.000053 | 0.000049 | 1.09 | 0.295 | 226.67 |
| Sand Size | 0.000000 | 0.000004 | 0.08 | 0.935 | 170.00 |
| Flow Rate | -0.00652 | 0.00490 | -1.33 | 0.206 | 57.67 |
| Design | | | | | |
| 2 | 0.000067 | 0.000034 | 1.98 | 0.069 | 1.50 |
| 3 | 0.000106 | 0.000034 | 3.12 | 0.008 | 1.50 |
| 4 | 0.000122 | 0.000034 | 3.60 | 0.003 | 1.50 |

The model summary in Table 19 provides key statistical measures, including the standard error, the coefficient of determination, and the adjusted and predicted R-squared values.

**Table 19:** Model summary

| S | R-sq | R-sq(adj) | R-sq(pred) |
|---|---|---|---|
| 0.0000537 | 84.89% | 77.92% | 59.57% |

The model summary indicates that the model fits the data well, explaining 84.89% of the variance. However, adjusted and predicted R-squared values are lower, demonstrating some limitations in the model's predictivity ability.

Table 20 shows the results of the analysis of variance (ANOVA) for the model, which has four factors: water velocity (WV), sand size (SS), flow rate (FR), and design. The model is significant for the design factor, which has a low P-value (0.015). The other influencing factors have high P-values, suggesting that they are not significant.

**Table 20:** Analysis of variance (ANOVA) for regression model

| Source | DF | Adj SS | Adj MS | F-Value | P-Value |
|---|---|---|---|---|---|
| Regression | 6 | 0.000000 | 0.000000 | 12.18 | 0.000 |
| Water Velocity | 1 | 0.000000 | 0.000000 | 1.19 | 0.295 |
| Sand Size | 1 | 0.000000 | 0.000000 | 0.01 | 0.935 |
| Flow Rate | 1 | 0.000000 | 0.000000 | 1.77 | 0.206 |
| Design | 3 | 0.000000 | 0.000000 | 5.13 | 0.015 |
| Error | 13 | 0.000000 | 0.000000 | | |
| Total | 19 | 0.000000 | | | |

Table 21 shows two unusual observations that significantly impact the validity and reliability of the regression model. Observation 5 falls significantly below the predicted trend, while observation 20 deviates substantially from the predicted trend in the opposite direction.

These unusual observations indicate potential errors or outliers in the data that can affect the accuracy of the regression model.

**Table 21:** Fits and diagnostics for unusual observations

| Obs | ER(Oka) | Fit | Resid | Std Resid | |
|-----|---------|-----|-------|-----------|---|
| 5 | 0.000090 | 0.000186 | -0.000097 | -2.32 | R |
| 20 | 0.000392 | 0.000309 | 0.000084 | 2.01 | R |

The standardized effects of various parameters on erosion rate in water-sand flow are presented in Figure 39. The Pareto chart of the standardized effects shows that design has the most significant effect on the model. The flow rate and water velocity also have a significant effect on the erosion rate, while sand size has the least effect on the erosion rate of the regression model.
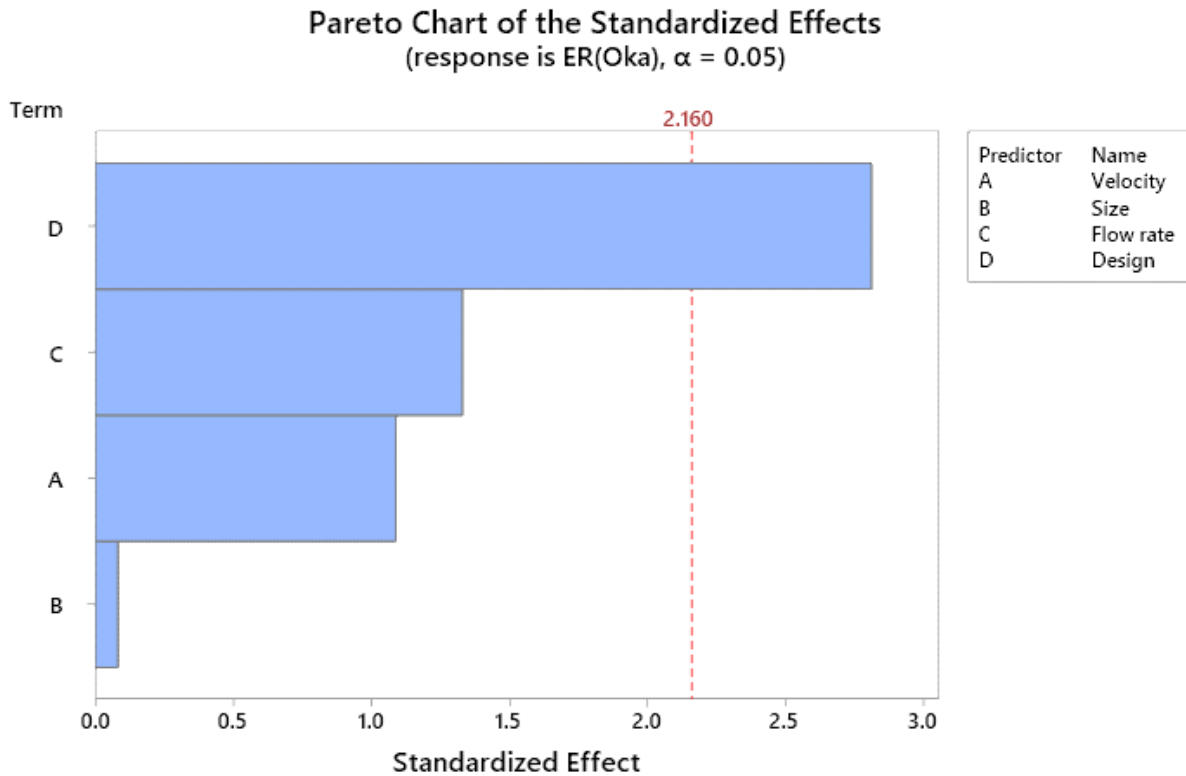


**Figure 39:** Standardized effects of various parameters on erosion rate in water-sand flow

*4.7.3        Main Effect Plots of Oka and Generic Model in Air-Sand Flow*

To investigate the optimal design, the main effect plot for the Oka and Generic erosion model in air-sand flow was generated in Minitab using the data collected for the first five cases of the CFD simulations. The main effect plot for the Oka erosion model is displayed in Figure 40. The figure indicates that the influencing parameters air velocity, sand size and flow rate are increased, and their numerical values are presented in their respective sections. The design section compares the performance of each design under the impact of the increasing influencing parameters. The Design sections 1,2,3 and 4 represent the design of a conventional 90-degree elbow, an 18-degree gored elbow, a 22.5-degree gored elbow, and a 30-degree gored elbow, respectively. The main effect plot reveals that the 22.5-degree gored elbow is the best design for resisting erosion for the specified data. The 30-degree gored elbow and the 18-degree gored elbow follow in the second and third place. The main effect plots show that the standard 90-degree elbow has the lowest potential to reduce erosion. From the main effect plots, it is evident that the gored elbows have higher erosion resistance in air-sand flow than the standard 90-degree elbow.



**Figure 40:** Main effect plot for the Oka erosion model in air-sand flow
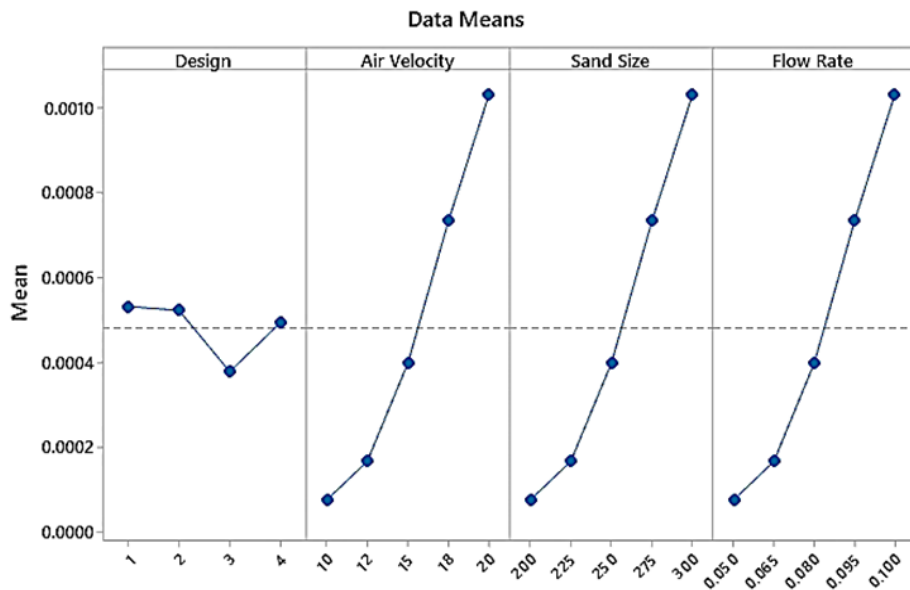
Figure 41 shows the main effect plot for the generic erosion model. The plot indicates that the 22.5-degree gored elbow has the highest erosion resistance, followed by the 30-degree gored elbow, similar to the Oka model. In contrast, the standard 90-degree elbow has more erosion resistance than the 18-degree gored elbow, which makes it prone to erosion.

73

**Figure 41:** Main effect plot for the Generic erosion model in air-sand flow

*4.7.4        Main Effect Plots of Oka and Generic Model in Worst-Case Scenario Air-Sand Flow*

Figures 42 and 43 present the main effect plots for the worst-case scenario with the highest influencing factors. Both the Oka and generic model indicate that the 22.5-degree gored elbow has the lowest erosion rate, while the 18-degree gored elbow has the highest for the particular data. The standard 90-degree elbow has higher erosion resistance than the 30-degree gored elbow in the Oka model, while it is reversed in the generic model.



**Figure 42:** Main effect plot for Oka erosion model in air-sand flow (worst-case scenario)

**Figure 43:** Main effect plot for Generic erosion model in air-sand flow (worst-case scenario)

### 4.7.5 *Main Effect Plots of Oka and Generic Model in Water-Sand Flow*

The main effect plots for the Oka model show that the best design order in the water-sand flow is the standard 90-degree elbow, 18-degree gored elbow, 22.5-degree gored elbow, and 30-degree gored elbow. The data from the first five CFD cases for the Oka erosion model are presented in Figure 44. The Generic model shows a different order, with the standard 90-degree elbow as the finest, followed by the 18-degree gored elbow, the 30-degree gored elbow and the 22,5-degree gored elbow as the worst, as shown in Figure 45.
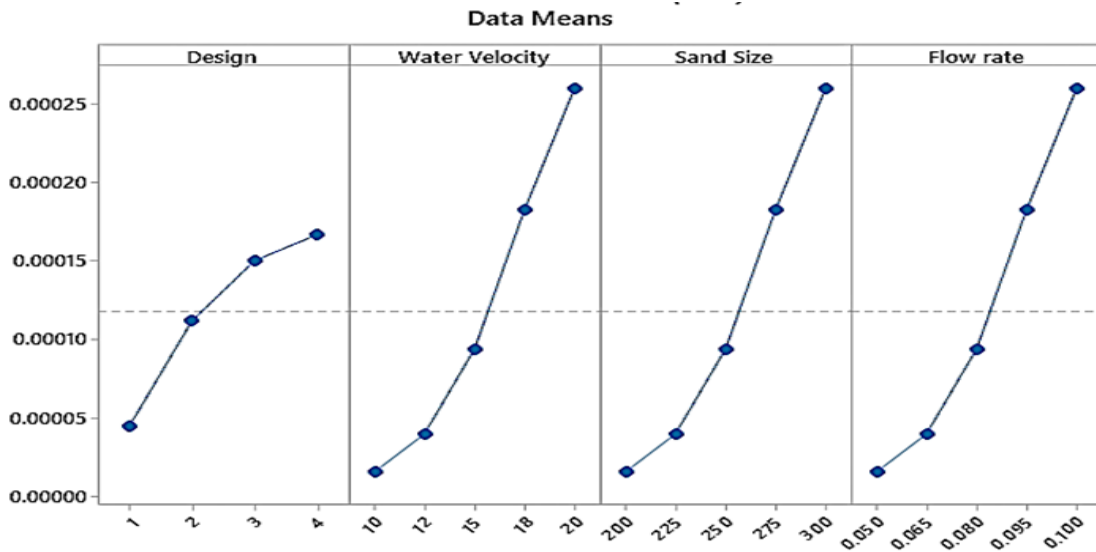


**Figure 44:** Main effect plot for the Oka erosion model in water-sand flow
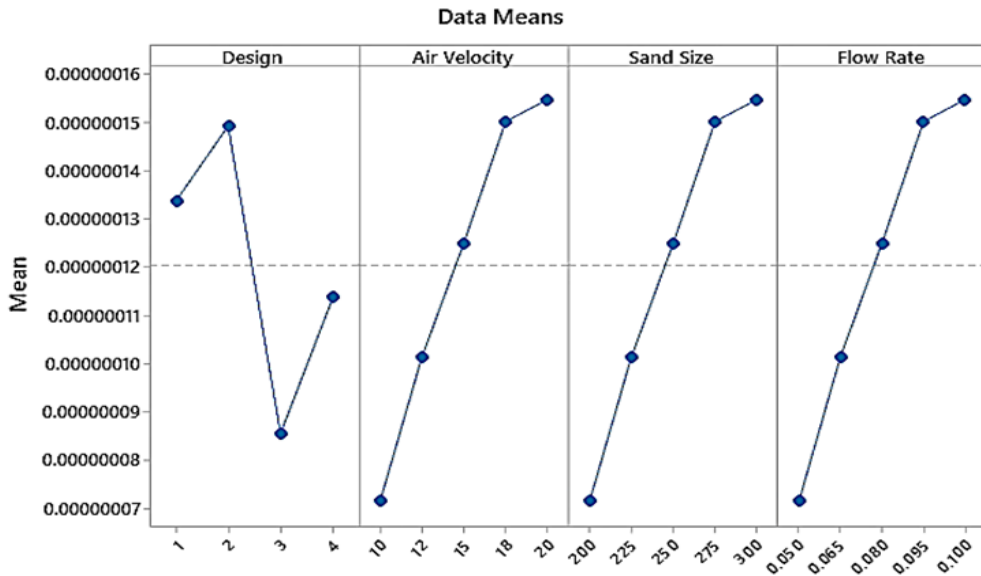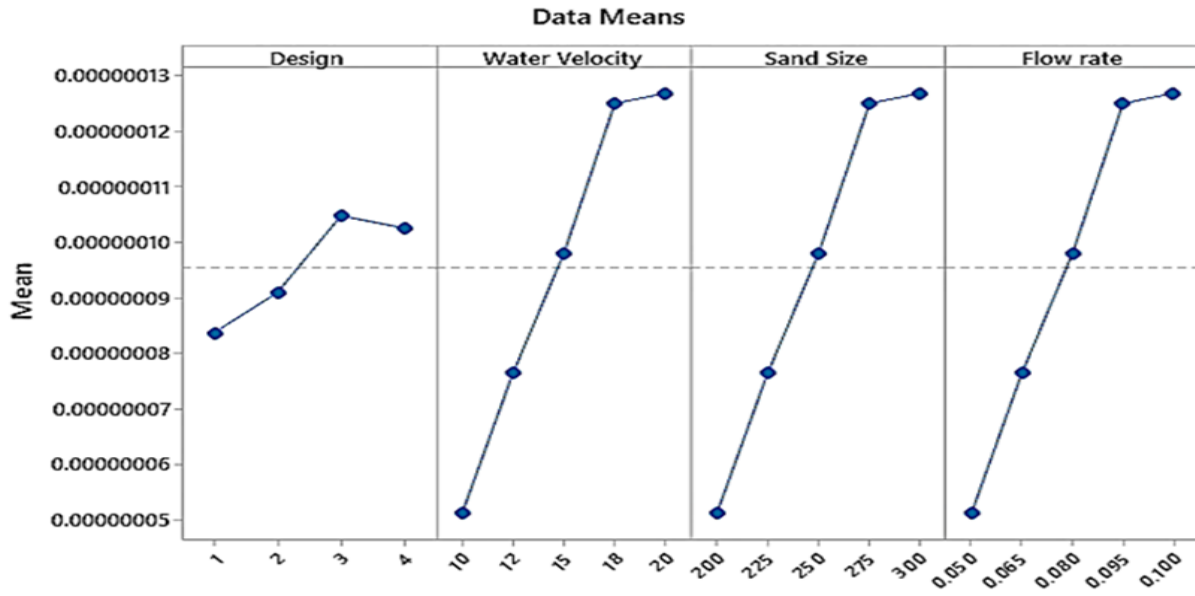
**Figure 45:** Main effect plot for the Generic erosion model in water-sand flow

*4.7.6     Main Effect Plots of Oka and Generic Model in Worst-Case Scenario Water-Sand Flow*

The main effect plots for the worst-case scenario with the highest value of the influencing factors are shown in Figures 46 and 47. In the case of the Oka model, the 90-degree elbow has the best response to mitigating erosion, followed by the 30-degree gored elbow, the 22.5-degree gored elbow, and the 18-degree with the worst response. The Generic erosion model indicates that the best elbow design to mitigate erosion is in the order of the standard 90-degree elbow, the 18-degree gored elbow, the 22.5-degree gored elbow, and the 30-degree gored elbow.
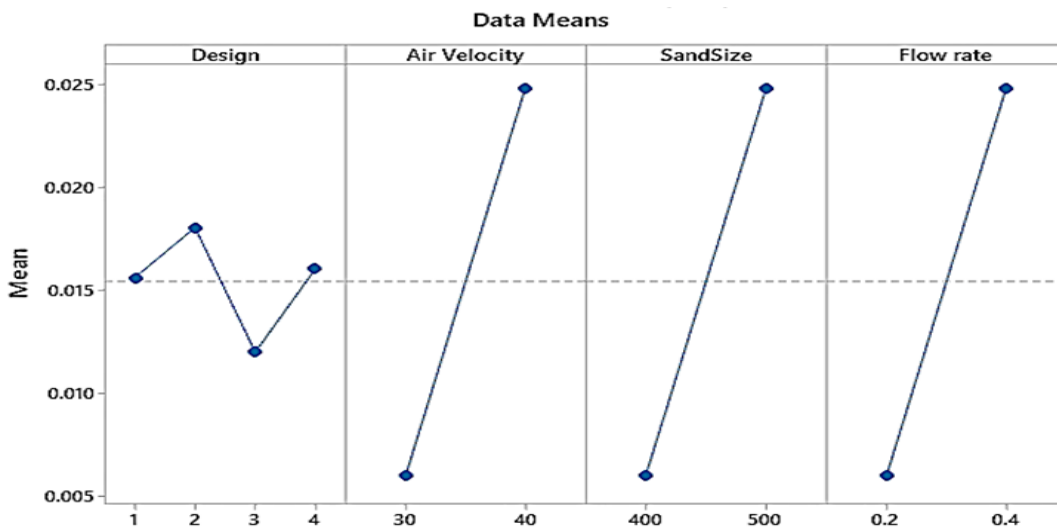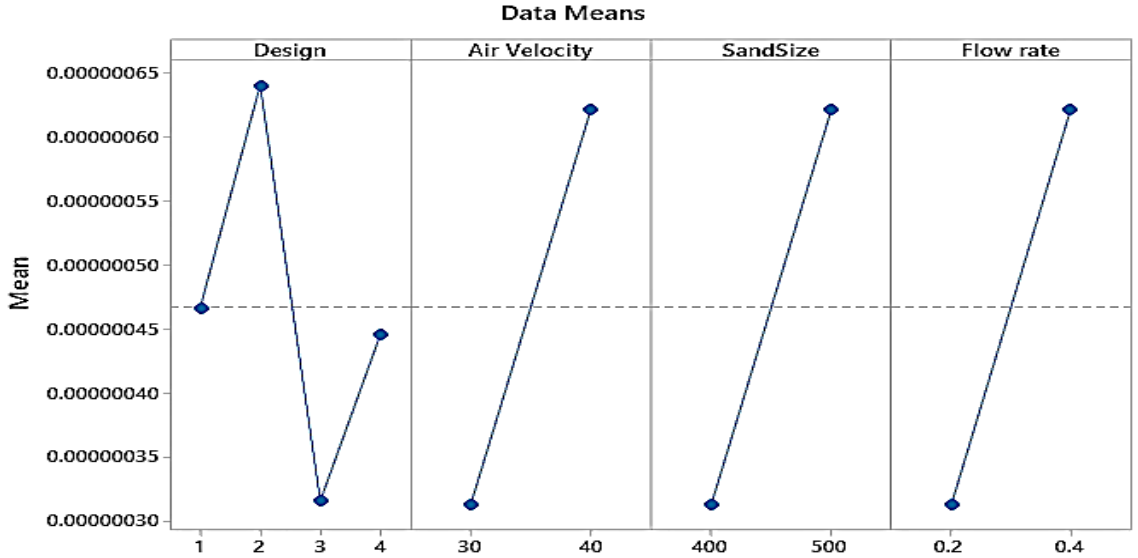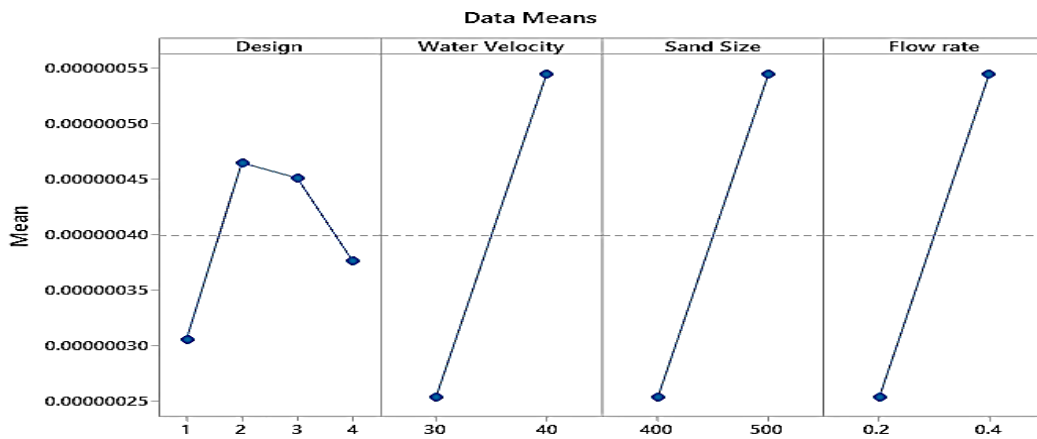


**Figure 46:** Main effect plot for Oka erosion model in water-sand flow (worst-case scenario)
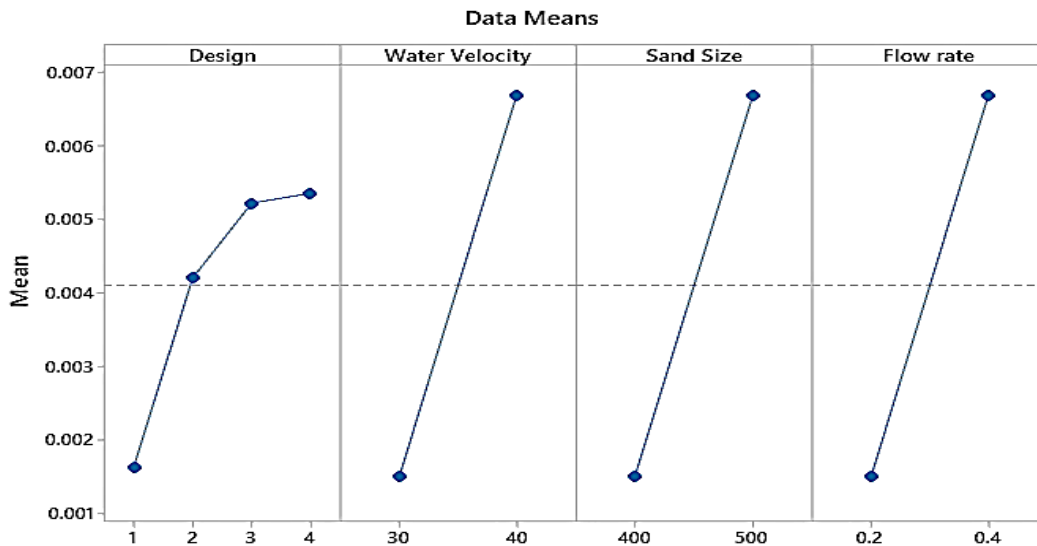
**Figure 47:** Main effect plot for Generic erosion model in water-sand flow (worst-case scenario)

## 4.8 Summary

This chapter comprehensively investigates the erosion rates of different elbow designs in air-sand and water-sand flows under a range of operating conditions. The pressure and velocity distributions within the elbows are also studied, identifying high and low-impact zones. The trajectories and impact patterns of the sand particles on the various elbow configurations are analyzed in detail, providing insight into the erosion mechanism at play. Regression models are developed to quantify the effect of different influencing parameters on erosion rates and elbow performance. The main effect plots presented in this chapter reveal the erosion resistance of different elbow designs, highlighting the most effective configuration for mitigating erosion.

# CHAPTER 5: CONCLUSION AND FUTURE RECOMMENDATIONS

This chapter summarizes the key findings of this research study and discusses its potential contributions to the field. This chapter also outlines the scope of the study and suggests directions for future research.

## 5.1 Conclusion

This study aimed to investigate the erosion caused by multiphase air-sand, and water-sand flows in various elbow designs and to identify the optimal design and operating conditions to mitigate erosion. The designs include the standard 90-degree elbow, 18-degree gored elbow and, 22.5-degree gored elbow, and the 30-degree gored elbow. The performance of all the designs was investigated under a range of operating conditions, including fluid velocities, sand sizes, and sand flow rates. The erosion phenomenon and its influencing factors were investigated by CFD simulations for different elbow geometries. The erosion rates of various elbow geometries were investigated under normal conditions with low values of influencing factors, as well as under worst-case scenarios with high-value influencing factors. The fluid velocity varied from 10 to 40 m/s, the particle size varied from 200 to 500 microns, and the sand flow rate varied from 0.05 to 0.4 kg/s to identify the optimal elbow design and mitigate erosion.

This research includes the analysis of pressure and velocity distributions to identify the high and low-pressure zones and to shed light on the fluid dynamics of the flow. The particle trajectories and high and low impact points predict the high and low erosion zones in different elbow configurations. These parameters provide insight into the erosion mechanism and fluid dynamics of the elbow configurations in multiphase flows.

This research also presents a regression analysis and the formulation of regression equations based on the simulation data for the air-sand and water-sand multiphase flows. This analysis highlights the relationships between the variables and the erosion rates of the elbow configurations. The standardized effect of the influencing factors on the elbow geometries reveals the correlation between the variables and how different factors influence the erosion rate. The main

effect plots examine the performance of various elbow configurations and their resistance against erosion.

The main findings of this research work are presented in detail in the following sections.

1. The results show that the gored elbows outperformed the standard 90-degree elbow in reducing erosion, with the 22.5-degree gored elbow showing the most consistent decrease of up to 32%. The 22.5-degree gored elbow consistently reduces erosion across various flow conditions and worst-case scenarios, ranging from 0.68 to 0.95 (5-32%) times the baseline. While the 18-degree and the 30-degree gored elbows exhibit erosion reduction, their performance was less consistent, with the 18-degree design showing an erosion increase of up to 1.32 times and the 30-degree configuration showing an increase of up to 1.06 times the baseline, respectively. Overall, the study suggests that gored elbows, particularly the 22.5-degree design, offer a promising approach for reducing erosion in air sand flows.

2. The gored elbow designs have different erosion scar shapes from the 90-degree elbow, which has an elliptical and V-shaped erosion scar influenced by the impact points and concentrations of sand particles. The 18-degree gored elbow has a curved rectangular scar with scattered points at the sides and upper portion of the elbow, the 22.5-degree gored elbow has a cylindrical scar similar to a semicircular closed arch, and the 30-degree gored elbow has a trapezium-shaped scar and dispersed erosion points at the sides and upper part of the elbow.

3. The gored elbows, regardless of angle, were ineffective in mitigating erosion in water-sand flows. All gored elbow designs (18-degree, 22.5-degree and 30-degree) exhibited significantly higher erosion rates than the standard 90-degree elbow under all water-sand flow conditions. Furthermore, the erosion rate generally increased with the angle of the gored elbow, with the 30-degree gored elbow experiencing the most severe erosion in most cases. These findings suggest that alternative strategies may be necessary for erosion control in water-sand flows.

4. The conventional 90-degree elbow has the highest erosion rate at the downstream end, especially on the pipe sides and the flow impact point. The three gored elbows have a comparable erosion pattern but with much higher erosion at the flow impact point,

especially at the segment edges. The segments also cause dispersed erosion points due to different impact angles.

5. Pressure and erosion vary greatly across the elbow designs in air-sand multiphase flow. The extrados has the highest pressure and particle impact, resulting in the most erosion, while the intrados have the lowest. The standard 90-degree elbow and the 18-degree gored elbow have similar pressure distributions, but the 18-degree gored elbow has a slightly higher value of maximum pressure. The gored elbows exhibit distinct pressure patterns at the extrados. The 22.5-degree gored elbow and the 30-degree gored elbow have different pressure distributions, with a 30-degree gored elbow having the highest at the extrados.

6. As in air-sand flows, the extrados has the highest pressure, and the intrados has the lowest in water-sand flows. The higher water density causes much higher pressure in water sand flows, and the highest-pressure points are the corners of the gored elbows. The pressure patterns in the standard 90-degree elbow and the gored elbows are consistent with those in air-sand flows.

7. Velocities are the highest at the intrados and lowest at the extrados, with a gradual decrease from the intrados to the extrados in the air-sand flows. A boundary region near the extrados has slower flow, then increases to a maximum at the intrados. The standard 90-degree elbow and the 18-degree gored elbow have similar velocity distributions due to the gored elbow design resembling the 90-degree elbow. The 22.50-degree and 30-degree gored elbows have different velocity variations, with different sections of low and high-velocity zones near the extrados and intrados. The geometry of the gored elbows, specifically at the edges, affects the flow streamlining within the elbow.

8. Water-sand flow velocity distribution in the elbows closely resembles that of air-sand flow, with minor variations. The water-sand flow has more noticeable low-velocity regions near the extrados and high-velocity regions near the intrados. The gored elbows have smaller high and low-velocity regions compared to the standard 90-degree elbow.

9. The particle trajectories and impact points in air-sand flows vary across different elbow geometries. Gored elbows, unlike standard 90-degree design, induce diverse particle impacts due to segmented arrangements. The segment angles in gored elbows

80

substantially influence impact distribution and erosion locations. This is achieved through higher collision rates and segment-driven trajectory variations.

10. Water properties significantly influence water-sand particle trajectories and erosion patterns compared to air-sand flow. Gored elbows, while varying impacts and reducing intense wear on the extrados, exhibit higher overall erosion due to segment-induced trajectory variations and restricted edge wear. Conversely, the standard 90-degree elbow experiences focused erosion on the outer end but less overall erosion due to straighter particle paths.

11. Using regression analysis, the study explored how various factors affect the erosion rate in air-sand multiphase flow. The findings revealed that air velocity, flow rate and elbow design significantly influenced the erosion rate, while sand size had a negligible impact. ANOVA analysis confirmed these findings, and the Pareto chart further illustrated the relative contributions of each factor. Flow rate was identified as the most significant factor, followed by air velocity and design.

12. The main effect plots for the Oka erosion model in air-sand flow indicated that the erosion resistance was highest for the 22.5-degree gored elbow, followed by the 30-degree gored elbow and the 18-degree gored elbow, while the standard 90-degree elbow had the lowest erosion resistance. The Generic erosion model gave similar results, but in contrast to the Oka model, the standard 90-degree elbow had greater erosion resistance than the 18-degree gored elbow, making it less prone to erosion.

13. Even under the worst conditions, the 22.5-degree gored elbow was the best design for mitigating erosion in both the Oka and Generic erosion models. The 18-degree gored elbow had the lowest erosion resistance in both models. In the Oka model, the erosion resistance was higher for the standard 90-degree elbow than for the 30-degree gored elbow, while the reverse was true in the Generic model.

14. In water-sand flow, the regression analysis using the Oka erosion model as the dependent variable suggested that the design had the most significant effect on erosion rate, followed by flow rate and water velocity. Sand size had the smallest effect on erosion rate. These results were further supported by the Pareto chart of standardized effects, which emphasized the dominance of the design factor in influencing erosion rate.

15. Different elbow designs have varying erosion resistance in multiphase water-sand flow, according to the main effect plots of the Oka and Generic models. The Oka model ranked the standard 90-degree elbow as the most erosion-resistant, followed by the 18-degree, 22.5-degree and 30-degree gored elbows. The Generic model, however, ranked the elbow designs as the standard 90-degree elbow, followed by the 18-degree, 30-degree, and 22.5-degree gored elbows.

16. In the presence of the highest influencing factors in the worst-case scenario, the Oka and Generic models provided conflicting results. The Oka model ranked the 90-degree elbow as the top choice, followed by 30-degree, 22.5-degree and 18-degree gored elbows. Contrary to this, the Generic model recommended the order of erosion mitigation as the conventional 90-degree elbow, followed by the 18-degree, 22.5-degree and 30-degree gored elbows.

## 5.2 Future Research Directions and Recommendations

This study suggests some possible directions for future work to advance this field further. The following are some key suggestions.

1. It is recommended to conduct experimental investigations on the gored elbows and analyze the erosion rate and locations of high impact points. This would verify the numerical models and examine the geometrical effects on the erosion of gored elbows.

2. The erosion performance of gored elbows depends on their shape and segment angles. To optimize the design, different angles of gored elbows need to be examined for their erosion resistance.

3. Gored elbows exhibited superior performance, especially the 22.5-degree gored elbow, in air-sand flows. However, their erosion resistance was poor in water-sand flows. Therefore, investigating the erosion rate of gored elbows in fluid with intermediate density between air and water is suggested.

4. Spherical particles were assumed in the numerical investigations, but sand particles have a variety of sizes and irregular shapes in reality. Therefore, both experimental and numerical investigations on the performance of different elbow designs using realistic sand particles are recommended.

5. The regression analysis revealed some unusual observations that require further investigation. More experimental data is needed to investigate the effects of the influencing factors, such as fluid velocity, sand size and flow rate, on the erosion rate. This will help to explain the unusual observations and improve the accuracy of the regression model.

# REFERENCES

[1]     W. Jia *et al.*, "Experimental and numerical simulation of erosion-corrosion of 90° steel elbow in shale gas pipeline," *J Nat Gas Sci Eng*, vol. 89, May 2021, doi: 10.1016/j.jngse.2021.103871.

[2]     C. B. Solnordal, C. Y. Wong, and J. Boulanger, "An experimental and numerical analysis of erosion caused by sand pneumatically conveyed through a standard pipe elbow," *Wear*, vol. 336–337, pp. 43–57, Aug. 2015, doi: 10.1016/j.wear.2015.04.017.

[3]     S. Rahman *et al.*, "Performance Prediction of Erosive Wear of Steel for Two-Phase Flow in an Inverse U-Bend," *Materials*, vol. 15, no. 16, Aug. 2022, doi: 10.3390/ma15165558.

[4]     X. Zhao, X. Cao, J. Zhang, H. Cao, Z. Xie, and N. Xiong, "Numerical investigation and dimensionless erosion laws of solid particle erosion in plugged tees," *Powder Technol*, vol. 402, Apr. 2022, doi: 10.1016/j.powtec.2022.117342.

[5]     A. Li, Z. Wang, L. Zhu, Z. Wang, J. Shi, and W. Yang, "Design optimization of guide vane for mitigating elbow erosion using computational fluid dynamics and response surface methodology," *Particuology*, vol. 63, pp. 83–94, Apr. 2022, doi: 10.1016/j.partic.2021.02.006.

[6]     X. Zhao, X. Cao, J. Zhang, H. Cao, Z. Xie, and N. Xiong, "Numerical investigation and dimensionless erosion laws of solid particle erosion in plugged tees," *Powder Technol*, vol. 402, Apr. 2022, doi: 10.1016/j.powtec.2022.117342.

[7]     Q. H. Mazumder, "S-bend erosion in particulated multiphase flow with air and sand," *Journal of Computational Multiphase Flows*, vol. 8, no. 3, pp. 157–166, Sep. 2016, doi: 10.1177/1757482X16668363.

[8]     R. Khan, H. H. Ya, W. Pao, M. Z. Bin Abdullah, and F. A. Dzubir, "Influence of sand fines transport velocity on erosion-corrosion phenomena of carbon steel 90-degree elbow," *Metals (Basel)*, vol. 10, no. 5, May 2020, doi: 10.3390/met10050626.

[9]     C. B. Solnordal, C. Y. Wong, and J. Boulanger, "An experimental and numerical analysis of erosion caused by sand pneumatically conveyed through a standard pipe elbow," *Wear*, vol. 336–337, pp. 43–57, Aug. 2015, doi: 10.1016/j.wear.2015.04.017.

[10]    Q. H. Mazumder, S. A. Shirazi, B. S. McLaury, J. R. Shadley, and E. F. Rybicki, "Development and validation of a mechanistic model to predict solid particle erosion in multiphase flow," in *Wear*, Jul. 2005, pp. 203–207. doi: 10.1016/j.wear.2005.02.109.

[11]    N. R. Kesana, S. A. Grubb, B. S. McLaury, and S. A. Shirazi, "Ultrasonic Measurement of Multiphase Flow Erosion Patterns in a Standard Elbow," *Journal of Energy Resources Technology, Transactions of the ASME*, vol. 135, no. 3, Sep. 2013, doi: 10.1115/1.4023331.

[12]    A. Abduljabbar, M. E. Mohyaldinn, O. Younis, A. Alghurabi, and F. S. Alakbari, "Erosion of sand screens by solid particles: a review of experimental investigations," *J Pet Explor Prod Technol*, vol. 12, no. 8, pp. 2329–2345, Aug. 2022, doi: 10.1007/s13202-022-01467-4.

[13]    B. Singh Chahar and A. Krishna Pun, EROSION WEAR OF DUCTILE MATERIALS: A REVIEW. Journal of Petroleum Exploration and Production Technology (2022) 12:2329–2345

[14]    M. Parsi, K. Najmi, F. Najafifard, S. Hassani, B. S. McLaury, and S. A. Shirazi, "A comprehensive review of solid particle erosion modeling for oil and gas wells and pipelines applications," *Journal of Natural Gas Science and Engineering*, vol. 21. Elsevier, pp. 850–873, Nov. 01, 2014. doi: 10.1016/j.jngse.2014.10.001.

[15]    P. M. Khodke, D. Mate, and & D. J. Tidke, "Impact erosion of brittle materials: Dependence of particle flow rate on particle velocity," 1999.

[16]    M. H. Buszko and A. K. Krella, "An Influence of Factors of Flow Condition, Particle and Material Properties on Slurry Erosion Resistance," *Advances in Materials Science*, vol. 19, no. 2, pp. 28–53, Jun. 2019, doi: 10.2478/adms-2019-0010.

[17]    V. B. Nguyen, Q. B. Nguyen, Y. W. Zhang, C. Y. H. Lim, and B. C. Khoo, "Effect of particle size on erosion characteristics," *Wear*, vol. 348–349, pp. 126–137, Feb. 2016, doi: 10.1016/j.wear.2015.12.003.

[18]    D. Kanesan and M. E. Mohyaldin, "A REVIEW: THE EFFECTS OF PARTICLE PROPERTIES ON SOLID PARTICLE EROSION FOR OIL AND GAS PIPELINES APPLICATIONS," vol. 13, no. 18, 2018, [Online]. Available: www.arpnjournals.com

[19]    N. Lin, H. Arabnejad, S. A. Shirazi, B. S. McLaury, and H. Lan, "Experimental study of particle size, shape and particle flow rate on Erosion of stainless steel," *Powder Technol*, vol. 336, pp. 70–79, Aug. 2018, doi: 10.1016/j.powtec.2018.05.039.

[20]    J. A. F. O. Correia, M. S. Parancheerivilakkathil, S. Parapurath, S. Ainane, Y. F. Yap, and P. Rostron, "Flow Velocity and Sand Loading Effect on Erosion-Corrosion during Liquid-Solid Impingement on Mild Steel," 2022, doi: 10.3390/app.

[21]    J. G. Liu *et al.*, "Effect of flow velocity on erosion–corrosion of 90-degree horizontal elbow," *Wear*, vol. 376–377, pp. 516–525, 2017, doi: 10.1016/j.wear.2016.11.015.

[22]    R. Khan *et al.*, "Influence of Elbow Angle on Erosion-Corrosion of 1018 Steel for Gas–Liquid–Solid Three Phase Flow," *Materials*, vol. 15, no. 10, May 2022, doi: 10.3390/ma15103721.

[23]    M. R. Banakermani, H. Naderan, and M. Saffar-Avval, "An investigation of erosion prediction for 15° to 90° elbows by numerical simulation of gas-solid flow," *Powder Technol*, vol. 334, pp. 9–26, Jul. 2018, doi: 10.1016/j.powtec.2018.04.033.

[24] C. A. R. Duarte, F. J. de Souza, and V. F. dos Santos, "Mitigating elbow erosion with a vortex chamber," *Powder Technol*, vol. 288, pp. 6–25, Jan. 2016, doi: 10.1016/j.powtec.2015.10.032.

[25] H. Zhu and S. Li, "Numerical analysis of mitigating elbow erosion with a rib," *Powder Technol*, vol. 330, pp. 445–460, May 2018, doi: 10.1016/j.powtec.2018.02.046.

[26] A. S. Al-Ithari, N. Al-Zurfi, and L. Z. A. U. L. Kareem, "Reducing the mechanical wear of elbows and pipes due to solid particles flow by using nano coating technique," *Sci Rep*, vol. 11, no. 1, Dec. 2021, doi: 10.1038/s41598-021-01563-1.

[27] H. Zhou *et al.*, "Study on reducing elbow erosion with swirling flow," *Colloids Surf A Physicochem Eng Asp*, vol. 630, Dec. 2021, doi: 10.1016/j.colsurfa.2021.127537.

[28] C. A. R. Duarte, F. J. de Souza, D. N. Venturi, and M. Sommerfeld, "A numerical assessment of two geometries for reducing elbow erosion," *Particuology*, vol. 49, pp. 117–133, Apr. 2020, doi: 10.1016/j.partic.2019.01.004.

[29] C. A. R. Duarte and F. J. de Souza, "Innovative pipe wall design to mitigate elbow erosion: A CFD analysis," *Wear*, vol. 380–381, pp. 176–190, 2017, doi: 10.1016/j.wear.2017.03.015.

[30] R. Li, Z. Sun, A. Li, Y. Li, and Z. Wang, "Design optimization of hemispherical protrusion for mitigating elbow erosion via CFD-DPM," *Powder Technol*, vol. 398, Jan. 2022, doi: 10.1016/j.powtec.2022.117128.

[31] X. Zhao, X. Cao, Z. Xie, H. Cao, C. Wu, and J. Bian, "Numerical study on the particle erosion of elbows mounted in series in the gas-solid flow," *J Nat Gas Sci Eng*, vol. 99, Mar. 2022, doi: 10.1016/j.jngse.2022.104423.

[32] G. Haider, P. Kane, S. A. Shirazi, T. Wood, and R. McNaught, "Testing and validation of a new state-of-the-art erosion control technology in multiphase flow," *Wear*, vol. 476, Jul. 2021, doi: 10.1016/j.wear.2021.203638.

[33] F. Xiao *et al.*, "Numerical investigation of elbow erosion in the conveying of dry and wet particles," *Powder Technol*, vol. 393, pp. 265–279, Nov. 2021, doi: 10.1016/j.powtec.2021.07.080.

[34] M. H. Zolfagharnasab, M. Salimi, H. Zolfagharnasab, H. Alimoradi, M. Shams, and C. Aghanajafi, "A novel numerical investigation of erosion wear over various 90-degree elbow duct sections," *Powder Technol*, vol. 380, pp. 1–17, Mar. 2021, doi: 10.1016/j.powtec.2020.11.059.

[35] N. Lin, H. Lan, Y. Xu, S. Dong, and G. Barber, "Effect of the gas-solid two-phase flow velocity on elbow erosion," *J Nat Gas Sci Eng*, vol. 26, pp. 581–586, Sep. 2015, doi: 10.1016/j.jngse.2015.06.054.

[36]    F. N. Mouketou and A. Kolesnikov, "Modelling and simulation of multiphase flow applicable to processes in oil and gas industry," *Chemical Product and Process Modeling*, vol. 14, no. 1, 2019, doi: 10.1515/cppm-2017-0066.

[37]    Y. I. Oka, K. Okamura, and T. Yoshida, "Practical estimation of erosion damage caused by solid particle impact: Part 1: Effects of impact parameters on a predictive equation," in *Wear*, Jul. 2005, pp. 95–101. doi: 10.1016/j.wear.2005.01.039.

[38]    Y. I. Oka and T. Yoshida, "Practical estimation of erosion damage caused by solid particle impact: Part 2: Mechanical properties of materials directly associated with erosion damage," in *Wear*, Jul. 2005, pp. 102–109. doi: 10.1016/j.wear.2005.01.040.

[39]    I. Finnie, "EROSION OF SURFACES BY SOLID PARTICLES." Wear, vol. 3(1), pp, 87-103, 1960

[40]    H. Arabnejad, A. Mansouri, S. A. Shirazi, and B. S. McLaury, "Development of mechanistic erosion equation for solid particles," Wear, vol. 332–333, pp. 1044–1050, May 2015, doi: 10.1016/j.wear.2015.01.031.

[41]    R. E. Vieira, A. Mansouri, B. S. McLaury, and S. A. Shirazi, "Experimental and computational study of erosion in elbows due to sand particles in air flow," Powder Technol, vol. 288, pp. 339–353, Jan. 2016, doi: 10.1016/j.powtec.2015.11.028.